

# Welcome to the PIIC Pipelines

Pointing & Imaging In Continuum

a code by Robert Zylka

Stefano Berta and Robert Zylka

September 16, 2021

**Acknowledgements:** we thank A. Sievers, C. Kramer and A. Schmiedeke for their careful reading of the Oct. 31st 2019 version of this document, and all users who sent us comments and suggestions (A. Beelen, G. Lagache, A. Rigby, J. Macias-Perez, S. Andreon, and many others). We are grateful to C. Kramer for his help and scripts for the Fourier analysis in App. C.

# Contents

|          |   |           |
|----------|---|-----------|
| <b>1</b> | <b>Welcome to PIIC!</b>   | <b>7</b>  |
| 1.1      | Acknowledging and citing PIIC . . . . .                             | 7         |
| 1.2      | This release . . . . .  | 8         |
| 1.3      | The PIIC calibration files . . . . .                                | 8         |
| 1.4      | Setting up PIIC . . . . .   | 8         |
| 1.5      | Starting PIIC . . . . .   | 9         |
| 1.5.1    | The graphic interface . . . . .                                     | 9         |
| 1.5.2    | Using external commands . . . . .                                   | 9         |
| <b>2</b> | <b>Blind use of the PIIC science pipeline</b>                       | <b>10</b> |
| 2.1      | Important warning . . . . .   | 10        |
| 2.1.1    | Note about scan speed . . . . .                                     | 10        |
| 2.2      | Weak compact sources . . . . .                                      | 11        |
| 2.3      | Strong compact sources . . . . .                                    | 11        |
| 2.4      | Deep fields . . . . .   | 11        |
| 2.5      | Sunyaev-Zeldovich clusters . . . . .                                | 11        |
| 2.6      | Complex sources . . . . .   | 12        |
| <b>3</b> | <b>The science data-reduction pipeline</b>                          | <b>13</b> |
| 3.1      | Principles and challenges of NIKA2 science data reduction . . . . . | 13        |
| 3.2      | Setup . . . . .   | 14        |
| 3.2.1    | The directory tree . . . . .  | 14        |
| 3.2.2    | The list of scans . . . . .   | 15        |
| 3.2.3    | The template script . . . . .                                       | 16        |
| 3.2.4    | Define your source . . . . .  | 18        |
| 3.2.5    | Specific cases . . . . .  | 20        |
| 3.2.6    | Order of baseline correction . . . . .                              | 22        |
| 3.2.7    | Deep field and weak source options . . . . .                        | 22        |
| 3.2.8    | Measuring the noise r.m.s. . . . .                                  | 22        |
| 3.2.9    | Additional parameters . . . . .                                     | 23        |
| 3.2.10   | Correlating pixels . . . . .  | 23        |
| 3.2.11   | Correlating pixels: the case of extended sources . . . . .          | 23        |
| 3.2.12   | Pixel size . . . . .  | 23        |

|          |  |           |
|----------|--|-----------|
| 3.2.13   | Exclude noisy timelines/maps . . . . .   | 24        |
| 3.2.14   | Pausing . . . . .  | 24        |
| 3.2.15   | Producing diagnostic diagrams and saving them as PNG figures . . . . .                   | 25        |
| 3.2.16   | Overwriting . . . . .  | 25        |
| 3.3      | Run it! . . . . .  | 26        |
| 3.3.1    | Information about re-gridding . . . . .  | 29        |
| 3.4      | Quick analysis of the 0-th iteration results . . . . .                                   | 29        |
| 3.4.1    | The intensity maps . . . . .   | 29        |
| 3.4.2    | The weight maps . . . . .  | 30        |
| 3.4.3    | Compute r.m.s. and S/N maps . . . . .  | 31        |
| 3.4.4    | Verify the source defined in the script . . . . .  | 32        |
| 3.4.5    | The noise r.m.s. polygon . . . . .   | 32        |
| 3.5      | Iterative mode . . . . .   | 33        |
| 3.5.1    | Verify convergence . . . . .   | 33        |
| 3.6      | Products . . . . .   | 33        |
| <b>4</b> | <b>Additional tips and advanced use</b>  | <b>35</b> |
| 4.1      | Non-azimuthal scans . . . . .  | 35        |
| 4.2      | Scans with different centers . . . . .   | 36        |
| 4.3      | Flux units . . . . .   | 36        |
| 4.4      | Effects of sky noise removal and of instabilities on extended and diffuse emission . . . | 37        |
| 4.4.1    | Faint extended sources . . . . .   | 37        |
| 4.4.2    | The effect of NIKA2 instabilities . . . . .  | 38        |
| 4.4.3    | Uniform emission . . . . .   | 38        |
| 4.5      | Noise of the final map . . . . .   | 39        |
| 4.5.1    | Noise r.m.s. across the map . . . . .  | 39        |
| 4.5.2    | Trimmed edges . . . . .  | 41        |
| 4.5.3    | Excluding the outer regions from the computation of the source map) . . . . .            | 41        |
| 4.6      | Noise of individual scans . . . . .  | 42        |
| 4.7      | Number of KIDs effectively used . . . . .  | 42        |
| 4.8      | Manually define, verify and optimize the noise r.m.s. polygon . . . . .                  | 44        |
| 4.8.1    | Produce the noise r.m.s. polygon . . . . .   | 44        |
| 4.8.2    | Verify the polygon . . . . .   | 45        |
| 4.8.3    | Optimize the polygon a posteriori . . . . .  | 45        |
| 4.9      | Scans of very different length . . . . .   | 46        |
| 4.10     | Cumulative signal and weights . . . . .  | 46        |
| 4.10.1   | Saving only the last cumulative map . . . . .  | 47        |
| 4.10.2   | Combining cumulative maps of sub-sets of data . . . . .                                  | 47        |
| 4.10.3   | Linking <code>rgw</code> and effective exposure time . . . . .                           | 48        |
| 4.10.4   | Using <code>rgs</code> and <code>rgw</code> to produce individual scan maps . . . . .    | 48        |
| 4.11     | The source map . . . . .   | 48        |
| 4.11.1   | Continuing where PIIC was stopped (during the iterative mode) . . . . .                  | 49        |
| 4.11.2   | Using a pre-defined source map . . . . .   | 49        |

|                     |   |           |
|---------------------|---|-----------|
| 4.11.3              | Produce the source map a posteriori . . . . .               | 50        |
| 4.11.4              | Enhance detections by smoothing . . . . .                   | 50        |
| 4.12                | Adding artificial sources to the timeline . . . . .         | 51        |
| 4.12.1              | Null maps (a.k.a. jackknife) . . . . .                      | 52        |
| 4.13                | Saving maps of individual scans . . . . .                   | 52        |
| 4.14                | Hit map . . . . .   | 53        |
| 4.15                | Pointing and calibration correction between scans . . . . . | 54        |
| 4.16                | Saving time . . . . .                                       | 55        |
| 4.16.1              | Reduce the read and pre-processing time . . . . .           | 56        |
| <b>5</b>            | <b>The quick look monitor</b>                               | <b>57</b> |
| 5.1                 | On the fly data reduction at the telescope . . . . .        | 57        |
| 5.2                 | Quick Look . . . . .  | 57        |
| 5.3                 | Simple use of QL . . . . .                                  | 58        |
| 5.4                 | Advanced example: use the QL on a refined list . . . . .    | 59        |
| 5.5                 | Operations and results . . . . .                            | 60        |
| 5.6                 | Products . . . . .  | 60        |
| 5.6.1               | Save FITS files . . . . .                                   | 60        |
| 5.7                 | Additional setup parameters . . . . .                       | 63        |
|                     | <b>References</b>   | <b>64</b> |
| <br><b>Appendix</b> |   |           |
| <b>A</b>            | <b>Content of PIIC NIKA2 DAFs</b>                           | <b>65</b> |
| A.1                 | CAL files . . . . .   | 66        |
| A.2                 | DRP files . . . . .   | 66        |
| A.3                 | NKFR files . . . . .  | 66        |
| A.4                 | RPP files . . . . .   | 67        |
| A.5                 | TAU files . . . . .   | 68        |
| <b>B</b>            | <b>Effects of re-gridding</b>                               | <b>69</b> |
| <b>C</b>            | <b>Transfer function examples and challenges</b>            | <b>71</b> |
| C.1                 | List of term and acronyms used in this Appendix . . . . .   | 71        |
| C.2                 | Point-like sources transfer function . . . . .              | 72        |
| C.2.1               | Recovered point-like sources flux . . . . .                 | 73        |
| C.2.2               | Noise properties of Null Map <i>vs.</i> Final Map . . . . . | 73        |
| C.2.3               | The effect of changing baseline fitting order . . . . .     | 74        |
| C.2.4               | The ideal case of simulated pure Gaussian noise . . . . .   | 76        |
| C.3                 | Extended sources transfer function . . . . .                | 76        |
| C.3.1               | Properties of the input artificial map . . . . .            | 79        |
| C.3.2               | The effect of the zeroing radius . . . . .                  | 80        |

|          |   |           |
|----------|---|-----------|
| C.3.3    | Re-shuffling the list of scans . . . . .                  | 82        |
| C.3.4    | Caveats, warnings and null maps . . . . .                 | 82        |
| C.3.5    | Instabilities induced by the scanning direction . . . . . | 84        |
| <b>D</b> | <b>History of PIIC releases</b>                           | <b>87</b> |

# Chapter 1

## Welcome to PIIC!

The *Pointing and Imaging In Continuum* software is developed by Robert Zylka at IRAM. It is the extension of the MOPSIC data reduction software (for MAMBO) to the case of NIKA2 data. It consists of two main components: the so-called *Quick Look monitor* (briefly known also as QL); and the data reduction *pipeline* aimed at producing science-graded products.

The core of PIIC is written in Fortran-90 and defines the commands to be used for the data reduction and analysis. The data reduction is carried out by scripts that combine the core commands to perform all operations on the data. Plotting is also included in the main scripts and calls GREG/SIC functions, which are part of the GILDAS distribution.

This tutorial is a brief hand-in-hand guide to accompany the users through PIIC operations. **For support, questions, doubts, suggestions, please do not hesitate to contact us, by writing to [piic@iram.fr](mailto:piic@iram.fr).**

### 1.1 Acknowledging and citing PIIC

If you are using PIIC for the reduction and analysis of NIKA2 (or other) data, please acknowledge the efforts of the developer by adding a note in your related publications and citing the PIIC seminal paper.

Please include in your acknowledgements the sentence: *The NIKA2 data were processed using the Pointing and Imaging In Continuum (PIIC) software, developed by Robert Zylka at the Institut de Radioastronomie Millimetrique (IRAM) and distributed by IRAM via the GILDAS pages. PIIC is the extension of the MOPSIC data reduction software to the case of NIKA2 data.*

Please be also so kind to cite the Zylka (2013) seminal paper<sup>1</sup> in your publication. Thank you.

---

<sup>1</sup><https://ui.adsabs.harvard.edu/abs/2013ascl.soft03011Z/abstract>

## 1.2 This release

The first release of PIIC was on October 2019. The software is distributed via the GILDAS pages<sup>2</sup>. It consists of a tarball file containing the main components of PIIC, an archive of the calibration files (regularly updated), a Read-Me file, and this tutorial. To install PIIC, simply follow the instructions found in the Read-Me file.

A history of PIIC releases is provided in Appendix D.

## 1.3 The PIIC calibration files

The PIIC calibration database (called DAFs) contains five different main types of files: calibration files (CAL), defining the response of KIDs (*kinetic inductance detectors*) for flux calibration; deleted receiver pixels (DRP) files, listing those KIDs that are known to be defective; frequency files (NKFR), listing the natural resonance frequencies of all KIDs, for different sweeps<sup>3</sup>; receiver pixels parameters (RPP), listing the position of each KID in the field of view of NIKA2, for different sweeps; atmospheric conditions over all observing runs (TAU files), containing the values of the atmospheric opacity,  $\tau$ , produced by the Observatory's tau-meter. Appendix A describes the content of the DAFs files.

After each observing pool, the PIIC support team processes calibration data and produces new calibration files. The DAFs database is thus updated and a new version is available online. This process might take some time, therefore there is a natural delay between science observations during a pool and the release of the related DAFs. The DAFs directory includes a PDF document that summarizes the properties of the available DAFs for each science pool, including calibration uncertainties.

At the moment, DAFs cover the period from October 2017 until March 2021. This means that DAFs for all NIKA2 science pools so far have been produced and are released. There is no plan to produce DAFs for non-science weeks carried out before October 2017.

## 1.4 Setting up PIIC

Install PIIC following the instructions provided in the release Read-Me file. PIIC does not need GILDAS to be installed first. See the PIIC installations notes for instructions on how to avoid conflicts with pre-existing GILDAS installations on your computing machine. The PIIC installation directory contains the following sub-directories:

```
dafs/  
doc/  
etc/  
pro/  
x86_64-generic/
```

where `dafs/` contains the calibration files; `doc/` includes the PIIC online documentation files; `pro/` is the repository of all PIIC scripts; and `x86_64-generic/` is the actual code installation folder.

---

<sup>2</sup>[www.iram.fr/~gildas/dist/index.html](http://www.iram.fr/~gildas/dist/index.html)

<sup>3</sup>a *sweep* is practically a re-definition of KIDs resonance frequencies, performed regularly for each new season.



## 1.5 Starting PIIC

Once the necessary environmental variables are set (see the INSTALL instructions file), start PIIC by simply typing `piic`. The PIIC prompt will look like this:

```
PIIC>
```

### 1.5.1 The graphic interface

Plots, diagrams and image displays are visualised on a graphical window, following the GILDAS' syntax. The QL and the science pipeline open the graphical device automatically. If other operations need to be performed — without running the QL or pipeline — the user needs to explicitly open the graphic device. This can be done either after starting the software, i.e. from the PIIC prompt, or at the start itself. Three graphical examples follow.

In the PIIC prompt type either

```
dev i
dev i b
dev none
```

or while starting PIIC type:

```
piic dev i
piic dev i b
piic dev none
```

An “i” device is a (possibly interactive) graphical window with white background; if the user likes a black background better, the chose “i b”; finally, if no device is wished, then use the option “none”.

If PIIC is operated remotely — e.g. with a low-speed net — or if the user is experienced enough to trust all operations without the need for visual inspection, or if a huge workload is foreseen and the user would like to avoid slowing down the processes by displaying many diagrams, then `dev none` could be the option of choice.

It is very important to note that `dev none` is *different* from not specifying any device. If the given PIIC script plots diagrams, it will stop in case no device is specified. On the other hand it will redirect the plot to the `none` device if specified as such, thus proceeding with script operations without stopping but also avoiding slow downs due to displaying graphics.

### 1.5.2 Using external commands

Just as in GILDAS, to use an external command (e.g. shell) from PIIC, simply type the name of the command, preceded by the “\$” sign, e.g. `$ls`.

# Chapter 2

## Blind use of the PIIC science pipeline

Performing data reduction with PIIC is simple. It consists of simply editing a template script, setting it properly for the given dataset, and running it. This short Chapter is a description of typical setups for common types of targets, dedicated to those users who do not want to enter much in the details of PIIC setups. A more detailed description of operations can still be found in Chapter 3.

If this is your case — after preparing PIIC and its environment as described in Section 3.2 — edit the template script as described in this Section.

We start, however, with a very important warning about the setup and optimization of the observing strategy (Sect. 2.1). **Do not omit to read it!** The outcome of data processing depends also on the adopted observing setup.

### 2.1 Important warning

As a general rule for multi-beam, sub-mm continuum mapping observation, the size of maps along the scan direction, shall be at least:

$$\text{NIKA2 FoV} + 2 \times \text{NIKA2 beam width} + \text{source size (above the noise)} \quad (2.1)$$

plus an additional term accounting for the NIKA2 instability triggered by the 30m telescope tracking behaviour (see, e.g., the IRAM/NIKA2 call for proposals). Note that it is assumed that the source is centered in the map. If not, the map size should be increased by the value of the offsets from the center.

Using this formula ensures that the correction of data instabilities (intrinsic to NIKA2 or induced by the chosen mapping strategy) is optimized. If this condition is not fulfilled, the results might become unpredictable, because some crucial processing steps cannot be performed properly. The header of the template scripts includes some additional comments about this topic.

#### 2.1.1 Note about scan speed

The map size is not the only parameter defining the scan strategy. The choice of the scan speed plays also an important role in optimizing the results. A high scan speed lowers the  $1/f$  noise and allows

to approach the stability timescale of the instrument. On the other hand, it can also induce other instabilities of the system (e.g. enhanced shaking when changing direction, magnetic fields produced by the motors, acoustic noise, etc.).

For setting up the optical observing strategy for your project, please refer to the technical description of observations on the IRAM/NIKA2 Spanish web pages<sup>1</sup> and to the documentation accompanying the call for proposals.

## 2.2 Weak compact sources

Targets are considered *compact* if their radius is  $< 2.5$  times the half power beam width (HPBW) of NIKA2/30m. In this case, use the template script with its default settings (simply change filenames).

## 2.3 Strong compact sources

If the target is a bright source, expected to be detected at  $S/N > 10$ , and visible on individual scans, use the template script with its default settings, switching the `weakSou` option from *yes* to *no*.

## 2.4 Deep fields

If the target is a *deep* (blank) *field*, potentially including several weak sources, edit the template scripts such that:

```
let souRmxAS 0
let souRmnAS 0
let blOrderOrig 3
let deepField yes
let nIterSource 5
```

Don't omit to read Sections 3.4.5 and 4.8 about the r.m.s. polygon.

## 2.5 Sunyaev-Zeldovich clusters

This is a special case of weak, extended sources, with moderate size. Keep the default setup, but re-define the source a priori using the available knowledge about the target: its expected position and size (see Sect. 3.2.4).

If using the iterative mode, in order to detect the negative signal, switch the `souSign` parameter to “-”. If both positive and negative signals are present (e.g. both the SZ cluster and foreground/background/lensed galaxies are in the field), set `souSign` to “+-”.

Finally, take a look to Section 4.11.4 that describes how to use the “source map smoothing”: important in the case of SZ targets.

---

<sup>1</sup><https://publicwiki.iram.es/Continuum/PoolPreparation>

## 2.6 Complex sources

By these, are meant extended objects with complex geometries, possibly including diffuse emission. Adopt the iterative mode, and do not use any a priori definition of the source. For a first, quick data processing, edit the template script changing the default settings of the following parameters:

```
let souRmxAS 0
let souRmnAS 0
let nIterSource 10 ! for example
```

Note that — at odds with the deep fields case — now `blOrderOrig=3` and `deepField=no`.

If the dataset consists of scans of very different lengths (e.g. in different directions), please read Sect. 4.9. Moreover, Sect. 3.2.11 gives indications about advanced sky noise evaluation for this case.

# Chapter 3

## The science data-reduction pipeline

NIKA2 observations are carried out with a raster-scan scheme. The field of view is moved on the sky, scanning a region centered on the target, and covering an area around it large enough to allow for a proper characterization of sky noise and instrumental effects.

The main issues to deal with, when reducing science maps, are instabilities, both due to the KIDs behaviour itself and due to changes in elevation when scanning in directions other than azimuthal.

The science data reduction consists of a combination of PIIC commands and GREG/SIC (GILDAS) macros. The combination of the two performs all needed operations and produces several diagnostic diagrams.

The data reduction of a science data set is carried out using a single PIIC script, which calls all needed procedures.

### 3.1 Principles and challenges of NIKA2 science data reduction

NIKA2 data include the signal of the sources, of the sky, of the system telescope+instrument and noise. Sky signal and its low-frequency noise, as well as instrumental instabilities, should be removed as much as possible before transforming the NIKA2 data into a science-quality product.

The essential steps are: flat field correction, correlation correction, sky subtraction, baseline subtraction, calibration, geometry association (given by the known RPPs), re-gridding on the final map. During these operations, particular care should be taken in properly dealing with the emission of the sources, in order to preserve it.

The sky signal and its variations are monitored and measured during the time-line of each KID (also known as receiver pixel, RP). The correlation of each KID to all others is studied and only the best correlating KIDs are used to compute the correlated noise to be subtracted from each timeline.

When performing these measurements, the records of those KIDs observing sources at the given time need to be excluded, in order to avoid compromising the measurement of the sky and instrumental properties. This is done by defining the sky area covered by sources (either as an ellipse or a polygon, see Sects. 3.2.3 and 3.2.4).

If the position, size and shape of the sources is known, and the size is smaller than the NIKA2 field of view (FoV), then it is possible to define the area to be avoided in the sky. If not, it is possible to

let PIIC define it on the basis of the signal to noise (S/N) ratio in the final map, during the iterative process. Similarly, a pre-defined source will be improved on the basis of S/N.

*The data reduction procedure is an iterative (and interactive) process.* At each iteration, all data reduction operations are repeated, using the improved source definition. To compute the S/N ratio, the weight map produced at the previous iteration is rescaled into a noise map, by simply measuring the r.m.s. of the signal map within a source-free polygon defined by the user. Thus the S/N ratio is computed for each pixel, and pixels about a certain S/N threshold are identified. In this way a *source map* is built and is subtracted from the data timeline at the next cycle of the loop.

The standard procedure can be thus summarized in two broad main steps:

1. in the so called *0-th iteration*, PIIC performs all operations using the definition of source given by the user (see Section 3.2.4). This can be either an ellipse, a polygon or no a-priori definition of the source. The sky area covered by the source is excluded from the computation of baselines to be subtracted from the data.
2. in the subsequent *iterative mode*, PIIC loops  $N$  times and performs again the data reduction, improving the source definition on the basis of a S/N ratio thresholding method.

Between these two main steps, it is possible to use the results of the 0-th iteration to improve and optimize the setup of PIIC (e.g. the source definition itself), before proceeding to the proper iterative mode.

## 3.2 Setup

Before running PIIC, we need to prepare the necessary files and environment:

- the directory and sub-directories tree in which PIIC will work;
- the list of scans to be processed (and combined together);
- the template data reduction script, that will be modified and renamed, depending on your needs, taste and on the type of data to be dealt with;
- the definition of the source on the sky (if needed), also included in the data reduction script;
- a polygon defining a source-free region of sky, to be used for the computation of the noise r.m.s.

### 3.2.1 The directory tree

First of all, let's set up the working directory where PIIC will be used. For example, create the directory `my_data_red_with_piic/`. Similarly to the QL case, PIIC needs a whole directory tree to work properly. Prepare it in the following way:

```
cd
mkdir my_data_red_with_piic
cd my_data_red_with_piic/
```

```
mkdir png red stat
ln -s directory_containing_data imbfitsDir
```

The list of scans needs to be produced only once, for each array, unless scans filenames or number change.

Note that the data files in the data directory are *not* modified by the PIIC data reduction, nor is anything going to be written in the data directory.

### 3.2.2 The list of scans

The list of scans is an ascii file containing the names of the IMBFITS files belonging to the dataset of interest. It can be produced with any tool. Here an example is given to use PIIC to produce the list of all array-2 scans belonging to observations of an *hypothetical* source called “Superantennae”:

```
cd
cd ql
cd imbfitsDir
ls iram-30m*-2-* > ~/ql/all_ar2.LIST      ! lists all Ar2 IMBFITS files
cd ..

piic

indir imbfitsDir          ! define the input directory
inlis all_ar2              ! load the list
sel type m                 ! select scans with observation type = map
find obje /wri             ! find the names of all objects that were
                           ! observed with scans in the list
                           ! and writes one list of scans per objects
sel obje SUPERANTENNAE    ! selects only scans of object SUPERANTENNAE
write inlist SUPERANTENNAE_a2.LIST ! write the list of selected scans on file
init inlist                ! if needed, resets the starting list (in memory)
                           ! the user will need to start from scratch,
                           ! if they wish to produce a new list
```

In this way, one ascii list has been produced for array 2 containing the names of all Superantennae IMBFITS files to be processed.

If the data IMBFITS files are all stored in the same directory, then the list can include only filenames, and the `imbfitsDir` symbolic link points directly to that directory. If, instead, the data are spread over several directories, the `imbfitsDir` points to the parent directory common to all of them and the list includes paths (starting from the common parent directory). In this case, in order to comply to Fortran’s conventions, path+filenames need to be written in double quotes: “path/imbf\_filename.fits”.

The filename of the list is to be inserted in the data reduction script (see Sect. 3.2.3). By default, it is “yourSource\_a”’nikaBand’.LIST. In the above example, for the target called “Superantennae” and array 2, the default name is therefore `Superantennae_a2.LIST`.

*Very importantly*, the data belonging to each array need a different list of IMBFITS data files. In fact, remember that the data of each scan are stored into three separate IMBFITS files, each belonging to one single NIKA2 array.

If the user would like to process 1.3 mm data all together, i.e. would like to combine array-1 and array-3 data together, then the list shall be labelled **a13** and shall include both array 1 and 3 scans filenames. This means that the length of the arrays 1+3 IMBFITS list must be double the one of array 1 *or* 2 *or* 3 individual lists.

### 3.2.3 The template script

PIIC comes with a template script for science data reduction. It is found in the **pro/** folder under the installation directory and it is called **mapTP\_a2\_wc\_template.piic**. This template script needs to be edited and optimized for the given science case and the give kind of observations (target type, map size, scan strategy, etc).

This and the following Sections describe the key parameters of the script and give some guidelines for choosing their optimal values. The users are encouraged to test different configurations and design the best setup for their project.

This script assumes that all the needed calibration files have been already produced and are in place in the PIIC **dafs/** database.

Figure 3.1 shows an example of template script, as found in the **pro/** folder and with an additional custom commands section.

As mentioned, the template script includes several parameters that can be optimized depending on goal and on type of data/targets. Nevertheless, the default values of most parameters are already a valuable start for almost any kind of data set and it is worth to perform a first test run leaving most of them unchanged.

The most critical parameters, to which the user should take special care are:

- **inList, inDir, ...**: basic filenames;
- **souRmxAs, souRmnAs, souPA, souRAoffAS souDECoffAS**: size, position angle and possible offset of an elliptical source, to be used during the 0-th iteration to exclude the area covered by the source(s), during baseline computation;
- **polSeq**: in alternative to an elliptical source, it is possible to define a polygon that describes the source, stored in a separate ascii file;
- **blOrderOrig**: order of baseline correction (i.e. of the polynomial fit to the baseline) over individual subscans;
- **deepField**: flag that indicates if we're dealing with "deepfield" observations;
- **nIterSource**: the number of iterations to be performed;
- **maskLevel**: the S/N threshold to be used in iterative masking;



```

mapTP_a2_wc_template.piic v
!
! Written by Robert W. Zylka, zylka@iram.fr
! created 02.10.2016, version 15.09.2021
!
! usage: @scriptName (.piic is the default extension)
!
! Pipeline to reduce maps of sources with sizeAboveTheNoise <FoVdiameter-2*HPBW in the scanning direction,
! i.e. souRmxAS<recArRmxAS-HPBW;
! the usable max. radius of the FoV (Receiver Array R max., recArRmxAS) for NIKAA2 is <180arcsec.
! It is assumed that the source is centered, i.e. appears at (0,0) in (R.A.,DEC); if not the map size
! in the scanning direction has to be increased by the offset values.
! Contrary to MAMBO2, for NIKAA2 data the cascade Correlated Signal Filter (CSF) cannot be used, therefore
! for data of sources which do not satisfy the above condition the source distribution has to be supplied
! with sbSource (single beam source) or - if the S/N>snrLevel - the iterative mode has to be used (nIterSource>4).
! Depending on NIKAA2 instabilities and source structure the best in the iterative mode might be to put
! the source size to 0, i.e. souRmxAS=souRmnAS=0. However, with this setting smooth extended emission
! below the chosen limit of S/N will not be recovered (see the appendix "Transfer Function" in the tutorial).
! If the maps in the scanning direction are shorter than 2*(souRmxAS+recArRmxAS+HPBW+scanVelocity, scanVelocity
! in arcsec/s) some crucial processing steps cannot be performed. As a consequence, due to inevitable data
! instabilities (intrinsic to NIKAA2 or induced by the chosen mapping strategy), the results in such cases
! will be questionable. The only way to make the results a bit more reliable is to set blOrderOrig to <3
! and minimize the size of the BASE RANGE (polygon polBReq or brRmxAS, brRmnAS).
! Important: due to NIKAA2 instabilities & very low integration time, at map edges appear S/N spikes.
! To avoid their propagation while iterating towards map centre, either polZmEq or rZmEq should be used.
! Defaults are set for A2 and weak (sigMax<5*rms0fNIKA2pixel) and compact (souRmxAS<2.5*HPBW) sources.
! <rms0fNIKA2pixel> is roughly ~33mJy/23.8Hz for a2, ~110mJy/23.8Hz for a1 and ~87mJy/23.8Hz for a3
!
dev none          ! see help g\device, if display required e.g. dev i b
@ mapTPdefs
let nikaBand "2"   ! process NIKAA2 A2 data, 1=A1, 3=A3, 13=A1+A3; other names not accepted
!----- loading the list of observations and selecting -----
init inList
init outList
inDir imbfitsDir
outDir red
inList "yourSource_a" 'nikaBand' ! e.g. Superantennae_a2
select type m                    ! only maps
sort inList
list
!----- parameter setting -----
let weakSou yes      ! signal > 5*rms0fNIKA2pixel masked after sky noise subtraction, no check if set to no
let deepField no     ! yes for e.g. G00DSNorth, COSMOS, HDF, DeepField1, ...
let souSign "+"      ! "-" if source with negative signal, e.g. SZ; "+" if positive and negative sources
let polSeq " "       ! polygon in EQ system defining the source border
if polSeq.eq. " " then
  if deepField then
    let souRmxAS 0
    let souRmnAS 0
  else
    if nikaBand.eq."2" then
      let souRmxAS 40 ! [arcsec] max. source semi-diameter above the noise
      let souRmnAS 40 ! [arcsec] min. source semi-diameter above the noise
    else
      let souRmxAS 30
      let souRmnAS 30
    end if
  end if
  let souPA 0.0      ! [deg] source position angle in EQ system
end if
let posSeq " "       ! [H M S D AM AS] centre of the final (R.A.,DEC) map and of polSeq
! necessary only if individual maps have different centres
let eqExtraS 0.0     ! [arcsec] half map extent in EQ, 0 to calculate it (if all maps have the same centre)
let souRAoffAS 0.0   ! [arcsec] R.A. offset of the source relative to posSeq
let souDECoffAS 0.0  ! [arcsec] DEC offset of the source relative to posSeq
let blOrderOrig 2    ! order of instability corrections in subscans, >2 might be better
let nIterSource 0    ! number of iterations
if nIterSource.ge.1 then
  let rZmEq 0.0      ! if >0 outside of this radius the data in the iterative source are neglected (set to 0)
  let polZmEq " "    ! outside of this polygon the data in the iterative source are neglected (set to 0)
end if
@ mapTPfurtherSets
pause main
!----- Ste's custom parameters -----
let nrPause 0        ! =1: pause after processing each map; =2: after "plot"; ...
!----- Run it! -----
@ mapTPrun
exit

```

Figure 3.1: Example of data reduction script: default template plus few custom parameters.

In order to better understand the meaning of these parameters, a very brief introduction to the main operations performed during the PIIC NIKA2 data reduction is needed. A brief overview was given in Sect. 3.1. More details are given in Section 3.3. Additional, important parameters are described in Sect. 3.2.9.

### 3.2.4 Define your source

During the data reduction, sources need to be excluded from baseline computation and subtraction for two reasons: 1) avoid the sources in the computation of sky (noise) removal; 2) do not cross the sources while performing the baseline subtraction (which would alter the flux and the profile of the sources). The *iterative* mode automatically accounts for this.

At best, the data would have already been gone through the QL (see Chapter 5), so to have a first initial guess of where the source lies, in order to be able to have a first guess of the region of sky it covers. Note, however, that the QL does not combine maps together, hence if the source is faint, it won't be seen in the QL results yet.

A source can be defined as a circular/elliptical or a polygonal shape. Such source area is defined on the final map, i.e. on sky coordinates, using GILDAS/PIIC conventions: the (0,0) point is at the center of the map; units are [arcsec]<sup>1</sup>; x-axis values increase to the left and y-axis values increasing towards the top, i.e. as in a RA-Dec map with East to the left and North up. The position angle is defined starting from the y-axis, in the counter-clockwise direction. Figure 3.2 depicts these conventions.

When only a simple source is present in the maps, a simple circular/elliptical patch covering it all could be the easy and correct way to proceed. The parameters `souRmxAs` and `souRmnAs` define the major and minor axis of an ellipse defining the source on sky, in arcseconds. The position angle of the major axis, with respect to the vertical axis of the image (North in Equatorial coordinates) is given by `souPA`.

If the parameters `souRmxAs` and `souRmnAs` are set to 0.0, then simply no source patch is defined, nor used to exclude sky areas. This option is used, for example, when adopting the iterative mode with no initial source guess.

For a proper use of elliptical source patches, the `deepfield` needs to be set to “no” (see Sect. 3.2.7).

Although conceptually very simple, defining the source correctly might not be always trivial. Such an ellipse should not be too big, in order to leave enough KIDs for a proper computation of sky noise. This means that the ellipse should certainly be smaller than the array size. Note that — however — this simple precaution might not be enough to produce a reliable science-quality final map, e.g. if the final map is small or if the sky conditions were particularly unstable, or if KIDs were not well tuned. It is therefore recommended to experiment with different ellipse sizes and geometries, if the results look doubtful.

A sub-optimal definition of the source patch can generate spurious features in the final map. It can produce “fake” sources, both positive and negative. If a negative spurious signal is produced (e.g. a negative lobe), and if the iterative method is used, then the adaptive protection of positive sources

---

<sup>1</sup>Note that some GILDAS component have [radians] units default. Therefore it is recommended to use the `polygon` command within PIIC.

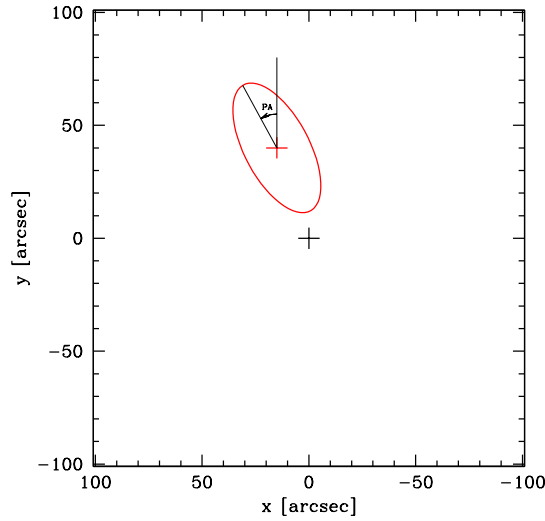


Figure 3.2: Scheme of GILDAS graphical conventions. The pixels coordinates origin (0,0) is at the center. Coordinates are defined in units of [arcsec] as in Equatorial coordinates (North is up, East is to the left). Position angles are defined starting from the y-axis, in the counter-clockwise direction. In this example, an ellipse centered at (15,40), with major and minor semi-axes equal to 15 and 32 [arcsec], and position angle of 30 degrees was defined.

based on the S/N ratio can gradually make it disappear. On the contrary, a positive spurious signal is detected by the iterative process and recognized as a source. Hence it is much more difficult to identify a positive spurious signal. If a positive spurious signal is produced by a improper source definition, then it will persist on the final map, no matter how many iterations are employed. Finally note, that even negative spurious sources can survive the iterative process and can end up on the final product.

The overall message here is that — although conceptually simple — defining the source area to be excluded from computations is a delicate process and its complex consequences should not be underestimated.

A typical data reduction performs the 0-th iteration using a first-guess ellipse, for then verifying on the product map if the initial choice was properly designed or if it needs to be modified, optimised, or turned into a polygon. With an improved source definition, the reduction proceeds either directly in the iterative mode, or repeating the 0-th step.

Keep in mind that — for example — a 10-iterations process on a typical (small-ish) map of a Galactic cloud (SF region) can take approximately 24h to process. Hence it is better to spend some more time defining the source region and optimize it, rather than finding out later that it was not correctly defined and thus wasting a 24h time.

### Offsetting the source patch

In some specific cases, it might be necessary to apply an offset to the ellipse that defines the source. An offset might also be relevant for a polygonal region, but one could imagine that polygons are

defined directly at the position of the source.

The parameters that define the offset of the ellipse with respect to the center of the final map are called `souRAoffAS` and `souDECoffAS`. If all maps are centered at the same coordinates (i.e. all scans were observed using the same scan center), then defining `souRAoffAS` and `souDECoffAS` is sufficient.

On the contrary, if the scans to be combined have different scan centers, then PIIC does not know a priori where the final map will be centered, and the central coordinates of the final map must be given manually defining the parameter `posSeq` (in Equatorial coordinates). In this case, the offsets are computed with respect to the position given by `posSeq` itself.

Summarizing, six parameters need to be used in order to entirely define the size, shape and position of the elliptical source patch:

```
souRmxAS      ! size of major half-axis in arcsec
souRmnAS      ! size of minor half-axis in arcsec else
souPA         ! source position angle on sky, in degrees (equatorial conventions)
posSeq        ! equatorial coordinates of the center of the final image,
               ! in the format "H M S D AM AS"
souRAoffAS    ! R.A. offset of the source relative to posSeq (in arcsec)
souDECoffAS   ! Dec  offset of the source relative to posSeq (in arcsec)
```

## Polygonal source definition

A polygonal source definition follows the same principle as the ellipse, but is defined ad-hoc to cover sources with irregular or complex shapes. It can be easily defined using the GILDAS command `polygon`. The polygon needs to be written in an ascii file, listing in two columns the coordinates (x,y) of each vertex of the polygon.

Importantly, the vertices sequence must be clockwise or counterclockwise, but not mixed. This means that one should not mix the vertices, neither make intersections while defining the polygon, because otherwise its “inside” and “outside” region might get inverted (see GILDAS tutorials<sup>2</sup>).

Remember that, if multiple objects are present, it is necessary to define a single polygon covering them all. This can make intersections difficult to avoid if the geometry is very complex. All we need is just a little patience.

Finally, also for a proper use of polygonal source patches, the `deepfield` needs to be set to “no” (see Sect. 3.2.7).

The filename of the polygonal source definition is given in input as parameter `polMeq`. This is to be found in the script `mapTPfurtherSets.piic` (see Sect. 3.2.9).

### 3.2.5 Specific cases

The details and tuning of the data reduction procedure depend on the kind of sources one is dealing with. This is particularly true when it comes to properly define source areas.

---

<sup>2</sup>Note that some GILDAS components adopt [radians] units, while PIIC uses [arcsec]]. Therefore use the `polygon` command from within PIIC.

Simple sources, i.e. with simple and compact geometry are easy to deal with. A typical example is one single point-like source or a small extended source. In this case, a simple ellipse covering the target is sufficient.

More complex objects (e.g. extended sources still smaller than the FoV of NIKA2) are more difficult, but can still be dealt with without problems. A polygon defining an extended source smaller than the FoV of NIKA2 can be built with success.

Note that the polygon or ellipse must be smaller than the FoV of NIKA2 and should allow some pixels to be kept, in order to allow a proper computation of sky noise. The FoV of NIKA2 has a radius of  $\sim 200$  [arcsec]. Hence the source “mask” should be in general  $\ll 200$  [arcsec] in radius and undoubtedly not larger than 180 [arcsec] in radius (which anyway is already very big).

See Sect. 4.4 for a description of the effect of sky noise removal on extended sources and diffuse emission.

### Faint sources or blank-field case

In the case of a blank field, several faint sources are present on the final map, but one does not necessarily know a priori where they are. At the moment a multi-ellipse definition of several source is not implemented in PIIC and, in order to manually exclude all sources from the baselines computation, one should define a very complicated polygon covering all (mostly point-like) sources.

The straightforward PIIC approach is to adopt the iterative method, using no source patch at all during the 0-th iteration. In order to do this, simply set the sizes of the ellipse `souRmxAs` and `souRmnAs` to 0.0 [arcsec].

An unintended advantage of this choice is that — with no source defined on sky — PIIC avoids to transform back and forth from sky coordinates to Nasmyth and FoV coordinates the source patch, thus sparing a lot of spherical trigonometry computations and speeding up the 0-th iteration.

### Very large objects

Very large, extended objects, larger than the NIKA2 field of view are an interesting, complicated case.

In such case, the diffuse emission extended over an area larger than the NIKA2 FoV is suppressed by definition, during sky noise subtraction (see also Sect. 4.4). Only the small, more compact structures (e.g. cores and filaments embedded in a big Galactic cloud) make it to the final map.

The small structures can be treated similarly to faint sources in a deep field (see Sect. 3.2.7), i.e. simply letting PIIC to identify them on the basis of the S/N ratio on the final map. The easiest approach is therefore to adopt the iterative processing, with no a priori source definition. In this way, the flux of these structures is preserved and is not affected by filtering/baseline suppression. On the other hand, obviously no measurement of diffuse emission is possible with this approach.

### Negative signals

Compton scattering of CMB (Cosmic Microwave background) photons by free electrons in the plasma of galaxy clusters produce the well known Сюняев - Зельдович effect (SZ). The NIKA2 bands are

designed such that the signal in the 1.3 mm band is roughly neutral and the 2 mm band detects the negative distortion of the CMB due to the SZ effect.

In order to detect negative signals, switch the `souSign` parameter to “-”. If both positive and negative signals are present (e.g. both the SZ cluster and foreground/background/lensed galaxies are in the field), set `souSign` to “+-”.

Being faint and extended, the S/N thresholding is likely to miss part of the SZ source. It might therefore be needed to defined an elliptical patch covering it. Although this might seem the easiest kind of targets to deal with, the combination of instabilities, small map sizes and the choice of the ellipse and other PIIC parameters can cause the production of spurious (negative/positive) signal, depending on the adopted settings (see Sects. 2.1 and 3.2.4, for example). Some experimentation might be needed in order o produce the best final product. Good luck!

### 3.2.6 Order of baseline correction

By default, the order of the baseline correction over single sub-scans (`blOrderOrig`) is 2. This should not be confused with `btOrder`, the order of baseline correction over the whole timeline, which is set equal to 1 and should not be modified.

It is surely possible to experiment with larger values of `blOrderOrig`, but keep in mind that enough KIDs should be available to evaluate higher-order polynomials.

Note also that a higher order baseline fitting risks: *a)* to diverge at the edges; *b)* to fit not-perfectly “masked” sources or sky variations or other smooth, faint features, and thus might easily produce spurious signals; *c)* to remove real features of sources.

Vice versa, under particular conditions (e.g. small maps) a lower value of `blOrderOrig` might give better results.

If the map is produced with scans of very different lengths (e.g. in different directions), please read Sect. 4.9.

### 3.2.7 Deep field and weak source options

In case of blank fields or very faint, point-like, sources, it is useful to switch the `deepField` parameter on. This activates the `weakSou` option, which tells PIIC that we are in presence of faint sources, i.e. sources that potentially are below the  $5\sigma$  level.

When this option is active, the elliptical source definition is ignored and baselines are computed over the whole area, sources included. Therefore, for a proper use of elliptical source patches, the `deepField` option has to be switched off.

Finally, note that the `weakSou` option can be activated independently of the `deepField` parameter.

### 3.2.8 Measuring the noise r.m.s.

During the iterative process, source pixels are identified based on a S/N ratio threshold on the final map. PIIC does not produce noise maps explicitly, but it provides weight maps. A noise map can be produced by simply rescaling the weight map to the r.m.s. value of the final signal map (see Sect.

3.4.3). This implies that the r.m.s. should be measured in order to determine the S/N of each pixel of the final map and apply the thresholding on the iterative mode.

The r.m.s. of the signal map should be obviously measured in a region where no sources are present. By default, PIIC define automatically a polygon in an empty region of the map, in which the noise r.m.s. is measured (see Sect. 3.4.5). Alternatively, this polygon can also be defined manually by the user (see Sect. 4.8).

### 3.2.9 Additional parameters

The main data reduction script calls the script `mapTPfurtherSets.piic`, that defines additional parameters.

If users feel like modifying this file, for example to switch some special features on or to fine-tune some expert-mode parameters, they can proceed in two ways. They can simply re-define the “further sets” parameters in the main (template). script, after the call to the `mapTPfurtherSets.piic` macro, or they can make a copy of the `mapTPfurtherSets.piic` script in the working directory and edit it there. In fact, PIIC finds its scripts and components in the `pro/` folder in the installation directory but — following GILDAS’ conventions — equivalent scripts, with the same name, found in the working directory have priority.

#### 3.2.10 Correlating pixels

By default the number of best correlating KIDs to be used when subtracting sky noise is `nBest=16`. One can experiment using more (e.g. 32, 64, ...) to see if the end products of the data reduction show a better source recovery. This parameter is defined in the “further sets” macro.

#### 3.2.11 Correlating pixels: the case of extended sources

As said, `nBest` is the number of KIDs used to calculate the approximation of sky noise. This can be computed as an average or a median over the `nBest` KIDs.

In the case of a median, point-like (or compact) objects are naturally rejected, because its signal is larger. If the source is extended, there is a chance that a subset  $n$  of the `nBest` KIDs is off-source. Two cases are possible: *a)* if  $n > 50\%$  then the source is successfully removed using the median; *b)* if  $n \leq 50\%$ , then not.

In this latter case, the parameter `nBest2` comes to help: it specifies how many KIDs with the lowest signal out of the `nBest` are to be taken to evaluate the sky noise.

*Note that a combination of `nBest` and `nBest2` is different than using a smaller value of `nBest` only. For example, `nBest=64` combined to `nBest2=16` is different than `nBest=16`!*

#### 3.2.12 Pixel size

Among the many other available parameters, let us mention the pixel size of the final map (parameter `eqPixSizeAS` in the “further sets” macro). By default, the pitch of the pixels of the final map are defined to be of 3 arcsec at 1 mm and 4 arcsec at 2 mm.

The HPBW is  $\sim 11$  arcsec at 1 mm and  $\sim 17$  arcsec at 2 mm. Therefore the chosen pixel size is more than sufficient for Nyquist sampling. A finer pixel scale is not necessary and would result into an enhanced noise.

### 3.2.13 Exclude noisy timelines/maps

PIIC checks the r.m.s. of timelines (signal as a function of time along the scan) of each KID. If such the average r.m.s. over all KIDs is above a given threshold, the entire map will be rejected from the dataset and will not be part of the final map.

In this way, scans taken in particularly unstable conditions can be discarded and will not degrade the quality of the final product.

The parameters that define these thresholds are found in the further settings script and are called:

```
let mxA1todAvRMS 250.0      ! [mJy/beam/smplRateHz], A1 map will be excluded
                             ! if the TOI mean r.m.s. of all KIDs larger than this
let mxA2todAvRMS  70.0      ! [mJy/beam/smplRateHz], A2 map will be excluded
                             ! if the TOI mean r.m.s. of all KIDs larger than this
let mxA3todAvRMS 190.0      ! [mJy/beam/smplRateHz], A3 map will be excluded
                             ! if the TOI mean r.m.s. of all KIDs larger than this
```

These limits are set according to the statistics of NIKA2 data over the past years.

If users prefer not to exclude the noisy maps, they simply have to set these three thresholds to very high values.

The lists of scans, excluded from the final maps following this and other criteria, are saved in the `stat/` directory in files with `.err` extension.

### 3.2.14 Pausing

If no problems arise the data reduction script proceeds without stopping. Nevertheless, it might be of interest to verify the operations performed on individual scans, or visualize and study the diagnostic diagrams shown on the active plotting device. It is possible to change if, when and how often the script pauses, by changing the value of the parameter `nrPause`, found in the `mapTPfurtherSets.piic` script.

By default `nrPause=0`, which means that the data processing makes no pause, if not one at the very beginning after having loaded the list of scans to be processed.

Setting `nrPause=5` implies that the data reduction script makes a pause after having completed the reduction of each individual scan. If the number of scans is large, this implies a large number of breaks. In iterative mode, the whole process is repeated `nIterSource` number of times, hence producing even a larger number of pauses, which one should then manually resume by pressing “c”.

Other possible values of `nrPause` are listed in the script.

At every pause, it is possible to change the value of the `nrPause` variable, as well as of any other variable, if needed and if the user has enough experience to do that. While the script is idling, it is also possible to perform any other operation, run other scripts, display the combined image (map),



verify if the polygon adopted for measuring the r.m.s. is positioned in a reliable, clean, well centered, etc, and/or verify that the data reduction is proceeding correctly. It also possible to re-define the polygon and use a new, better, version at the next iteration (or after pressing “c”).

If `nrPause` is set to 0 but one would like to make a pause and verify something or change the values of some parameters, it is always possible to interrupt the procedure, pressing `ctrl-c`. The script will pause at the first viable point, i.e. when the currently-running command ends, and it will be then possible to manually perform the desired operations.

It is possible to include the definition of `nrPause` in the template script. When doing so, take care to add it after the call to the `mapTPfurtherSets.piic` script (see Fig. 3.1).

### 3.2.15 Producing diagnostic diagrams and saving them as PNG figures

The pipeline produces several diagnostic diagrams and plots them on the chosen graphical interface. The user can activate or de-activate the production of different types of such diagrams, depending on their needs. Plotting takes time. In order to speed up the processing, it is suggested to switch off those plots that are not used or not interesting for the specific project. The parameters controlling which diagnostics to plot are found at the end of the `mapTPfurtherSets.piic`. The names and default values of these parameters are:

```
let plCC      yes      ! plot the Correlation Coefficient CC
let plRMS     yes      ! plot the rms in the TOD
let plRG      no       ! plot the maps of each KID
let plSig     no       ! plot the signals of each KID
let plFFc     no       ! plot the Flat Field Corrections
let plTPvar   no       ! plot the total power variations
let plNuRPs   yes      ! plot the Number of Used Receiver Pixels
```

Since the Spring 2021 release, PIIC does not save PNG diagrams by default anymore. This choice is driven by the evidence that not many users took advantage of the saved plots and by the wish to save space in the default setup of the data reduction template script.

All the diagnostic diagrams shown on the active plotting device can be saved on file by activating the *hardcopy* option. The parameter that controls it is called `hc` and is also found in the `mapTPfurtherSets.piic` script. By default its values is “no”. Turn it to “yes” to switch it on.

### 3.2.16 Overwriting

The execution of the data reduction scripts halts before overwriting already existing FITS files and polygons. The user may continue running the script by using the write command written on the prompt, adding the `/overwrite` option to it, and typing continue.

Alternatively, cleaning or backup-ing the `red/` directory before starting a new reduction can be a valuable way to avoid these interruptions.

### 3.3 Run it!

After preparing the working environment, the data reduction script and associated data files, it is now time to run the PIIC data reduction. Start PIIC in the working directory and run the script:

```
cd
cd my_data_red_with_piic/
piic dev i
```

```
@reduce_my_data_Ar1.piic
```

PIIC will load the list of scans and pause. Verify that everything is correct and continue by pressing “c” and “enter”.

The data reduction operations start and PIIC will perform in sequence the following:

1. assign sky positions to each KID; perform main-beam flat-fielding; exclude known problematic KIDs;
2. transform the KIDs signal into flux density and calibrate it to physical units [mJy/beam];
3. perform sky-noise (forward-beam) flat-fielding;
4. compute the correlation coefficient of each KID to all others; KIDs with bad correlation statistics are rejected;
5. analyse the time line of each KID and compute the r.m.s. of each KID’s signal along the timeline (excluding the source positions, if requested); the most noisy KIDs are rejected;
6. subtract sky noise, using only the **nBest** KIDs best-correlating to each KID, and ignoring those records covering the source in the sky (if defined a priori);
7. subtract baselines to remove instabilities that could not be dealt with during sky-noise subtraction;
8. apply extinction correction;
9. distribute the signal of all KIDs onto the final pixel grid, using the appropriate kernel linking the NIKA2 PSF and KIDs size to the grid;
10. after the 0-th iteration (steps 1 to 9 above), the final map pixels with S/N ratio above the requested threshold are identified and a *source map* is produced;
11. in the iterative mode, the source map is subtracted from the data timeline (after calibration) and steps 2 to 8 are repeated **nIterSource** times.

Figures 3.3 to 3.6 show an example of the main steps for array 1, during a scan on the planet Uranus.

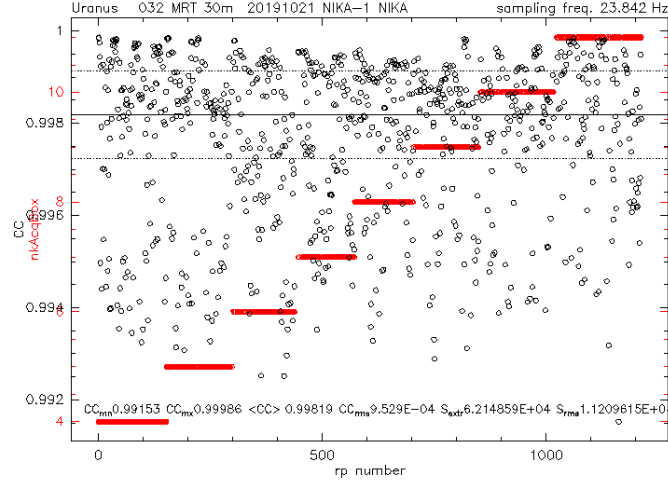


Figure 3.3: Average correlation coefficient of each receiver pixel (RP, i.e. KID) to all others, for array 1. In red are marked the RP id ranges belonging to NIKA2's 8 acquisition boxes of which array 1 consists (see also red y-axis label).

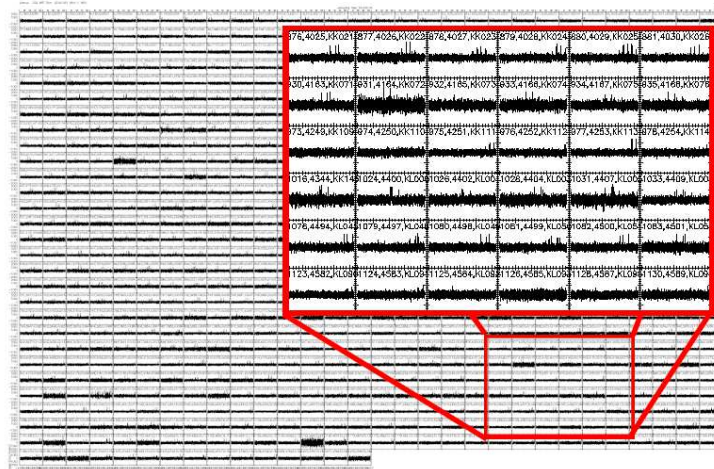


Figure 3.4: Time line of all KIDs of array 1, after the first baseline subtraction. The KIDs with the noisiest time lines are rejected (see also Fig. 3.6). The more pronounced spikes in the timelines are the bright source, crossed by the given KID at the given moment along the time line while scanning on sky.



Figure 3.5: Array-1 scan maps of each individual KID, during the Uranus observation already shown in Figs. 3.3 and 3.4. The ellipse defining the area covered by the source is depicted. Those KIDs “seeing” the source (ellipse) at the given record along the timeline are not used to compute baselines for that record.

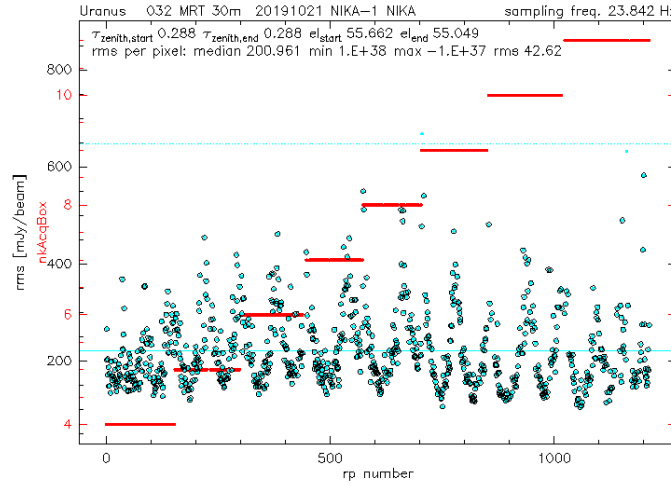


Figure 3.6: Timeline r.m.s. of all KIDs of array 1 (see also Fig. 3.4). The solid blue horizontal line marks the median value and the dot-dashed line marks a threshold set to  $n0fRPrms \times$  the r.m.s. (corresponding to  $n0fCCrms$  in Fig. 3.3). As in Fig. 3.3, in red are also marked the RP id ranges belonging to the 8 electronic boxes of array 1.

### 3.3.1 Information about re-gridding

The re-gridding strategy adopted as default by PIIC works in Fourier space. The kernel used to re-distribute the flux of each KID onto the final grid is a sinc function ( $\sin(x)/x$ ) in this space. This function is truncated at the 4th period and then weighted. Weighting involves 6 parameters, i.e. two weighing functions are used, each one having 3 parameters to be optimized. The net result is a kernel that corresponds to  $\sim 43\%$  of the HPBW.

The values of the free parameters have been optimized already in 1992. Thanks to this optimization, such regridding method reproduces the original point-like source shape to better than 1%.

The algorithm was first described by Haslam (1973) and later modified and optimized by R. Zylka, as mentioned above. Appendix B analyses the effects of re-gridding on point-like sources.

## 3.4 Quick analysis of the 0-th iteration results

After running the 0-th iteration, it is advisable to quickly verify that the initial assumptions were commensurate to the target and the dataset, and if necessary modify them.

The maps produced by PIIC are stored in the `red/` directory. Here follow some examples of basic operations that can be performed on these maps.

PIIC produces three FITS files at each iteration: 1) the signal map; 2) the corresponding weights map; 3) the source map, based on S/N, to be used during the next iteration, in combination with the source (ellipse or polygon) defined at the beginning. Typical filenames are:

- 1) `Uranus_a1_..._0.fits`
- 2) `Uranus_a1_..._0rgw.fits`
- 3) `Uranus_a1_..._0f1.fits`

The three dots omit part of the filenames; their content reflects the setup chosen in the data reduction script, i.e. the labels and numbers found in the filenames are basically the values of some of the key parameters of the data reduction.

As for the source map, the label `0f1` indicates that it was produced at the 0-th iteration and will be used in the 1st iteration to protect the area of sky where the source signal was detected (see Sect. 3.1).

### 3.4.1 The intensity maps

The intensity map combines the signal that hit all KIDs of all scans, excepted those KIDs and scans that were rejected during the data reduction process. In each pixel of the final grid (i.e. the final image), the intensity is the weighted mean of the intensities of all KIDs that have “seen” that given pixel

$$\frac{\sum_{i,j} s_{i,j} \times w_{i,j}}{\sum_{i,j} w_{i,j}} \quad (3.1)$$

where  $s_{i,j}$  is the signal of the  $i$ -th KID of the  $j$ -th scan and  $w_{i,j}$  its weight. By default, weights are proportional to the inverse of r.m.s. squared.

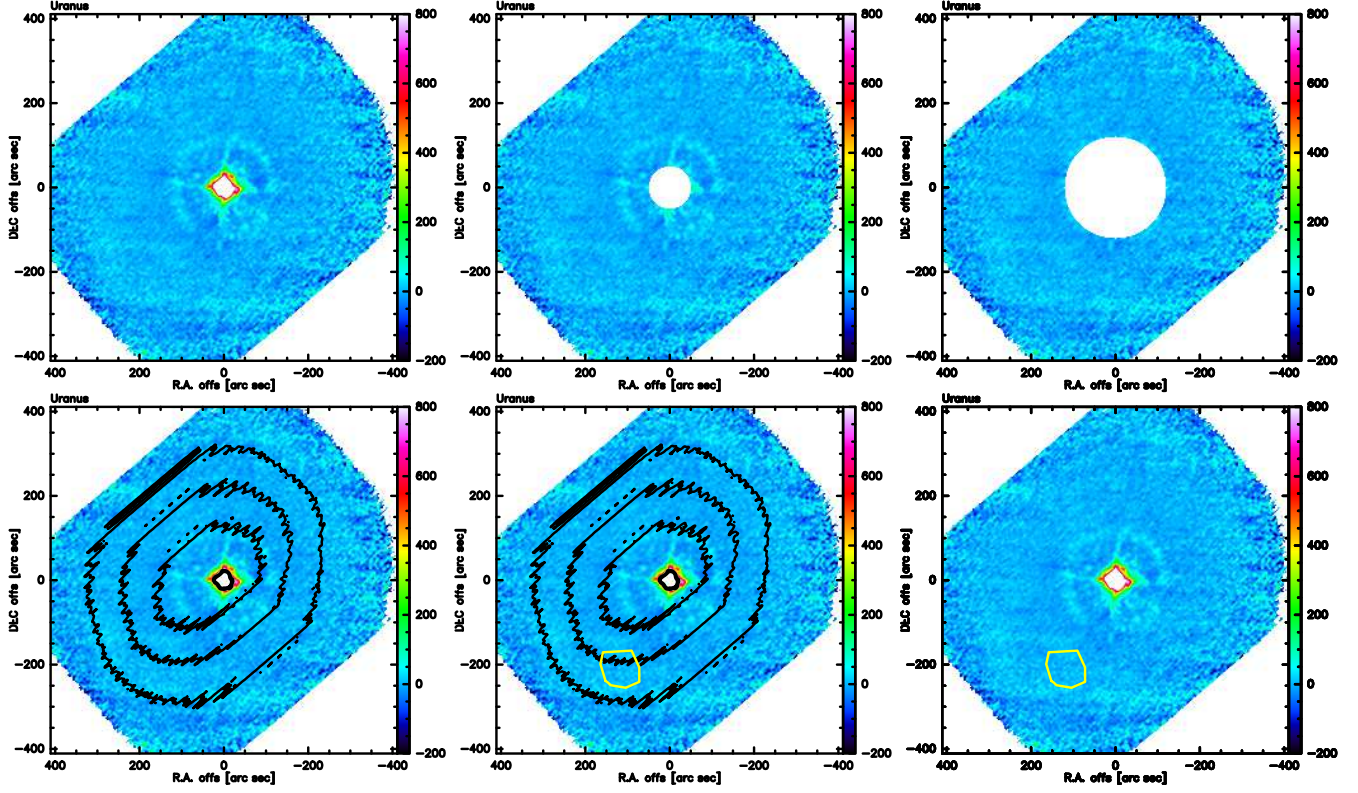


Figure 3.7: *Top-left*: array 1 intensity maps of Uranus. *Top-middle*: source area defined as a circle with radius 50 arcsec. *Top-right*: source definition with radius 120 arcsec. *Bottom-left*: 25%, 50% and 75% coverage levels (black lines). *Bottom-middle* and *right*: definition of the r.m.s. polygon (yellow line). See main text for details.

The intensity of each KID is distributed on the final grid according to the beam, i.e. its contribution to the intensity of each pixel of the grid implies a convolution with a proper kernel. The construction of the final map in Equatorial coordinates from the KIDS timelines of all scans is performed using the algorithm by Haslam (1973), also described by Emerson et al. (1979) and adopted in the MOPSIC data reduction software (Zylka 1998).

The WCS of the final maps is not based on any projection (e.g. TAN, Mercatore, or others). It is simply in spherical coordinates. Then, of course, it is displayed on a flat screen. This kind of WCS is called “Cartesian” in the header and in WCS jargon.

The top-left panel of Fig. 3.7 shows the 0-th iteration intensity map obtained for array 1 of our example Uranus case.

### 3.4.2 The weight maps

Along with the intensity map, the PIIC script produces the map of weights, labeled `rgw` (regular grid weight). Its value is the denominator of Eq. 3.1. Each KID of each scan enters into `rgw` with a different weight, which depends on electronic noise, KIDs instabilities, KIDs tuning, sky noise, etc. Hence a possible proportionality of `rgw` to exposure time is not trivial and actually is distorted by



weighting.

In order to compute a quantity that is directly proportional to the effective exposure time per pixel, one should in principle re-compute the terms (nominator and denominator) of Eq. 3.1 without weighting. Note, nevertheless, that even in such case, the proportionality constant between  $\mathbf{rgw}$  and  $t_{\text{eff}}$  would be not straightforward to evaluate, because the contribution of each KID to the pixels of the final grid is convolved with a kernel. See Section 4.10 for more on this subject.

### 3.4.3 Compute r.m.s. and S/N maps

As mentioned earlier, r.m.s. maps can be computed by rescaling weight maps to the r.m.s. of the intensity map measured within a given area. This area is — for example — what is here called “the r.m.s. polygon”. The PIIC `pro/` repository includes the script `creaRMS.piic`, already prepared to produce the r.m.s. map. Use it as follows:

```
@creaRMS mainName polName
```

where `mainName` is the main file name, without the `rgw` suffix, and `polName` is the polygon file name (as produced automatically by PIIC or as defined manually by the user). The result is the `mainName_rms.fits` map.

Similarly, the script `creaSNR.piic` can be used in a similar way to produce the S/N ratio map `mainName_snr.fits`.

#### Manual computation of the r.m.s. map

If wished, the user can compute the r.m.s. map manually as follows:

```
read Superantennae_rgw.fits      ! read the rgw map produced for the source Superantennae
init spik /all
calc ^0.5                        ! take the sqrt of the rgw
pol Superantennae.pol           ! load the polygon in which to compute the r.m.s.
mean in                         ! compute the avg value of sqrt(rgw) within
                                ! the polygon
div 'MEANVAL'                   ! divide the current array by this MEANVAL
store                           ! store it in the "BACKUP" array
read Superantennae.fits         ! read the intensity map
rms in                          ! compute the r.m.s. within the polygon
take                            ! recovers what was stored before (i.e. the
                                ! BACKUP array = sqrt(rgw)/sqrt(rgw(polygon))
div 'rmsDEV'                    ! this is now sqrt(rgw/rgw(polygon))/rms(polygon)
calc ^-1                        ! invert and obtain
                                ! rms(polygon)/sqrt(rgw/rgw(polygon))
                                ! which is nothing else than the r.m.s. map,
                                ! our final result!
write Superantennae_rms.fits     ! save on file
```

## Manual computation of the S/N ratio map

The S/N ratio map can be computed manually in the following way:

```
read Superantennae_rgw.fits      ! read the rgw map produced for the source Superantennae
store rgw                        ! save it in the rgw array

read Superantennae.fits          ! read the intensity map

pol Superantennae.pol            ! load the polygon in which to compute the r.m.s.
statistics in                    ! compute statistics within the polygon
calculate snr                    ! compute the S/N ratio

plot sca lin -1 5                ! plot the result

write Superantennae_snr.fits     ! save the S/N ratio map
```

### 3.4.4 Verify the source defined in the script

We can now verify if the definition of the source on sky, that we have adopted during the 0-th iteration was appropriate, e.g. if it includes the whole object, or if some features are missed.

In the Uranus example, initially a circular source with radius of 50 [arcsec] was used. Proceed as follows in PIIC:

```
read Uranus.fits
mask in 50 50 0                ! mask all pixels within a ellipse with
                                ! maj/min axes = 50 arcsec and PA=0 deg,
                                ! centered at (0,0)
                                ! [this specific case could also be simply written as
                                ! mask in 50 ]

plot sca lin -200 800
```

The top-middle panel of Fig. 3.7 shows the results: a 50 arcsec radius is too small for this bright object; the first diffraction ring and the signature of the tetrapod is missed. We can let PIIC “detect” it on the basis of the S/N ratio during the iterative mode, or we can enlarge the circle to 120 [arcsec] (top-right panel of the same Figure).

For more complex sources and polygonal geometries, the principle is similar, but one needs to load the source polygon and use `mask in` to verify the area actually covered.

### 3.4.5 The noise r.m.s. polygon

The polygon, within which the r.m.s. of the map is to be measured, is by default defined automatically. PIIC seeks for a square area on the map, with minimum size  $5 \times 5$  HPBW<sup>2</sup> and maximum size  $8 \times 8$  HPBW<sup>2</sup> with as low as possible noise r.m.s. In iterative mode this region might change as



the processing advances, because the properties of the map change. If `nIterSource`>0, the r.m.s. polygon is re-computed at each iteration.

The polygon thus defined is saved for each iteration. Its extension is `.pol`.

Alternatively, it is possible to define the noise r.m.s. polygon also manually, and to input its file name with the parameter `polRMSeq` (in the further settings macro). Section 4.8 describes the procedure to define and verify the r.m.s. polygon manually. It is worth to mention that, thanks to the automatic search of the region with minimum r.m.s., the polygon defined automatically produces a lower r.m.s. value than what any manually-defined polygon has done so far, even when expert hands are operating. Having the lowest possible r.m.s. produces a lower “detection” threshold and therefore a better treatment of sources’ signals.

## 3.5 Iterative mode

After the optimization of the script and associated files has been completed, it is time to proceed with the second main step of the data reduction, i.e. the iterative loop. This time, PIIC iterates on all data reduction operations (see Sect. 3.3), each time modifying the source map based on the S/N ratio. The negative features due to poor “masking” gradually disappear.

Depending on the kind of targets observed, the number of iterations needed to reach “convergence” might vary significantly. For faint and simple sources, 4-5 iterations can be enough; for extended emission and complex geometries, more than 10 iteration might be necessary.

### 3.5.1 Verify convergence

In order to verify if `nIterSource` iterations are sufficient to the project’s goal, or if more are needed, one should simply compare the final intensity maps obtained with  $N$  iterations to those obtained with `nIterSource`–1 iterations only.

To do this, simply take the difference of the two. Generally speaking, if the average difference across the field is a small fraction of percent of the typical sources’ flux, then `nIterSource` iterations are sufficient. Typical acceptance values are of the order of few percent. Each science project has indeed different needs and the users are invited to define their own “convergence” metrics.

## 3.6 Products

The PIIC pipeline produces a large number of files. These files are stored in the directories created at the beginning, as in Sect. 3.2.1. Here we summarize them very briefly, and we defer to specific Sections of this tutorial for further details:

- final maps are stored in the directory `red/`. Three FITS files are produced at each iteration: the signal map; the `rgw` weight map; the source map (see Sect. 3.4 and also Sect. 4.11).
- noise r.m.s. polygons produced automatically by PIIC (if `polRMSeq` is not used, see Sect. 3.4.5) have extension `.pol` and are stored in the directory `red/`.

- if requested by the user, cumulative `rgs` and `rgw` maps (see Sect. 4.10) are stored in the directory `red/`.
- files containing statistical information about each scan are stored in the `stat/` directory (e.g. see Sect. 4.6).
- the same `stat/` directory contains also files that list all scans that have been excluded from the final maps. One possible exclusion criterion is based on the r.m.s. of timelines (see Sect. 3.2.13), among others. These files have a `.err` extension.
- if the `hc` option is switched on, all plots that are displayed on the graphical device of PIIC are also printed on file and stored in the `png/` directory.

# Chapter 4

## Additional tips and advanced use

In this Chapter we include some material for further thoughts: possible hints to improve the observing strategy; and some extra data analysis tips for the most advanced users.

### 4.1 Non-azimuthal scans

Scanning on the sky in a direction different from azimuth (e.g. with an angle in Equatorial coordinates) produces a quasi-periodic saw-like instability, of the order of 10's of Jy or more, mostly due to the change of airmass (a.m.) during the scan. This behaviour is not exactly periodic and the saw teeth are actually not linear. Such drifts do not correlate perfectly because each KID reacts differently to the movement of the telescope. Therefore we cannot fully correct this behaviour; we can only obtain an approximative “cleaning”.

The FoV of NIKA2 is large and therefore different KIDs (e.g. one pixel at the low-el side and one at the high-el side of the array) have different airmass and cover different a.m. ranges during the scan. Therefore the saw-like quasi periodic instability is different for each KID.

Moreover the NIKA2 array(s) rotate(s) on sky as time goes by and as the scan is performed. Hence the saw-like “trajectory” (in noise space) is NOT linear (the saw teeth are not linear), but is slightly curved. The consequence of this curvature is that a linear base-line fitting approximation can cause over-/under-subtraction of instabilities, thus producing spurious negative signals on one side and spurious positive signals on the other side of the “tangent point” to the curve, where the linear fit is pivoted.

Using an iterative procedure (see, e.g., Sect. 3.1), source “protecting” is adapted and optimized. By doing this, the negative signal is avoided and corrected, but the fake positive signal cannot be removed and will stay until the end. Hence a good evaluation of the source map (i.e. those regions of the sky that contain a source and must be protected) at the very beginning is critical, in order to avoid producing spurious effects on the final map.

## 4.2 Scans with different centers

When large fields are observed, or different structures of complex sources are targeted, it is possible that the scans to be combined together have different centers in the sky. In this case PIIC does not know a priori where to position (center) the pixel grid on which the final map will be built.

It is therefore necessary to define the (RA, Dec) position of center of the final map using the parameter `posSeq`. Its value must be in the format “H M S D AM AS”.

Similarly, the extension of the final map must be defined by setting `eqExtraS` in units of [arcsec].

## 4.3 Flux units

The maps produced by the PIIC data reduction are in units of [mJy/beam]. Flux calibration is based on the DAFs CAL files, which are based on observations of standard flux calibrators, e.g. (primary calibrators) and a number of other sources (secondary calibrators). The calibration factors are obtained fitting the main beam (MB) with a Gaussian profile.

Let’s say that one would like to transform the map in different flux units, for example in [MJy/sr], which is another typical unit used in the literature, for example to build color maps with Herschel.

The equivalent source angle under a Gaussian profile, in units of [arcsec<sup>2</sup>], is  $2\pi\sigma_x\sigma_y$ , where  $\sigma_{x,y}$  is expressed in [arcsec] and is related to the FWHM of the Gaussian by the well known relation  $\sigma = \text{FWHM} / (2\sqrt{2\ln(2)})$ . In case of a circular Gaussian profile and point-like sources, we can write  $\text{FWHM}_x = \text{FWHM}_y = \text{FWHM} = \text{HPBW}$ .

Therefore, expressing the HPBW on units of [arcsec], we obtain:

$$[\text{mJy/arcsec}^2] = \frac{[\text{mJy/beam}]}{2\pi\sigma^2} = \frac{[\text{mJy/beam}]}{\frac{\pi \times \text{HPBW}^2}{4\ln(2)}} \quad (4.1)$$

Converting to steradians, one obtains<sup>1</sup>:

$$[\text{MJy/sr}] = \frac{[\text{mJy/beam}]}{\frac{\pi \times \text{HPBW}^2}{4\ln(2)}} \times \frac{(206264.8062)^2}{10^9} \quad (4.2)$$

The size and shape of the NIKA2 beam depend on a several factors, some intrinsic to the instrument, some related to the observing conditions:

- the focal surface changes from the centre to the edges of the arrays, e.g. at the frequency of 1 mm this variation is of  $\sim 0.8$  mm; this results in different beams at different location across on one given array;
- the three arrays not perfectly at a common “average” focus, e.g. array 1 and array 3 are off by  $> 0.1$  mm; this results in different beams on different arrays;

---

<sup>1</sup>the number of arcsec in one radian is  $3600 \times 180/\pi = 206264.8062$ .

- day and night observations are taken under different environmental conditions; for example during the day the main dish is under direct sun illumination, which heats it and induces distortions on the primary surface of the telescope;
- the coating of the telescope dish evolves with time, thus so do also the environmental effects on the beam.

The ideal beams — defined under perfect conditions (telescope, instrument, atmosphere, ... — have HPBW  $\sim 11.3$  arcsec at 1 mm and  $\sim 17.7$  arcsec at 2 mm, but these widths are never observed, even for really good sky conditions. Therefore more conservative values of 11.8 and 18.5 arcsec are used here, as measured for average good conditions (see for example Fig. 4.2).

## 4.4 Effects of sky noise removal and of instabilities on extended and diffuse emission

When dealing with faint extended sources or diffuse emission, the effects of sky noise removal and of the NIKA2 instabilities can play a non negligible role. In the former case, the retrieved flux and source profile can be affected. In the latter, the signal can be suppressed or enhanced.

### 4.4.1 Faint extended sources

For extended sources — smaller than the NIKA2 FoV — an ellipse or a polygon are used to define the source boundaries in the sky. The records with coordinates inside these boundaries are not used during the subtraction of sky noise.

It is possible that the source profile extends beyond the boundaries defined by the ellipse or the polygon, still being well contained in the FoV of NIKA2. In this case, its emission outside the source boundaries is recovered during the iterative processing, if it is above the S/N threshold defined by `snrLevel` (found in the further settings script). On the other hand, if it's too faint then it is lost when subtracting the sky noise.

A smoothing of the source map can be applied (`smSourcePar`; see Sect. 4.11.4) to help detect more extension of the sources<sup>2</sup>. This is highly recommended for faint extended targets.

Figure 4.1 shows the fraction of recovered flux, as a function of the source radius. A circular source was defined in the data reduction setup, i.e. `r=souRmxAS=souRmnAS`. A `blOrderOrig=2` was used. The smaller the radius of the circle used to isolate the source emission, the larger is the fraction of flux lost due to sky-noise subtraction. Note that this is not an artificial source. The curve is normalized to 100% at 120 arcsec radius. This is just an example limited to a given intrinsic size of the source, a given flux and a given noise r.m.s. reached by the observations. If any of these factors changes, the curves in Fig. 4.1 change. The users shall compute their own curves, if needed by their analysis (see also Sect. 4.12).

In reality, some flux is also lost within the radius  $r$ , because the real profile of the source is not a sharp box. How much inside  $r$  this effect extends, depends on the actual profile of the object.

---

<sup>2</sup>only the source map is smoothed, the data are not.

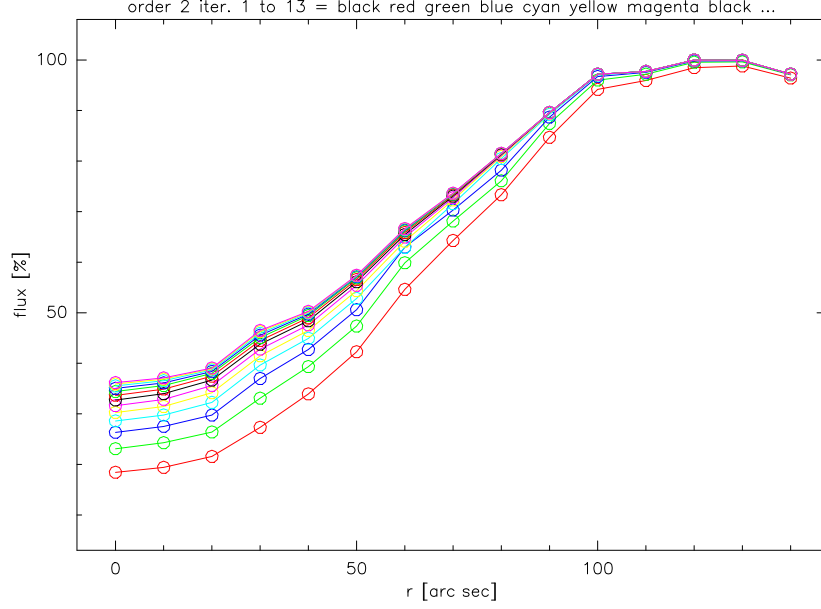


Figure 4.1: Fraction of flux recovered for an extended faint source, as a function of the source radius defined by `souRmxAS=souRmnAS`. Different lines (colours) refer to a different iteration, from 1 to 13. A `blOrderOrig=2` was used.

The fraction of recovered flux is exactly  $=1$  *only* if the source is *entirely* contained inside the circle. To be precise, this is true only if the median calculated using `nBest` records outside the source boundaries is not polluted by the source signal (see Sect. 3.2.11). In practice,  $\sim 100\%$  of the flux is recovered, if the source is smaller than  $r + x \times \text{HPBW}$ . Here,  $x$  is a constant that depends on the profile shape, and whose value is usually between 1 and 2.

Similar considerations can be made for elliptical or polygonal shapes.

#### 4.4.2 The effect of NIKA2 instabilities

Inside the boundaries of the source area (defined either by an ellipse or a polygon), a second effect plays an important role: NIKA2 instabilities, related to the atmospheric condition, the observing strategy, the reply of KIDs to the sky load, and so on.

Instabilities can decrease or increase the source flux, depending on the order of baseline corrections, and on the location of the source in the map (i.e. if it falls onto an instability “valley” or a “hill”).

Under strongly unfavorable conditions, even spurious signals can be generated (see Sect. 2.1).

The map size, the scanning strategy, and the choice of `blOrderOrig` are key factors to be carefully defined at the observing stage and when using the PIIC pipeline.

#### 4.4.3 Uniform emission

Very extended, diffuse emission — which can extend beyond the size of the NIKA2 FoV — is suppressed by the sky noise subtraction. This suppression extends also inwards, inside the source ellipse

(or polygon), because a common “background” is subtracted, and it includes the diffuse emission too.

A straightforward way to show this effect is to study an almost uniform signal: the beam of NIKA2, extended over large scales.

Observations of Mars were taken in excellent conditions: the source was  $\sim 1000$  [Jy], and any sky effects were negligible in comparison. This allowed to produce the beam without any sky-noise subtraction. Figure 4.2 compares the NIKA2 beam obtained in this way to the one produced subtracting the sky-noise (see also Sect. 4.3 for notes about the possible effects that can affect the NIKA2 beam).

When applying the sky-noise subtraction, a circle of radius 190 [arcsec] defined the source in the sky. Remember that the radius of the NIKA2 FoV is  $\sim 200$  [arcsec]. Using such a large source radius was possible only thanks to the special conditions of these observations.

The suppression of the uniform/diffuse emission are clear.

## 4.5 Noise of the final map

The final map comes with an associated noise r.m.s. map, that can be produced following the instructions given in Sect. 3.4.3. The noise r.m.s. map is not uniform and its value can show large variations across the field observed with NIKA2.

The outer regions (or edges) of maps are always noisier than the central parts, because they are covered by a smaller number of KIDs while scanning in the sky. In low number conditions the usual law of statistics are not a good representation of the noise, and the r.m.s. at the edges can be thus erroneously measured. For this reason, scaling the r.m.s. from the central to the outer regions of the map on the solely basis of the lower exposure (e.g. lower weights) can lead to an erroneous (underestimated) noise prediction at the edges.

For the same reason, associating one single value of the noise r.m.s. (or depth) to an observed map does not properly characterize the map nor the performance of the instrument during that specific data set.

### 4.5.1 Noise r.m.s. across the map

Figure 4.3 presents three examples, built for three different data sets that observed areas of different sizes in the sky: a very large field, observed in two different scan directions parallel to the Equatorial coordinates; an intermediate-size field observed in two directions rotated with respect to the coordinate system; and a small field observed at multiple scanning directions.

The bottom panels of the Figure represent the noise r.m.s. map, normalized to its deepest level (at the center of the map). The top panels show the distribution of the normalized noise r.m.s. along  $\delta$  (Dec) = 0.0 (i.e. along the x-axis).

As can be seen, the noise r.m.s. literally “explodes” in the outer regions of the maps, increasing by up to a factor much larger than 10 at the edges. In the case of smaller maps (central panel), the region with enhanced noise has a larger impact in relative terms: the area with “flat” r.m.s. value near the central minimum covers a smaller fraction of the map. In the case of the smallest map, the central region with minimum r.m.s. nearly becomes curved and the flat area almost disappears.

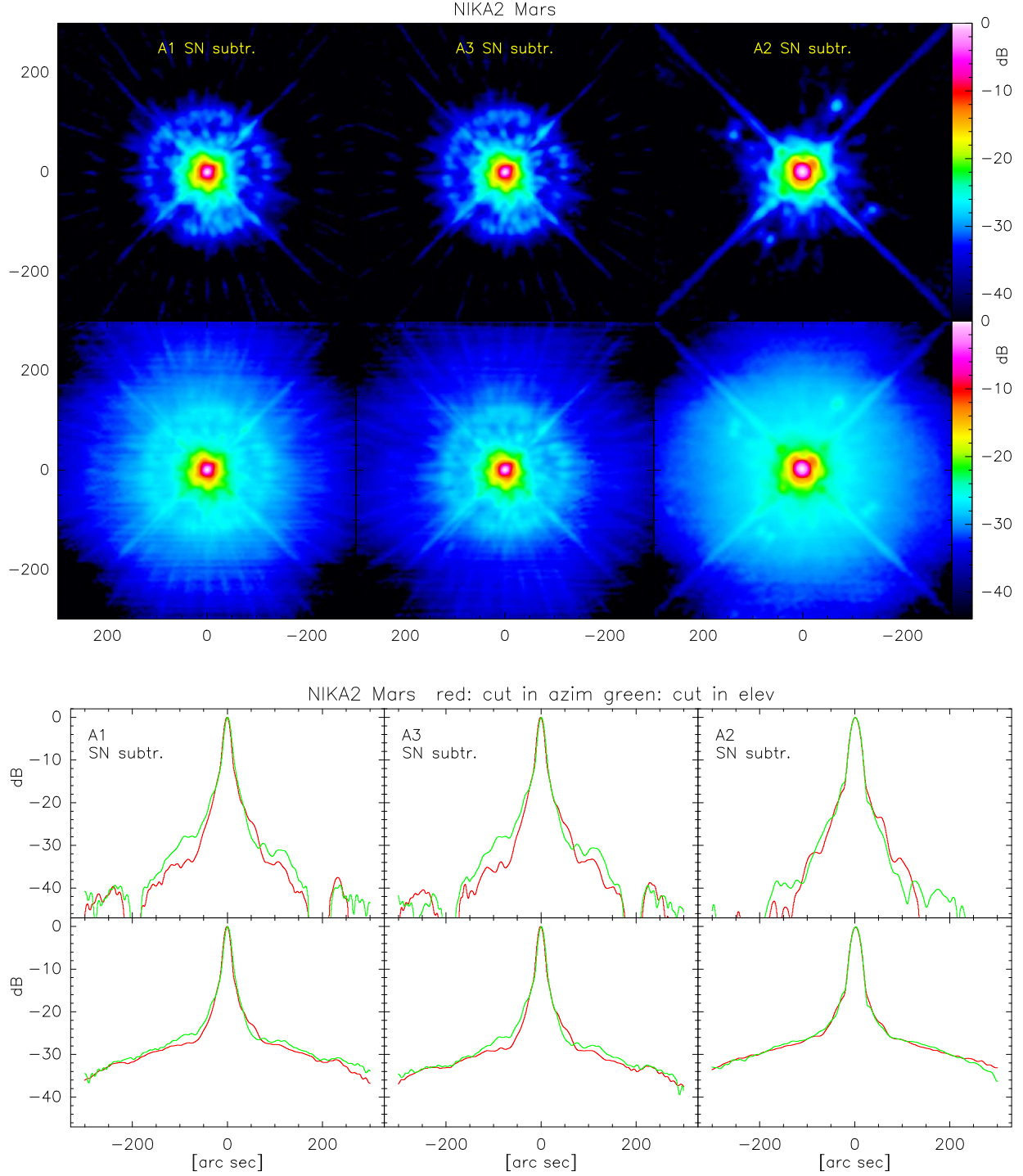


Figure 4.2: NIKA2 beam, based on Mars observations. The *top* maps and profiles show the beam as obtained with sky-noise (SN) removal. The *bottom* ones without it. The *left*, *middle*, *right* panels belong to arrays 1, 3, and 2, respectively. The profiles were obtained cutting the 2D maps along the central line and column (red/green lines).



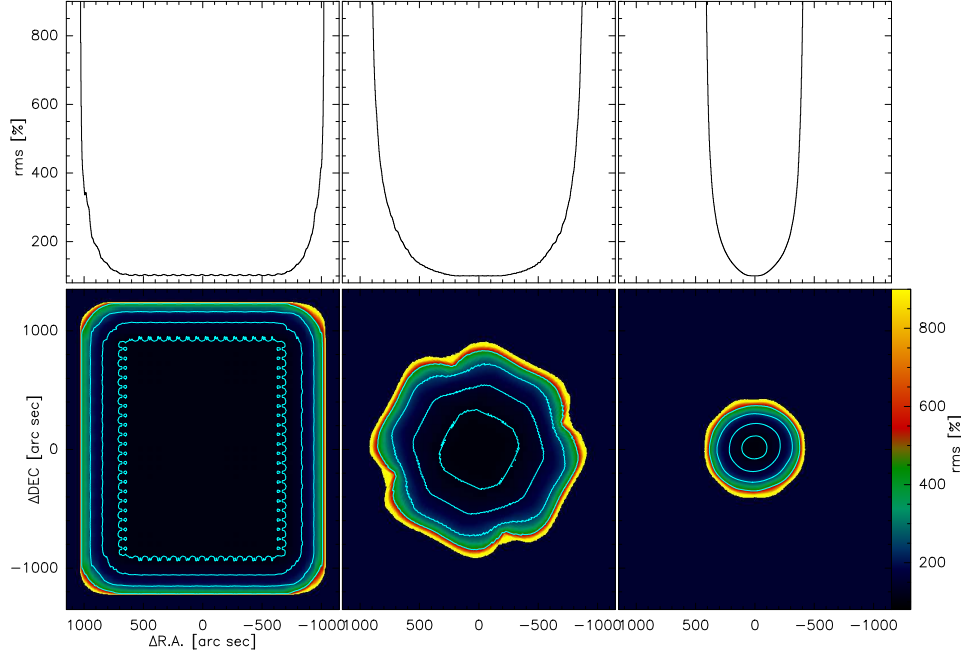


Figure 4.3: Noise r.m.s. across maps of different sizes. *Bottom* panels: r.m.s. maps built as described in Sect. 3.4.3 and normalized to the maximum central depth. The contours are traced at 102%, 150%, 250% and 500% of the central minimum r.m.s. *Top* panels: distribution of the noise r.m.s. across the map, along the x-axis, as measured on the central lines of the maps.

If the map size would be smaller than  $\sim 2\times$  the diameter of the field of view, the areas with r.m.s. larger than the minimum would start to overlap and the r.m.s. profile would become completely curved. In this case there would be no region of the final map that observed by all KIDs and therefore no region would reach the full nominal depth.

### 4.5.2 Trimmed edges

At the very edges of the map the r.m.s. tends to diverge. Moreover, because gridding is performed using the sinc function, the weights map at the edges become negative.

PIIC trims the edges of the final map, blanking out all those pixels for which the weight is  $< 0.3 |\mathbf{rgMn}|$ , where  $\mathbf{rgMn}$  is the minimum weight value of the map (always negative if the size of final map is equal or larger than that of the area covered by the scans).

### 4.5.3 Excluding the outer regions from the computation of the source map)

The source map is the result of a S/N thresholding of the signal map produced at the  $i$ -th iteration using the optimized r.m.s. polygon. This polygon is usually chosen automatically to minimize the noise r.m.s. itself. It is therefore possible that the enhanced noise in the outer regions of a map is identified as a source by the thresholding procedure.

Moreover, note that the r.m.s. noise measured on the map is dominated by high spatial-frequency noise, but the so-called “baseline instabilities” are low-frequency noise. In other words, the high-frequency noise determines the detection threshold in defining the source map, and the low-frequency noise may be detected as if it were a source. Also this effect is enhanced in the outer regions of scan maps.

In both cases, such sources are obviously spurious and shall be discarded. One way to do this is to define a polygon or a radius, outside of which the source map will be set to zero. These are addressed as *zeroing* polygon or radius, and are controlled by the parameters `polZmEq` and `rZmEq` defined in the main template script.

Some consequences of adopting different values of the zeroing radius are described in Appendix C.

## 4.6 Noise of individual scans

In addition to the final products and the PNG images of intermediate diagnostics, the PIIC data reduction script also saves numerous files containing data statistics, as measured during the data reduction flow and at the end of it. These data files are stored in the directory `stat/`.

As an example, one quantity of special interest is the noise of the individual scans before and after applying the atmospheric opacity correction. This can be plotted using the GREG script `plTODrms.greg`, included in the `pro/` folder under the PIIC installation directory. Proceed as follows:

```
@plTODrms Superantennae_..._ECend ! [continue when it pauses]
```

One example obtained with a large dataset of more than 100 scans is shown in Fig. 4.4 for Array 1. In green is depicted the noise of the scans, before applying the opacity correction (and after sky-noise subtraction). It is flat, denoting how the instrumental noise kept constant during the whole observations and across different runs. In red the noise after opacity corrections is plotted. The behaviour of noise now reflects the sky conditions, with peaks for those scans observed in poor conditions.

## 4.7 Number of KIDs effectively used

During the data reduction, some KIDs can be excluded on the basis of different criteria. Some examples are: noise along the timeline; cross-talking; sub-optimal tuning; etc. PIIC stores the number of KIDs rejected for different reasons in `stat/` directory.

The GREG script `plNurps.greg` — included in the `pro/` folder, as usual — can be used to draw a diagram of the number of KIDs left in each scan, and that were effectively used to produce the final map. Identify the files with extension `.nUrps` and use the one belonging to the latest iteration. Proceed as follows:

```
@plNurps Superantennae_..._i5_5 ! [e.g. for the 5th iteration]
                                ! [omit the nUrps extension: it's added automatically]
```

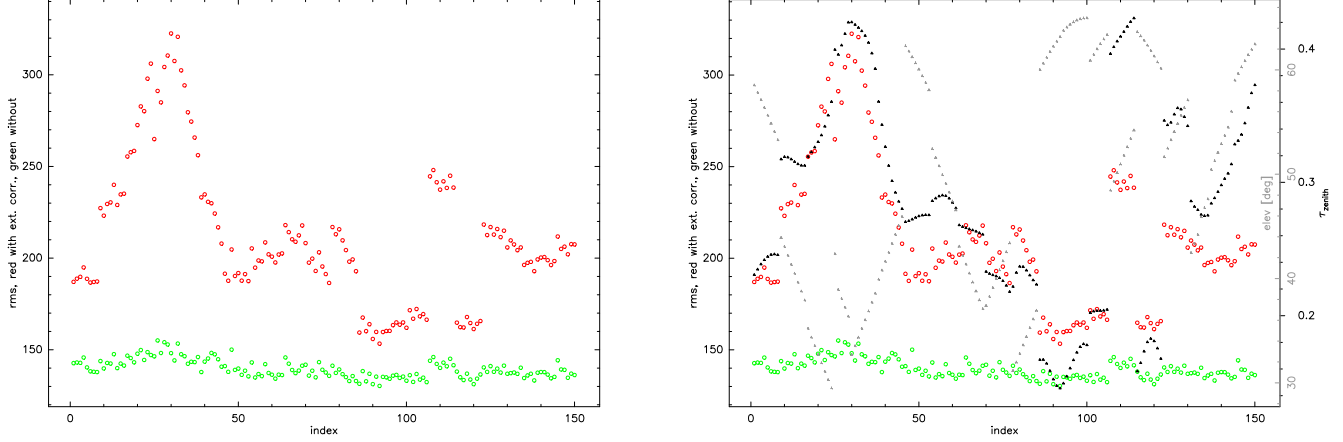


Figure 4.4: Array 1 noise of individual scans during observations. Green points depict the noise before applying the tau-correction. Red dots are the noise after the opacity correction. In the *right* panel, elevation and opacity information are plotted as grey and black symbols, respectively (see right-hand y-axes).

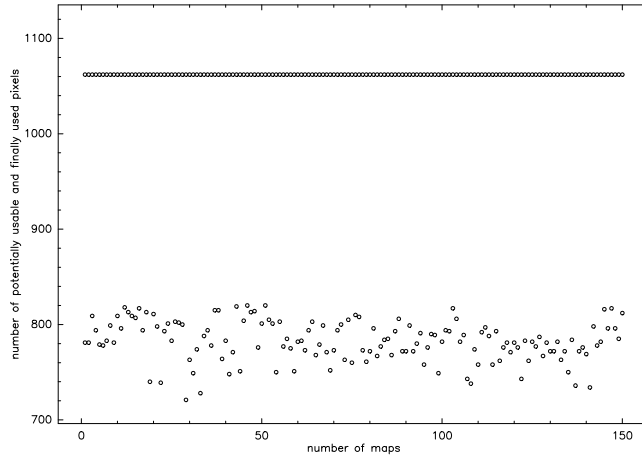


Figure 4.5: Number of KIDs that effectively made it to the final map, as part of a large dataset with more than 150 scans. For each scan, two quantities are shown: the total number of available KIDs defined by the sweep (note that this is not the number of hardware KIDs; top sequence); and the number of KIDs that survived the different selection criteria (bottom sequence).

One example, obtained with the same large dataset as before, is shown in Fig. 4.5 for Array 1. For each scan, two quantities are shown: the total number of available KIDs (named “potentially usable” on the y-axis label) and the number of KIDs effectively used to produce the final map.

## 4.8 Manually define, verify and optimize the noise r.m.s. polygon

The polygon, within which the r.m.s. of the map is measured, is by default defined automatically by PIIC (see Sect. 3.4.5). Alternatively, it can be also defined manually by expert users and given to PIIC as input. The parameter to be used in this case is found in the `mapTPfurtherSets.piic` macro (see Sect. 3.2.9) and is called `polRMSeq`.

The chosen area should ideally have deep enough coverage to be representative of the goal of the project and to allow excluding the presence of any source. In the case of large maps with very inhomogeneous coverage, this choice can turn out to be quite critical in properly defining the source area and in avoiding the creation of spurious signals.

Ideally one would like to define the r.m.s. polygon on the final map, in order to exclude possible sources from it, using the maximum possible S/N ratio. The result of the 0-th iteration can be used.

### 4.8.1 Produce the noise r.m.s. polygon

The polygon file is simply an ascii file, consisting of two columns:  $x$  and  $y$  of the polygon vertices (see the GREG commands help). The coordinates are in “world” units [arcsec], following GILDAS conventions (see Fig. 3.2 and related text). Knowing these rules, users can define the polygon using their favorite piece of software. Nevertheless, we find convenient to use PIIC/GREG themselves, since here the coordinates definition is completely transparent.

Display the final map with PIIC and use the GREG command `polygon` in interactive mode (just type “polygon”). Click on the image where you wish to define vertices, taking care to proceed in clockwise or counterclockwise direction, and without crossing paths (see also Sect. 3.2.4). The coordinates are written on screen. Exit pressing “e” and save the coordinates on file or using the command `write pol filename.pol`.

To define the polygon in a more refined way, one might like to help the hand by visualizing the N% coverage levels on the map. In this way, one could define the polygon within an area of high coverage (or within a desired coverage range). All this, translated in PIIC, looks like the following:

```
read Superantennae.fits      ! reads the intensity map
plot sca lin -1 5            ! plots it with linear scale within the
                             ! indicated range
store                        ! saves it in a backup array
read Superantennae_rgw.fits  ! load the weights map
store rgw                    ! store it in the rgw array
put                           ! transfer the rgw data from PIIC to GILDAS
levels 90                    ! define the 90% level
rgmap /percent 1              ! draw 90% coverage contours
levels 95                    ! 95%
rgmap /percent 1
...                           ! etc
polygon Superantennae.pol /plot ! load and plot an existing polygon
```

```

polygon                                ! use pol command in interactive mode to
                                      ! define a new one in the desired area
greg\write pol Superantennae.pol ! write on file the new polygon
                                      ! add the /overwrite option if the file
                                      ! already exists or use a different file name

```

The three bottom panels of Fig. 3.7 show the definition of the polygon as described here.

## 4.8.2 Verify the polygon

Let's verify that the area we have defined to be *inside* the polygon is effectively interpreted also by GILDAS to be *inside* the polygon. There different reasons for which this might not happen, for example if paths were crossed while defining vertices (easy to happen if complex geometries are involved), the direction was inverted, etc.

The procedure is simple: load the image; display the image; load and display the polygon; mask all pixels within the polygon; re-plot the image and visually verify that GILDAS actually masked those pixels that we meant to mask.

The same, translated into PIIC/GILDAS commands is:

```

read Superantennae.fits
plot sca lin -1 5
polygon Superantennae.pol /plot
mask in
plot sca lin -1 5

```

## 4.8.3 Optimize the polygon a posteriori

The basic principle on which we base our polygon verification is that the r.m.s. of the S/N map, in an empty area (i.e. without sources) in presence of white noise only, must be equal to 1.0.

In order to verify this, we need to produce the S/N map out of the intensity and weights map produced by PIIC (see Sects. 3.4.1 and 3.4.2).

The weight maps is proportional to the inverse the r.m.s. squared. In order to find the correct normalization and transform it into a r.m.s. map, it is necessary to measure the average value of the weight maps and the r.m.s. of the intensity map within the same area (polygon) free of sources. The rest is simple arithmetics.

Produce the S/N ratio map using the script `creaSNR.piic` (see Set. 3.4.3). Then measure its r.m.s. in different areas (polygons), defined where there are no sources. In this way we verify if the r.m.s. value is on average close to unity. If so, then the r.m.s. polygon is defined correctly. If not, the polygon needs to be re-defined. Let's do it in PIIC:

```

read Superantennae_snr.fits
plot sca lin -1 5
pol                                ! yes, all commands can be abbreviated
                                ! define a polygon somewhere appropriate

```

```

! press ``e''to exit
statistics in
pol          ! do the same at different locations, several times
statistics in ! do the same at different locations, several times

```

## 4.9 Scans of very different length

For some particular source geometries (e.g. long filaments), the user might have defined scans and cross-scans with very different lengths. In this case it is necessary to use different orders of the baseline fitting polynomials, because the data instabilities might have different spatial frequencies.

The parameter `blScale`, found in the `mapTPfurtherSets.piic` script, is used to this aim. If its value is larger than 0.0, the baseline polynomial order is modified such that:

$$\text{blOrder} = \text{nint} \left( \text{blOrderOrig} \times \frac{(x_{\max} - x_{\min})}{\text{blScale}} \right) \quad (4.3)$$

where *nint* represents the closest integer, and  $x_{\max}, x_{\min}$  are the maximum/minimum scan lengths. If `blScale` is set to 0.0 (i.e. its default value), no scaling of the baseline order is performed.

## 4.10 Cumulative signal and weights

For some project and science cases, it might be of interest to build — in addition to final maps containing all scans in the dataset — partial, cumulative maps. Given a list of  $M$  scans, partial cumulative intensity maps are obtained combining the first two, then three, then four, and so on scans of the list, up to  $M$ . Similarly, the associated cumulative weights can be produced.

We name these partial-depth maps cumulative **rgw** (regular grid weights) and **rgs** (regular grid signal). In practice, they represent the denominator and the nominator of Eq. 3.1, respectively.

Writing the “cumulative” **rgs** and **rgw** for each scan is switched on by setting the parameter `wrCumMaps` to “yes”. This parameter is found in the `mapTPfurtherSets.piic` script. The cumulative **rgs** and **rgw** are written in the `red/` directory for each scan, i.e. up to that given scan.

This option cannot be combined with the iterative mode, because when `wrCumMaps` is switched on, the final maps are not produced and therefore also the corresponding source maps are not available. Understandably, one might want to write the cumulative **rgs** and **rgw** maps only for the last iteration. To do this, proceed as follows:

- perform the data reduction with the iterative mode as usual and produce the final signal, weight and source maps. At this stage keep `wrCumMaps`=“no”.
- switch `wrCumMaps` to “yes” and perform a second run of PIIC, limiting to the 0-th iteration only. Use the source map produced at the last iteration as `sbSource` input (see Sect. 4.11);

Once the **rgs** and **rgw** cumulative maps have been produced, the intensity map — in units of [mJy/beam] — corresponding to the  $m$ -th **rgs** is computed as follows:

```

read Superantennae_i_rgw.fits
calc extre          ! shows map min/max values
< '0.3*abs(rgMn)'    ! (for example, the limit should be ~0.1 to 0.3 of abs(min)
store rgw
read Superantennae_i_rgs.fits
div rgw

! save it to fits with your favorite filename

```

### 4.10.1 Saving only the last cumulative map

It is possible to save on disk only the “final” cumulative **rgs** and **rgw**, i.e. cumulating all scans in the input list, instead of all cumulative maps. To switch on this option, set the parameter **wrCumLast** to “yes”, instead of **wrCumMaps**.

As in the case of **wrCumMap**, the **wrCumLast** option cannot be combined with **nIterSource**>0. The procedure to write the last cumulative maps after  $N$  iterations is similar to the one described for the case of **wrCumMap** and is not repeated here. See Sect. 4.10 for details.

One possible application of the **wrCumLast** option is when the user would like to split the input list of scans into sub-lists and process several sub-sets of data in parallel, using multiple CPU cores. For example split the input list of scans in as many sub-lists as the number of available CPU cores. Section 4.10.2 explains how to combine the results back into a final map. To run PIIC on several sub-lists in parallel, it is necessary to open several independent PIIC sessions.

If this is the aim of using **wrCumLast**, care must be taken that the maps obtained from the sub-lists have all the same dimension and are all centered and oriented in the same way in the sky. In other words, the final maps will be combined pixel-by-pixel, and each pixel in each map to be combined with the others must correspond to the same pixel of all other maps. Because scans can have different directions in the sky, this does not mean that all maps must have an identical data coverage, but they must have the same geometry (i.e. pixels can have no signal, but must be there). To assure that this happens, instead of letting PIIC define automatically the position and size of the maps, use the parameters **posSeq** and **eqExtrAS** (see Sect. 4.2) and set them to the same values for all sub-lists.

### 4.10.2 Combining cumulative maps of sub-sets of data

Once several cumulative maps are produced for different sub-sets of data (see Sect. 4.10.1), the script **creaAver.piic** (found in the **pro/** repository) shall be used to build the final map, thus effectively combining together all scans in the parent full input list, after data processing.

The script can be copied in the working directory and can be edited. It needs the file name of the output combined map, coded in the parameter **outName** and two input lists: one of all cumulative **rgs** maps and one of the **rgw** maps produced for the partial data sets. These lists have to be prepared by the user; their default names<sup>3</sup> are **'outName'\_rgs.LIST** and **'outName'\_rgw.LIST**. As mentioned in

---

<sup>3</sup>for example, if **outName=Superantennae\_a2** then the lists are called **Superantennae\_a2\_rgs.LIST** and **Superantennae\_a2\_rgw.LIST**.

Sect. 4.10.1, the user must take care that all maps of the partial data sets to be combined together have the same geometry in the sky.

The combination of `wrCumLast` and `creaAver.piic` can save a significant amount of processing time, especially for long scan lists and if a large number of CPUs is available. Nevertheless, it also requires a lot of preparatory work and a good bookkeeping of all sub-lists and partial results.

Before opting for this solution, the user should evaluate the effective gain in execution and analysis time with respect to — for example — a classic one-core only processing or a parallel processing of the full scan list with different PIIC setups on different cores, aimed at testing which pipeline configuration is best for the given data set.

### 4.10.3 Linking `rgw` and effective exposure time

It would be interesting to compute the effective exposure time per pixel, or at least a quantity proportional to it. As said before (see Sect. 3.4.2) the current `rgw` is not a correct representation of effective time because it is weighted. Moreover the kernel convolution performed by distributing (in Fourier space) the signal of each KID onto the final grid, makes the proportionality constant not easy to define analytically.

The first issue can be solved by performing an alternative data reduction, which avoids weighting. The resulting intensity and r.m.s. maps will *not* be correct, but the `rgw` will be a proper description of the effective exposure time per pixel, modulo a scaling factor.

The second issue can be solved by performing a naive re-gridding that uses a box-convolution instead of re-distributing the signal of each KID adopting the real kernel. The result would then be used only to compute the scaling factor, and for no other science-related purpose.

These solutions are described in Sect. 4.14.

### 4.10.4 Using `rgs` and `rgw` to produce individual scan maps

Representing the cumulative signal at each  $i$ -th scan in the list, including all scans from 1 to  $i$ , the `rgs` maps can be used to produce reduced maps of each individual scan, defined on the final grid. While doing this, one needs to take into account the necessary weighting.

Produce the map of the  $i$ -th scan in the list by simply applying the following equation:

$$\frac{\text{rgs}(i) - \text{rgs}(i - 1)}{\text{rgw}(i) - \text{rgw}(i - 1)} \quad (4.4)$$

Note that, when dealing with 1 mm data, it is important to avoid mixing Array 1 and 3 maps in this equation.

## 4.11 The source map

Each iteration step produces three files, just like the 0-th iteration. One of three is the source map, as defined detecting pixels above the S/N ratio given by the user (`snrLevel` parameter in the further settings script). This is not a mask, but an actual source map in FITS format. At each iteration, this



source map is subtracted from the data before performing all computations (e.g. baseline subtraction, etc., see Sect. 3.3), and then it's added back.

For example, the source map produced at iteration `nIter=20` is called `Superantennae...._20f21.fits` and will be used during the next iteration (`nIter=21`).

#### 4.11.1 Continuing where PIIC was stopped (during the iterative mode)

For specific, complex sources or data sets, it might be necessary to use a large number of iterations to reach convergence. In this case the PIIC data processing takes a long time. Similarly, very large data sets or very large maps also require long data reduction sessions.

It is possible that the data reduction is interrupted and stopped, for example in case of loss of net connection, black outs, unplanned reboots, other accidental reasons, or on purpose.

If the stop was during the iterative process, and — for example —  $m$  iterations out of  $N$  were already completed, not everything is lost: it is possible to re-start the data reduction and to continue from the same  $m$ -th iteration, slightly editing the data reduction script and taking care of few details:

- the source map produced at the  $m$ -th iteration shall be now used as input source map (parameter `sbSource` in the further settings script);
- in the new run, the 0-th iteration corresponds to the previous  $m$ -th iteration;
- in the iterative loop, the 1st iteration corresponds now to the  $(m + 1)$ -th iteration of the run that was stopped;
- filenames will now be different, because: *a)* now the `sbSource` option is used; *b)* the numbering of iterations starts again from zero;
- the number of iterations `nIterSource` of the new (restarted) run needs to be adjusted, otherwise the effective total number of loops will be  $m + N$ , instead of simply  $N$ .

In practice, the  $m$ -th iteration is repeated, but it is a smaller loss than if one would need to repeat all the  $m$  iterations from scratch (unless  $m = 1$ ).

#### 4.11.2 Using a pre-defined source map

It is possible to have a user-defined source map as input, to be adopted as initial source map. It will be used during the 0-th iteration and then it will be refined by PIIC during the iterative process, based on S/N as usual.

Such a user-defined map must simply be a two-dimensional map in FITS format, including an Equatorial coordinates system at the J2000 epoch. The actual size in pixels of the map is not important, because the WCS will be used.

Note that using a pre-defined source map is to be considered an *expert-mode* operation. Defining it properly, without knowing how the emission is at the NIKA2 frequencies, is complex and could involve a bit of gambling. For example, such a map might come from the analysis of shorter/longer

wavelengths (e.g. *Herschel*) data, or from physical assumptions, or from a combination of the two. It is, though, not granted a priori that the underlying assumptions are fully correct.

The parameter defining the file name of this input pre-defined source map is again `sbSource` in the further settings script.

### 4.11.3 Produce the source map a posteriori

In some cases, the user might like to produce new source maps a posteriori, for example to test how different noise r.m.s. polygons would influence the source detection and thresholding.

The script `creaSource.piic`, included in the PIIC `pro/` repository, is designed to produce a source map, starting from the `rgw` map produced by PIIC and a noise r.m.s. polygon. Use it as follows:

```
@creaSource mainName polName snrLevel
```

where `mainName` is the main file name (i.e. the map produced by PIIC at any  $i$ -th iteration), `polName` is the polygon file name, and `snrLevel` is the threshold above which pixels are selected (e.g. equal 4 in the default setup, see the further settings script).

### 4.11.4 Enhance detections by smoothing

Excluding sources from sky noise is based on source boundaries defined by the user (elliptical or polygonal) and on the source map generated during the iterative process. The latter is based on the identification of pixels above a given S/N ratio on the final map. In some cases with low S/N ratio, the detection of source pixels likely will miss some of the signal. As mentioned in the previous Chapter, this might cause an important loss of information, and can even create spurious effects.

In order to improve on the detection of source pixels, it is possible to apply a smoothing algorithm to the final map or to the source map. The parameter `smSourcePar`, found in the `mapTPfurtherSets.piic` script, controls this feature:

- if `smSourcePar` > 0, the S/N ratio is calculated using a smoothed version of the final map, but the source map is not smoothed. In this way one goes deeper in the detection.
- if `smSourcePar` < 0, also the source map is smoothed. This helps to cover more extension of the sources, i.e. it helps to go further than the contour defined by the mere S/N thresholding.

The first case is useful for faint sources in general, including point-like and compact sources. The second is specifically more interesting for weak, extended objects (e.g. SZ signals).

The details of the improvement obtained are difficult to predict, because they depend very much on the data (geometry, strategy, instabilities, etc.). Therefore a bit of experimentation is required, to optimize the smoothing parameters.

Two different smoothing algorithms are possible at this time:

1. if  $|\text{smSourcePar}| \leq \text{HPBW}$ <sup>4</sup> then a so-called “*conjugate gradient (CG) smoothing*” is adopted. The smoothed image is the equilibrium state of a thin flexible plate constrained to pass near each height data by a spring attached between it and the plate (see the `cgs` help for more details). The CG smoothing creates a very “clean” result, but it is not possible to tell what is the final resolution. It affects point-like sources less than a Gaussian smoothing, and is instead more effective in smoothing the noise.
2. if  $|\text{smSourcePar}| > \text{HPBW}$  then a Gaussian smoothing to the given resolution is used. In this case, the value of `smSourcePar` is the final HPBW of the smoothed map, in units of [arcsec].

If the smoothing is used for point-like sources, only small positive values shall be used:  $0 < \text{smSourcePar} \leq 0.5$ . When extended sources are analyzed, it is suggested to apply the smoothing also to the source map, i.e. `smSourcePar` < 0.

## 4.12 Adding artificial sources to the timeline

PIIC allows one to add artificial sources, models, or other other kind of signals to the data timeline, before undergoing the data reduction (and after the first calibration steps; see Sect. 3.3). This feature is useful in several different contexts.

One important application is the study of how the data reduction pipeline affects the data, computing a so-called “*transfer function*” (see Appendix C) for their typology or targets (e.g. point-like sources, galaxies with different profile shapes, SZ signal, Galactic clouds, etc.). Having a model that describes the expected or typical emission of the sources, one can inject it in the timeline and compare the result to the “intrinsic” model emission hitting the telescope and the KIDs, which is known a priori by definition.

Another possible use is the development of completeness and reliability simulations for (extragalactic) blank-field surveys. Once the flux distribution of the sources is known (or modeled), point-like objects are added to the timeline and processed. Comparing the output and input distributions, leads to the completeness characteristics of the data set and the incidence of spurious detections.

The parameter controlling this feature is called `addSource` and is found in the “further sets” script. Its value shall be the file name of a FITS map that will be added to the timeline. This map can consist of a source model, or anything else. In the blank fields example, this would be a map with null background and no noise, containing a number of artificial sources, spread over the field, with a point-like profile, and having a given flux distribution. Other kind of observations, obviously require different kinds of artificial sources (model maps).

The model map can be produced with any tool, be it PIIC or any external software. The size, pixel scale and shape of the artificial map can be any and are left to the user’s choice. It is paramount that the artificial map includes a *World Coordinates System* (WCS) in Equatorial coordinates at epoch J2000, that covers the position of the real scans in the sky. The signal on the artificial map is transferred to the timeline on the basis of the (Ra,Dec) coordinates of each pixel. The units of artificial input map must be [*mJy/beam*], where the NIKA2 beam is intended (see Sect. 4.3).

---

<sup>4</sup>Values of 12 and 18 [arcsec] are adopted, i.e. slightly broader than the nominal NIKA2/30m HPBW at 1 mm and 2 mm.

Note that no convolution with the 30m/NIKA2 PSF is performed at this stage, therefore the artificial map should already include the effects that light undergoes during its path from the source to the detector. Adding an artificial source and studying it a posteriori gives only a description of the effects of PIIC processing on the data.

PIIC does not provide the means to perform the post-processing analysis, e.g. the study of the “transfer function” or of the data “completeness/reliability”. It only gives the tool to add the artificial sources to the timeline. The rest of the analysis is left to the users and their dedicated procedures.

Appendix B makes use of this feature to evaluate the effects of re-gridding on the profiles of point-like sources.

### 4.12.1 Null maps (a.k.a. jackknife)

Artificial sources added to the time line will appear on the final combined map, that includes also the signal of the real sky. On the other hand, PIIC can produce *null maps*, setting the `nullMap` parameter to “yes”. This parameter is found in the “further sets” script.

When this option is used, after the rejection of problematic scans, the signal of each second scan among those that are left<sup>5</sup> is multiplied by **-1**, before processing. The final product is a null map, where real sources and background are cancelled.

In some astronomical contexts (see e.g. Herschel/SPIRE or SCUBA extragalactic surveys and Planck work), this method is also called “jackknife”. Note that this has nothing to do with the statistical jackknife, originally developed by M. Quenouille, that consists in producing subsamples of  $N - 1$  scans and studying the statistics between the subsamples.

When using the `nullMap` and the `addSource` options combined, the artificial signal is added after multiplying by -1 each second map. The `nullMap` option can of course be used also without adding artificial sources, in case it serves for any other purpose.

When the null map is requested, the products of data processing are three files as for the normal data reduction. The file names are the same as in the non-jackknife case.

## 4.13 Saving maps of individual scans

It is possible to save the maps of individual scan, computed on the final grid, i.e. the same used to produce the final, combined map. Such individual maps can be used — for example — to compute for pointing corrections between individual scans, identify and exclude scans of poor quality (for whatever reason), check the effects of scanning in different directions, etc.

Enable this feature by switching the parameter `wrIndMaps` to *yes*. This parameter is found in the “further sets” script.

Because these individual maps serve for other analysis purposes and are not instrumental to create the final map, when using `wrIndMaps`, PIIC does not produce the combined map, nor the associated

---

<sup>5</sup>the number of scans accepted by PIIC (out of the input list) might not necessarily be even. If it’s an odd number, then the signal of one scan is left in the final “null” map. The user is invited to double check the actual number of used scans printed by PIIC at the beginning of the reduction.

weights and source map. Similarly, it is not possible to associate the use of `wrIndMaps` with the iterative mode.

The ideal way to save individual maps and use them properly is then:

- perform the standard data reduction with PIIC, performing  $N$  iterations if needed, and producing the combined maps. At this stage keep `wrIndMaps`=“no”.
- set `wrIndMaps` to “yes” and perform a second run of PIIC, limiting it to the 0-th iteration only. Use the source map produced at the  $N$ -th iteration as `sbSource` input (in the further settings script, see Sect. 4.11).
- perform the analysis for which the individuals maps were intended.
- if necessary, as a consequence of this analysis, adjust the PIIC setup and perform again the standard (iterative; `wrIndMaps`=“no”) data reduction to now produce the final, optimal result.

## 4.14 Hit map

Some science projects might have interests in recording how many times the pixels of the final map have been *hit* by all the scans, records, KIDs of the data set under analysis. One possible application is to evaluate the effective integration time per pixel. It is possible to compute a so called *hit map* with PIIC using the parameter `calcNhits` that is found in the further settings macro. Three options are available:

`calcNhits=0` In this case, PIIC operates normally and no hit map is produced.

`calcNhits=1` The hit map is computed distributing the signals to the final grid according to the NIKA2 beam.

`calcNhits=2` The hit map is computed without distributing the signals, i.e. the hit is assigned on a 1:1 (KID:pixel) basis.

The resulting hit map is stored in the `rgw` file. This means that there is not a “hit map” specific file name and the user interested in this feature should rename the result themselves, using their favorite naming conventions.

It is important to point out that the signal map and `rgw` map produced by the standard data reduction (i.e. `calcNhits=0`) are obtained weighting the contribution of each KID by the inverse of the noise r.m.s. (along the timeline) squared. On the other hand, this weighting cannot be applied to produce the hit map, because otherwise one would simply obtain the `rgw` map, that has a different meaning (see Sect. 4.10.3).

The hit map gives — so to say — an estimate of the formal time per pixel that went into the observations, but it does not fully correspond to what goes in the final map r.m.s. because the latter takes into account the various instrumental and environmental effects (e.g. instabilities) via weighting. Moreover, the effect of the extinction correction is different in the two cases, because the noise properties are different.

For these reasons, a direct comparison of an effective integration time based on this (non-weighted) hit map to the properties (e.g. the r.m.s.) of a weighted map can give only qualitative results. In principle, to make a fully correct comparison, a non-weighted signal map should be used in combination to the hit map. Such a map is also produced when `calcNhits>0`, but it is much noisier than the proper signal map obtained with `calcNhits=0`.

Inverting the point of view: associating the non-weighted hit map to the weighted signal map can provide only a lower limit to the effective integration time per pixel, at a given map r.m.s.

With this caveats in mind, in order to produce the hit map in addition to the proper signal and weights map, it is necessary to perform a double PIIC pipeline run<sup>6</sup> (similarly to when maps of individual scans are saved, see Sect. 4.13). A simplified (quick) way to do it is as follows:

1. run the standard data `calcNhits=0`. Perform as many iterations as needed.
2. run PIIC with `calcNhits=1` or `2` and using the source map produced at the last iteration before. One iteration should be then sufficient at this stage (see Sect. 4.11).

Note that this procedure speeds up the operations, but the source map produced with the weighting setup is different from the one that would be produced without weighting because of the different noise level resulting from the two methods.

The file names of the maps produced by the two runs might seem similar but differ by the label linked to `calcNhits`.

## 4.15 Pointing and calibration correction between scans

The telescope pointing errors can have an impact on the products of NIKA2 observations. Since the final map is a weighted average of a number of scans/maps, if not corrected, pointing errors will broaden strong compact sources and will dilute their flux. Further more some flux fraction of weak wings might decrease below the detection limit and might be missed.

It is possible to correct the pointing offsets between the different scans of a data set, by setting the parameter `nrCorrPoiCal` to 1, 2, or 3. This parameter is found in the “further settings” script. A significant amount of extra work by users is required to use this feature.

The offsets to be applied to each scan are read from the file `NIKA2gfEqElli.pccIn`. The format of this file is:

```
arNr scanNr date    corrRA corrDEC corrCal
```

e.g.:

```
1    131 20190118  -0.727  3.114  0.94786
2    131 20190118  -0.507  2.896  1.04733
3    131 20190118  -0.635  3.308  1.07845
```

---

<sup>6</sup>The hit map and the weighted products are not produced in one single run because the operations and the execution time would be anyway doubled.

The adopted value of `nrCorrPoiCal` indicates the array to be used for the pointing correction. In this example, if `nrCorrPoiCal=2` the pointing corrections will be  $(-0.507, 2.896)$  in RA and Dec.

The pointing corrections are the difference between the offset position of the same source in the individual maps and the average map:

$$\begin{aligned}\text{corr}(\text{RA}) &= \text{off}(\text{RA})_i - \text{off}(\text{RA})_{\text{avg}} \\ \text{corr}(\text{Dec}) &= \text{off}(\text{Dec})_i - \text{off}(\text{Dec})_{\text{avg}}\end{aligned}$$

Where by “offset” it is intended the offset of the source from the center of the final map in units of [arcsec] (in PIIC/GREG coordinates conventions).

The flux calibration correction is the ratio of the fluxes obtained for the same source in the individual maps and the average map:

$$\text{corr}(\text{Cal}) = \frac{\text{flux}_i}{\text{flux}_{\text{avg}}}$$

These measurements shall be performed on compact sources, if not point-like, bright enough to be detected on individual scans. *Hence the correction of pointing offsets between scans is possible only for data sets that have such sources in the field.* There is no limit to the number of sources to use: the more the better.

To derive the fluxes of sources and the flux calibration correction, it is preferable not to use the peak fluxes; integrals of a Gaussian fit to the sources profiles are a better — and easy — solution.

The file `NIKA2gfEqElli.pccIn` must have an entry for each scan to be processed, for the array chosen as reference. Note that the reference array for the pointing corrections (i.e. `nrCorrPoiCal`) can be different from the array processed to derive the combined map. For example, when producing the Ar 1+3 map, one can use either Ar1 or Ar3 offsets; or for array 2 (1) maps, one can use array 1 (2) as reference for the corrections, depending on the desired angular accuracy of the corrections or on source brightness; etc. These are just examples and other cases might happen.

*The PIIC package does not include procedures to measure the position and fluxes of the sources and to build the `NIKA2gfEqElli.pccIn` file. This choice is driven by the fact that every project and data set has different characteristics, different kind of sources, and therefore different techniques might be preferred by the users. This file has to be produced by users with their own tools.*

Finally before using the `nrCorrPoiCal` option, one additional directory `pcc/` needs to be created. The corrections applied to each map will be written there.

## 4.16 Saving time

Here we list some ways to reduce the PIIC processing time. Before opting for any of these solutions, the user should be aware of its counter-indications and should evaluate if it brings sufficient advantages for their case. So far, the following possibilities are available:

- test different setups of the PIIC data reduction pipeline in parallel on different CPU cores, using different PIIC sessions (mentioned in Sect. 4.10.2);

- split the data set in sub-sets and proceed as described in Sect. 4.10.1;
- reduce the time spent reading and pre-processing scans (see Sect. 4.16.1).

#### 4.16.1 Reduce the read and pre-processing time

Reading IMBFITS data files and pre-processing scans takes up to  $\sim 30\%$  of the total PIIC data reduction time. By default, PIIC reads and performs the pre-processing of all KIDs.

It is possible to decrease the time spent on this phase of the data reduction by selecting a priori only those KIDs that are not flagged in the DAFs (see Appendix A) as unusable. If the `useDAFsFr` parameter (found in the further settings script) is set to “yes”, PIIC will use the information stored in the DAFs to exclude those flagged KIDs from the reading and pre-processing operations.

In this way, up to  $\sim 30\%$  of the reading and pre-processing time can be saved. This option comes, nevertheless, with a caveat: when using it, it can happen that PIIC won’t identify some couples of KIDs tuned too close in (tuning) frequency, because one of the two might have already been excluded a priori from reading using the DAFs pre-selection. This implies that setting `useDAFsFr` to “yes” there might be more KIDs contributing to the final map than when setting it to “no”. The information carried by these KIDs is affected by cross-talking.

The incidence of this effect and the number of extra KIDs left depends on the quality of tuning and can be up to  $\sim 3\%$  of the total number of KIDs per Array.



# Chapter 5

## The quick look monitor

PIIC includes scripts for quick data reduction. They can be useful to the science user to check — for example — under which conditions the observations were done (e.g. pointing, tracking, etc.). These scripts adopt different names, depending on purpose. On-the-fly data reduction at the telescope, processing new data as they are produced by NIKA2, is called *monitor*. Quick off-line (i.e. not during the data flow, e.g. at home) data reduction is called *quick look* (QL). The name “quick look monitor” can also be found.

The setup of the QL is similar to the default setup of the science pipeline, i.e. it is optimized to process centered, compact sources.

### 5.1 On the fly data reduction at the telescope

Usually the on-the-fly data reduction at the telescope is activated by the astronomer on duty (AOD). In case not, prepare the needed directory tree as follows:

```
cd
mkdir ql
cd ql
mkdir dat plAr1 plAr2 plAr3 redAr1 redAr2 redAr3
ln -s directory_containing_data imbfitsDir
```

Then run the *monitor* in one terminal, typing:

```
piic @monitor1
```

for NIKA2 array 1 (first 1 mm array). Similarly, do the same in other terminals for Arrays 2 and 3, if desired, by simply using *monitor2* and *monitor3*.

### 5.2 Quick Look

The *quick look* analysis (QL) is the off-line version of the PIIC *monitor*. By “off-line” it is intended not on-the-fly as the data are produced and stored on disk at the telescope. It exists in two different incarnations:

- work on one scan at a time;
- work on all scans taken from a user-generated list.

In the first case the QL scripts for the three different arrays are called:

```
qlAr1
qlAr2
qlAr3
```

In the second case, they are called:

```
qlAr1list
qlAr2list
qlAr3list
```

To use the QL, setup on your local disk a directory tree organized as for the *monitor* (see Sect. 5.1).

## 5.3 Simple use of QL

To run the QL scripts on one single scan, follow this simple example:

```
@qlAr1 scanname
```

and similarly for arrays 2 and 3. For example:

```
@qlAr1 20150627s40
@qlAr2 20150627s40
@qlAr3 20150627s40
```

To make use of the QL for lists, first create a list of all scans to be examined and then run the script. The list shall be called `ar1.LIST`, `ar2.LIST` or `ar3.LIST`, and shall contain the IMBFITS<sup>1</sup> filenames (the IRAM NIKA2 FITS files provided to the users after pool observations, stored in the `imbfitsDir/` defined before) without path.

For example, to run QL on all array-1 scans present in the `imbfitsDir/` repository, follow this simple example:

```
cd
cd ql
cd imbfitsDir
ls iram-30m*-1-* > ~/ql/ar1.LIST
cd ..
```

```
piic
```

```
@qlAr1list
```

---

<sup>1</sup>IMBFITS means *IRAM Multi-Beam* FITS files; it is the standard file format of IRAM/30m and NIKA2 data.

## 5.4 Advanced example: use the QL on a refined list

In some cases, the user might need to run the QL on restricted list of scans, for example those belonging *only* to the observations of a specific target. Such a list can be prepared using any of your favorite tools. One option is to use GILDAS or PIIC to select scans on the basis of different parameters (e.g. observation type) and/or on the basis of the observed object (see also Sect. 3.2.2). The list should contain only the IMBFITS filenames, without path, for a given array.

For example, using PIIC, the list of all array-2 scans belonging to observations of our favorite *hypothetical* source called “Superantennae” can be produced in the following way:

```
cd
cd ql
cd imbfitsDir
ls iram-30m*-2-* > ~/ql/all_ar2.LIST      ! lists all Ar2 IMBFITS files
cd ..

piic

inlis all_ar2                        ! load the list
sel type m                          ! select scans with observation type = map
find obje /wri                      ! find the names of all objects that were
                                   ! observed writes with scans in the list
                                   ! and writes one list of scans per objects
sel obje SUPERANTENNAE             ! selects only scans of object SUPERANTENNAE
write inlist SUPERANTENNAE_a2.LIST ! write the list of selected scans on file
init inlist                        ! if needed, resets the starting list (in memory)
                                   ! the user will need to start from scratch,
                                   ! if they wish to produce a new list
```

In this way, one ascii list has been produced for array 2 containing the names of all Superantennae IMBFITS files to be processed by the QL. Do the same for arrays 1 and 3. The QL script accepts only lists with names `ar1.LIST`, `ar2.LIST` or `ar3.list`. Rename your list accordingly, before starting the QL, for example:

```
cp SUPERANTENNAE_a2.LIST ar2.LIST
```

Note that selecting scans is not strictly necessary: one can run the QL on all the scans of a given data set (see Sect. 5.3).

Run QL on all your favorite scans. Note that if the *monitor* is running at the same time, QL might interfere with it. To avoid interferences, the *monitor* and the QL should run in different working directories.

## 5.5 Operations and results

As it runs, the QL (or *monitor*) produces different diagrams, that are shown in sequence in two different graphic devices. The same diagrams are also saved as PNG files.

First of all, the QL shows the timeline of all KIDs (detector pixels) after different operations have been performed on the signal (see Fig. 5.1). The timeline of each KID is plotted as a line of different color in units of signal [mJy/beam] vs. LST [s]. The many lines overimpose to each other.

In the top-left panel, only forward beam calibration, flat fielding and the correction of first order drifts (over the whole sscan timeline) are applied. The low-frequency modulation is due to variations of sky signal (e.g. due to intrinsic changes of sky conditions or due to changes of airmass during the scan) and KIDs instabilities (e.g. light-blue line in the Figure). Possible short-time peaks represent the signal of bright sources at the time when the given KID crosses them on sky.

As the data reduction proceeds, the QL computes and subtracts the *sky noise* from the data timeline of each KID (see also Chapter 3) and produces a flattened timeline (*top-right panel*). Those KIDs that do not comply to a number of selection criteria are then excluded (*bottom-left panel*). Finally the baseline subtraction, the main beam calibration and the extinction correction are applied and only the corrected source signal is left (*bottom-right panel*).

After these operations, the QL shows four different diagrams, as in Fig. 5.2. Depending on which type of observations have been carried out, different diagrams might be displayed. As describing all of them here would be unfeasible, we invite the users to explore the possibilities of the QL.

The case shown in Fig. 5.2 is a pointing scan on source MWC349. The four panels show: the tracking accuracy of the telescope in Azimuth and Elevation; the reduced map of the scan, including information about the beam size, source flux, and pointing corrections; the noise r.m.s. in the field of view and the position of the KIDs in Nasmyth coordinates; the Gaussian fit in the Azimuth and Elevation axes of the source profile, aimed at determining pointing offsets.

The QL performs a simplified data reduction. Generally speaking, the results (even if written in FITS files) are to be used for display and checking purposes only.

Nevertheless, using the QL with the correct values of the atmospheric opacity  $\tau$  for simple point-like, well-centered sources, the result does not differ too much from a proper thorough data reduction. The same does not hold if the source is not centered or is complex.

Note, finally, that the QL does not combine scans together; it reduces each scan separately.

## 5.6 Products

The QL script produces many PNG images, that are stored in the `plAr#` directories.

It also produces many data files, that are stored in the `dat` directory. It is important to keep in mind that the `.dat` files are appended. This means that each time the QL is run, the `.dat` files become bigger and bigger. One might want to check their size from time to time.

### 5.6.1 Save FITS files

The QL scripts, in their standard configuration, do *not* produce any FITS files of the *quickly reduced* data. If a FITS version of the result maps is needed, it is possible to override the standard setup of

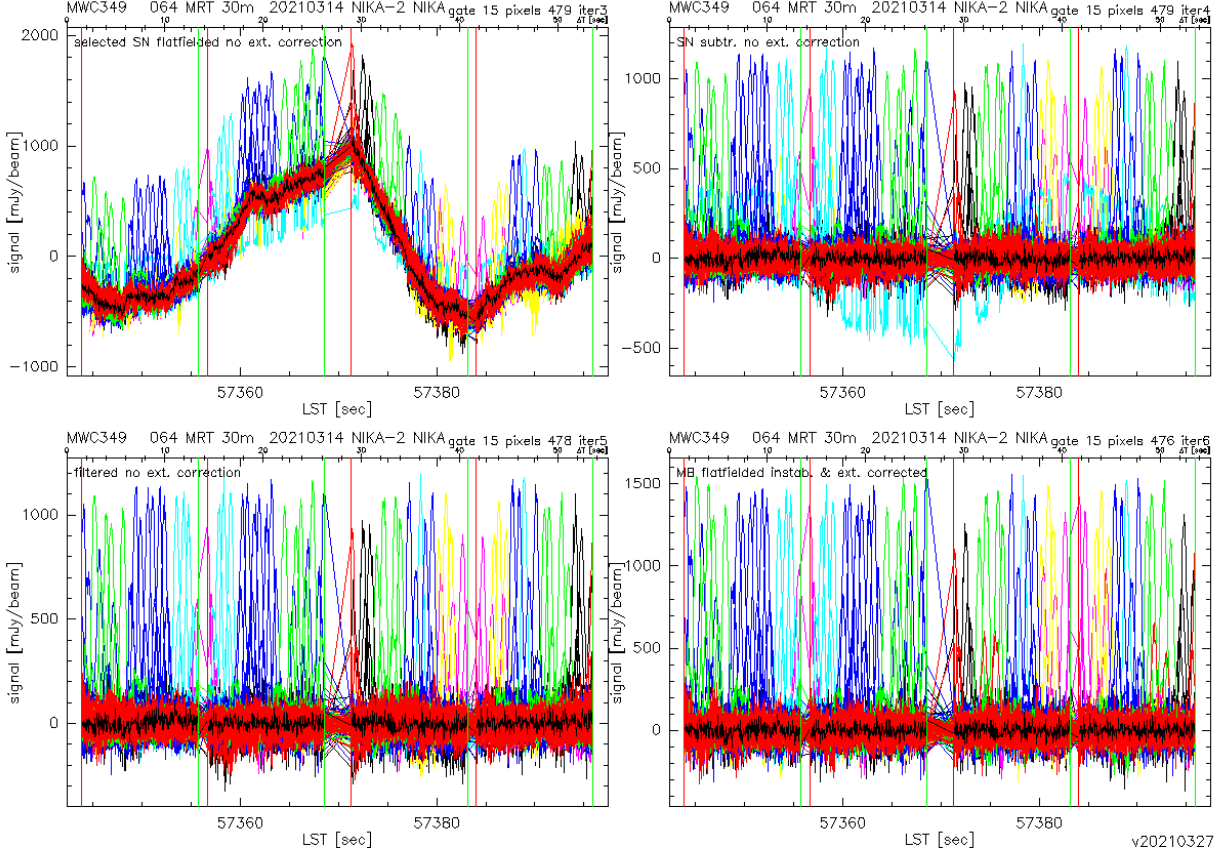


Figure 5.1: Example of timeline of a pointing scan on the source MWC349 (Array 2), after different operations have been performed on the signal: flat-field and forward beam calibration (*top-left*); sky-noise removal (*top-right*); exclusion of problematic KIDs (*bottom-left*); main beam, baselines and extinction corrections (*bottom-right*). Each line belongs to a different KID (detector pixel) of NIKA2. See main text for more details.

the QL scripts.

In order to do this, copy into the working directory, from the `pro/` folder in the installation directory, the scripts that define the QL parameters.

Generally speaking, PIIC finds the scripts in the `pro/` folder. Following GILDAS' conventions, if a script with the same name is in the working directory, then this has the priority. Therefore it is sufficient to copy the scripts of interest in the working directory and modify them there, in order to use a custom setup instead of the default setup, without the need to modify the installed version.

For the three arrays, these scripts are called:

```
qlDefsAr1.mopsic      for the individual-scan version
qlDefsAr2.mopsic
qlDefsAr3.mopsic
```

```
qlDefsAr1list.mopsic  for the list version
```

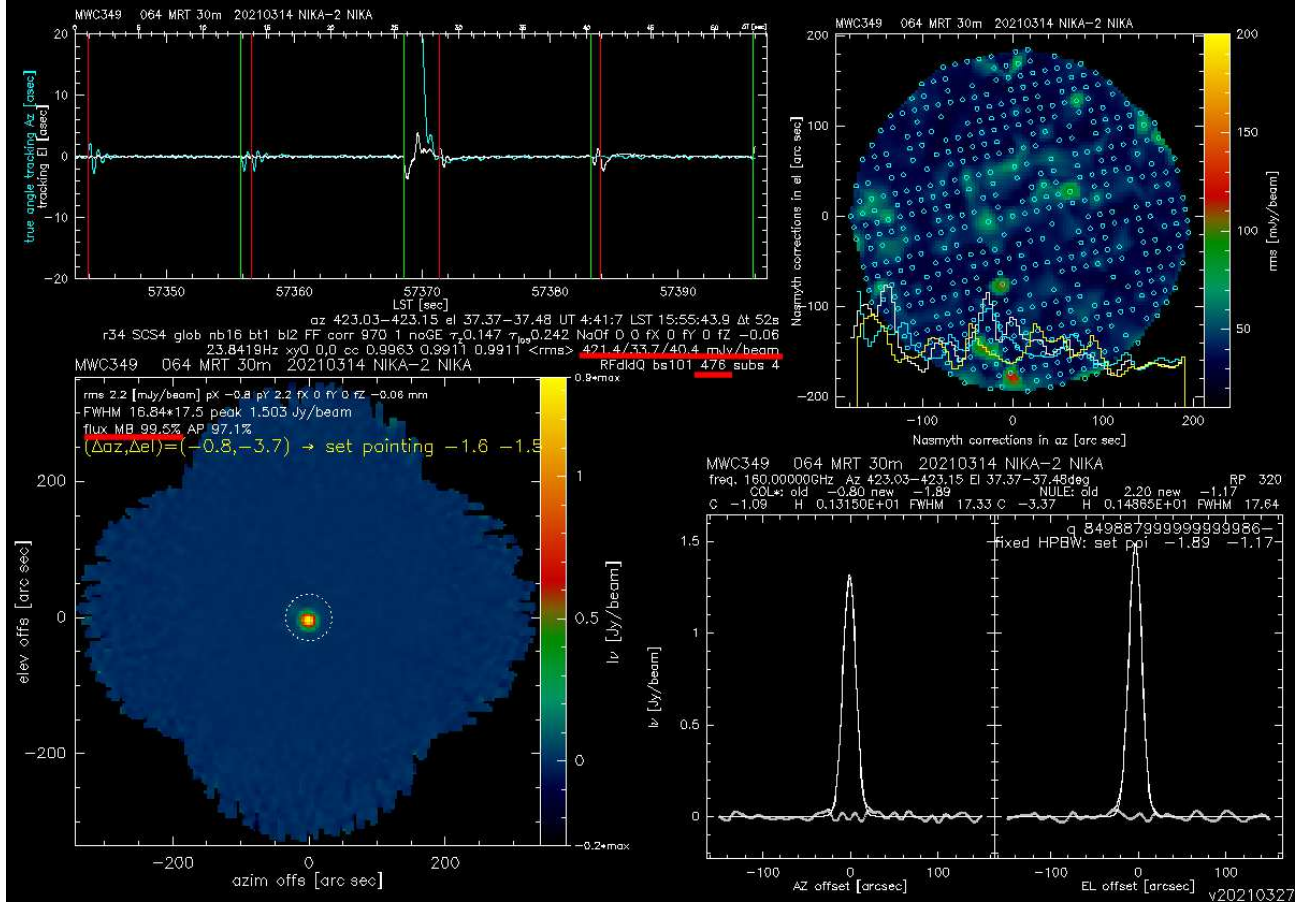


Figure 5.2: Result of QL analysis of a pointing scan on the source MWC349 (Array 2). Top-left: tracking accuracy in Azimuth (white) and Elevation (cyan), i.e. difference between commanded and effective coordinates as a function of time. Bottom-left: reduced map of the scan, including information about the beam size (HPBW), the peak flux, the main beam flux, the aperture flux (extracted within the aperture marked on the map), and pointing corrections (in yellow). Top-right: noise r.m.s. in the field of view and position of the KIDs in Nasmyth coordinates. Three histograms are also shown, representing a cut across the FoV at lines 0 (white), and  $\pm 100$  (yellow and cyan). Bottom-right: Gaussian fit in the Azimuth and Elevation axes of the source profile, aimed at determining pointing offsets. Among the many pieces of information reported in this diagram, the timeline r.m.s., the number of KIDs left and the fraction of flux (of a known calibrator) recovered in the main beam are underlined in red. Three values of the noise r.m.s. are given; they correspond to the top-left, the bottom-left and the top-right panels of Fig. 5.1, respectively.

```
qlDefsAr2list.mopsic
qlDefsAr3list.mopsic
```

Edit the variable `writeMap` and change it from “no” to “yes”:

```
let writeMap no      -> yes
```

Now the QL will write FITS files of the reduced data (maps) and will store them in the directory `redAr*/`.

## 5.7 Additional setup parameters

It is possible to optimize the value of some parameters in QL setup, to obtain a higher-quality QL products (both for simple sources and also more complex targets), or speed up the processing, etc.

The order of the baseline fit can be changed (e.g. from 1 to 3). This change needs to be taken with care, because — for example — if not enough data pixels (or not good enough data) are available, it might produce more damage than improvement. Nevertheless — assuming that you know what you are doing — the parameter to be changed is called `blOrderOrig`.

For increasing speed, just know that the parameter `nBest` defines how many best-correlating KIDs are considered in the computation of base-line corrections. A value of 32 does a good job; a value of 0 (zero) does a bad job, but is 10 times faster (because searching the `nBest` best correlating KIDs is not requested anymore).

In order to prevent the QL to stop after having processed each scan, set the parameter `usePause` to *no*.

# References

Emerson, D. T., Klein, U., & Haslam, C. G. T. 1979, A&A, 76, 92

Haslam, C. G. T. 1973, Kleinheubacher Berichte, 16, 451

Zylka, R. 1998, MOPSIC Cookbook, ITA Heidelberg

Zylka, R. 2013, MOPSIC: Extended Version of MOPSI, Astrophysics Source Code Library, record  
ascl:1303.011



# Appendix A

## Content of PIIC NIKA2 DAFs

In order to process NIKA2 data, PIIC needs a set of calibration files, that describe the properties of the KIDs arrays: geometry, resonance frequencies, cross-talking, response to incoming light (i.e. flux calibration). These are called *data associated files* (DAFs) and can be retrieved from the GILDAS download pages.

At each new release of PIIC, the DAFs database is included in the PIIC package. After each observing pool, the PIIC support team processes calibration data and produces new calibration files. The DAFs database is thus updated and a new version is available online, in a separate tar-ball, independent of the PIIC package. Therefore, when browsing the PIIC GILDAS pages for updates, always check for new PIIC *and* DAFs tar-balls.

The PIIC DAFs consist of five different main types of files. In alphabetical order:

- calibration files (CAL), defining the response of KIDs for flux calibration;
- deleted receiver pixels (DRP) files, listing those KIDs that are known to be defective;
- frequency files (NKFR), listing the natural resonance frequencies of all KIDs, for different sweeps<sup>1</sup>;
- receiver pixels parameters (RPP), listing the flat field, flag and beam properties of each KID in the field of view of NIKA2, for different sweeps;
- atmospheric conditions over all observing runs (TAU files), containing the values of  $\tau$  produced by the Observatory's tau-meter.

The DAFs are organized in the **dafs/** repository in the PIIC installation directory. This **dafs/** directory contains five sub-directories, one per each DAFs file type. The DAFs come with a PDF document that summarizes the calibration properties and quality of all NIKA2 science runs and includes many explicatory diagrams. In this Appendix the content of each DAFs file is described.

---

<sup>1</sup>a *sweep* is practically a re-definition of KIDs resonance frequencies, performed regularly for each new season.

## A.1 CAL files

For each NIKA2 array, this directory contains one file, called `MRT_NIKA-*.CAL` (where `*` is the array number). Each file lists a number of entries, structured as three columns and one line, for example:

```
2019-05-16T20:00:00 162.84 1.0
```

The three pieces of information in each line are:

```
Column 1:      the expiration date of the given flux calibration factor
Column 2:      the flux conversion factor from instrumental units to Jy
Column 3:      a further correction factor.
```

Additional notes and comments are provided, e.g. specifying the start of a given NIKA2 run or sweep changes. Exclamation marks indicate comment lines.

## A.2 DRP files

For each NIKA2 array, this directory contains one file, called `MRT_NIKA-*.DRP` (where `*` is the array number). These files list a number of entries, each one consisting of several lines. For example:

```
DATE 2019-09-18T23:13:04 1 12 20 21 32 37 38 71 72 73 74 77 78 91 92 93 98 ...
                        214 215 224 225 227 228 262 263 267 275 460 461 463 ...
                        344 350 351 352 361 362 377 393 403 426 441 442 453 ...
                        524 525 534 541 542 545 546 554 555 573 574 579 588 ...
```

These entries represent the identification numbers of the KIDs that are known to be affected by strong cross-talk or other problems and are therefore excluded a priori from the data analysis. The date and time of each entry indicate the expiration of the given entry. Usually, cross-talks are checked at least at each new sweep (because the logical order of KIDs changes) and whenever an intervention on the instrument is performed. Some times exceptional checks are also performed independently of these events.

## A.3 NKFR files

For each NIKA2 array, this directory contains one file, called `MRT_NIKA-*.NKFR` (where `*` is the array number). Several other files are also included. The `MRT_NIKA-*.NKFR` files list a number of entries, for example:

```
2019-02-12T12:00:00 N2R12_NIKA-1-20171019s3.nkFr
```

For a given expiration date, these entries point to a file that contains the intrinsic resonance frequencies of all available KIDs, as defined by a sweep. Specific comments indicate when a new sweep was performed.

The `N2*.nkFr` files consist of two columns: identification number of the KID (from 1 to  $n$ ) and their resonance frequency.

## A.4 RPP files

For each NIKA2 array, this directory contains one file, called `MRT_NIKA-*_MB.RPP` (where `*` is the array number, and MB means “main beam”). Several other files are also included. The `MRT_NIKA-*_MB.RPP` files list a number of entries, for example:

2019-01-29T12:00:00 NIKA2ar1allRPs\_run21med\_NO\_YES\_1\_92.rpp

For a given expiration date, these entries point to a file that gives the parameters describing the NIKA2 Array. Additional comments specify when new sweeps have been performed, or when other changes happened. These `.rpp` files consist of 25 columns; for data processing, the essential columns are only the following:

|           |  |
|-----------|--|
| Column 1  | identification number of the given KID for the current sweep       |
| Column 3  | main beam flat field   |
| Column 4  | forward beam flat field  |
| Column 5  | $\Delta x$ , Nasmyth x-offset at zero elevation                    |
| Column 6  | $\Delta y$ , Nasmyth y-offset at zero elevation                    |
| Column 7  | quality flag; if =0 the given KID might be usable (but see DRP)    |
| Column 14 | FWHMmaj [arcsec], major axis FWHM of beam, measured with beam-maps |
| Column 15 | FWHMmin [arcsec], minor axis FWHM of beam, measured with beam-maps |
| Column 16 | beam PA [deg], measured with beam-maps                             |

The ending line of each file defines the verse of the Nasmyth rotation and the pointing KID if the array is a pointing array; for NIKA2 it is Array 2.

Other parameters given in the `*.rpp` files might be used in PIIC internally for statistical purposes and are not essential.

For a given  $i$ -th NIKA2 data record, the offset position of each  $j$ -th KID, with respect to the reference (pointing) pixel, can be computed as:

$$\delta x_{ij} = \Delta x_i^{\text{tel}} - \delta x^{\text{corr}}, \quad (\text{A.1})$$

$$\delta y_{ij} = \Delta y_i^{\text{tel}} - \delta y^{\text{corr}}, \quad (\text{A.2})$$

where  $\Delta x_i^{\text{tel}}$  and  $\Delta y_i^{\text{tel}}$  are the telescope offsets defined by the observing mode for each record, and the  $\delta x^{\text{corr}}$  and  $\delta y^{\text{corr}}$  corrections are given by:

$$\delta x_{ij}^{\text{corr}} = \delta x_j^{\text{Nasmyth}} \cos(el_i) + \delta y_j^{\text{Nasmyth}} \sin(el_i), \quad (\text{A.3})$$

$$\delta y_{ij}^{\text{corr}} = -\delta x_j^{\text{Nasmyth}} \sin(el_i) + \delta y_j^{\text{Nasmyth}} \cos(el_i). \quad (\text{A.4})$$

In these Equations,  $\delta x_j^{\text{Nasmyth}}$  and  $\delta y_j^{\text{Nasmyth}}$  are read from the `.rpp` files, and  $el$  is the telescope elevation of the  $i$ -th data record.

## A.5 TAU files

For each NIKA2 array, this directory contains several files, called `MRT_NIKA-*run**`.TAUS (where `*` is the array number, and `**` is the NIKA2 run number to which the file belongs).

The structure of each file is of two columns: the modified Julian date (MJD) at which the value of the atmospheric opacity,  $\tau$ , was measured; and the value of  $\tau$  at the frequency of the given NIKA2 array (i.e. 1 or 2 mm).

The atmospheric opacity was measured by the IRAM 30m tau-meter instrument at 225 GHz and converted to the NIKA2 frequencies using standard procedures.

# Appendix B

## Effects of re-gridding

As mentioned in Section 3.3.1, gridding is performed applying the algorithm by Haslam (1973) modified and improved by R. Zylka. The kernel used to re-distribute the flux of each KID onto the final grid is a sinc function in Fourier space. It is important to truncate it properly, in order to avoid artefacts (because it extends to infinity).

Using the `addSource` option (see Sect. 4.12), simulations have been produced and analyzed to study the effects of gridding on the width of point-like profiles and on the flux of point-like sources. For extended sources, the issue of broadening due to gridding is not important.

The artificial input map consists of 50 sources with peak signals between 1 and 90 mJy/beam. The sources are assumed to be point-like and their profiles are Gaussian with  $\text{FWHM} = 12$  arcsec. Since these are point-like sources, peak fluxes correspond to total fluxes by definition. The sources were added onto a timeline of pure Gaussian noise with r.m.s. of 0.001 mJy. The noise r.m.s. was set so low in order to have a very high S/N ratio and be able to study the gridding effects on the point-like profiles without having to deal with the effects of poor S/N. The top-left panel of Fig B.1 shows the artificial map.

After processing with the default pipeline settings, the shape and fluxes of the artificial sources were measured by fitting elliptical Gaussian profiles, allowing re-centering. The profiles are described by their minor and major axes FWHM, their position angle (PA) and their peak flux (called “height” in the diagrams).

Figure B.1 presents the results. The profile geometrical parameters measured with the elliptical Gaussian fit (FWHM of minor and major axes and PA) are shown as a function of each other and as a function of the measured peak flux. The median measured  $\text{FWHM}_{\text{min,maj}}$  are  $12.059 \times 12.055$  arcsec, to be compared to the 12 arcsec input FWHM. This demonstrates that the broadening of the point-like profiles due to the adopted gridding algorithm is  $< 0.5\%$ . The retrieved peak fluxes agree with the input ones within a  $\sim 0.2\%$  difference.

We reiterate that the simulation is based on very high S/N artificial sources. In the real world, the limitations of the data play also an important role. By these are meant the limited exposure time (i.e. a higher intrinsic noise), the instrumental imperfections (including telescope deformations above all) and the sky and instrumental (KIDs and electronics) instabilities, and so on. Therefore the broadening inferred from real data may differ from the one measured under the ideal conditions shown here, but is not dominated by the effects of the gridding algorithm.

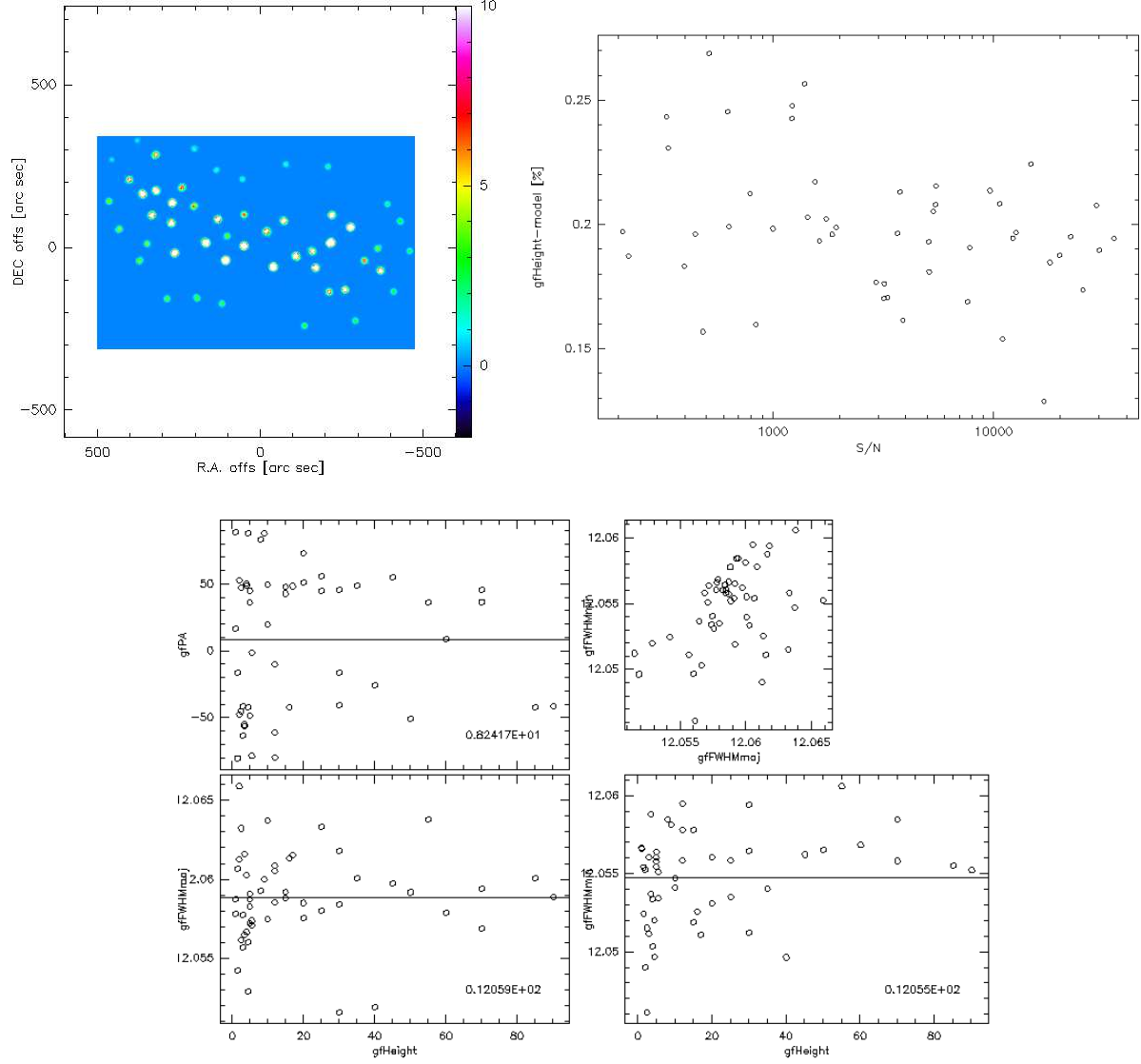


Figure B.1: Simulation to study the effects of gridding. *Top-left panel:* artificial map used in the simulation. *Top-right panel:* different between output (measured) and input peak fluxes, as a function of S/N ratio. *Bottom panels:* measured source geometry (elliptical Gaussian fit, gf, FWHM of minor and major axes and position angle as a function of each other and of peak flux, Height).

# Appendix C

## Transfer function examples and challenges

To the aim of performing an accurate and correct analysis of science data, it is necessary to handle the effects that are not related to the astronomical source itself, i.e. to study what happens to the light emitted by the target from the moment it leaves the object to the moment the final map is ready on one's hard disk.

The path starting from just outside the Earth's atmosphere and ending on the KIDs detectors has been commented before and is subject of the NIKA2 documentation. The possible effects induced by data processing can be studied by adding an artificial source to the KIDs timelines with the same characteristics as the original data (i.e. ideally *into the original timelines*), and by processing it in the same exact conditions as the original data (e.g. with the same PIIC setup).

This process is conveniently called “study of the *transfer function*” (TF), where it is meant the transfer from the raw data to the final map as operated by the data reduction process. During this process, possible idiosyncrasies of the data themselves might be highlighted, therefore the TF can also come in help to optimize the observing strategy for a given target.

Section 4.12 describes how to add artificial sources to the timelines. Appendix B discusses the effects of re-gridding on the profiles of point-like sources. Here we deal with the fundamental question: how does data processing affect the source flux distribution and total flux?

Some experiments with the TF of point-like and extended sources are presented in this Appendix, with the aim to show the principles and some caveats of the TF analysis. We do not have the pretension to be complete, nor exhaustive of all possible cases, hence each science project needs to perform its own specific TF analysis. Those presented here are only general examples, but can be still used as inspiration to define one's methodology to study the TF.

### C.1 List of term and acronyms used in this Appendix

This *transfer function* Appendix makes use of a quite variegate and complex nomenclature of cases and of PIIC features. Here we list them, so that the reader can have an easy and direct reference to look at any time:

|      |   |
|------|---|
| AS   | AddSource or Artificial Source; i.e. the input artificial map/object used in the simulations.   |
| FM   | Final Map; i.e. the map produced by PIIC processing the real data, without the null map option.   |
| FMAS | Final Map plus AS; the AS has been added to the KIDs timelines, without using the NM option.  |
| NM   | Null Map; i.e. the map obtained multiplying each second scan by $-1$ .  |
| NMAS | Null Map plus AS; i.e. the result of PIIC processing, obtained adding the AS to timelines and using the NM method.  |
| RZ   | zeroing radius (see Sect. 4.5.3).   |
| SMAS | Simulated Map using AS; the AS is added to an empty, simulated timeline that includes only artificial Gaussian noise (linked to the NIKA2 sensitivity and sky noise). |
| S/N  | Signal to Noise ratio.  |
| TF   | Transfer Function.  |

## C.2 Point-like sources transfer function

The analysis of the *transfer function* for the case of point-like sources is based on the same artificial map presented in Appendix B. It includes 50 sources with peak signals between 1 and 90 mJy/beam, and it's added to the timelines of a large deep dataset reaching down to  $\sim 0.15$  mJy/beam r.m.s. in the central regions. Different pieces of analysis and data processing approaches have been carried out and are presented here:

1. NMAS; the artificial map was combined with the null map technique to study the TF of point-like sources.
2. FMAS; to highlight the different noise properties between NM and FM, the AS was added to the timelines without using the NM technique, taking care to avoid any overlap to real sources.
3. SMAS; a completely simulated dataset was defined and studied: empty timelines containing only Gaussian noise, to which the AS is added.

In the FMAS and NMAS cases, the data processing was carried out with five different values of `blOrderOrig` = 1, 2, 3, 5, 7 and in iterative mode with up to 12 iterations.

In the SMAS case, the Gaussian noise in the timelines is made of two components: the NIKA2 sensitivity and the sky noise. This noise is symmetric around zero by construction and it is not affected by the “zig zag” due to crossing a range of airmasses. This experiment represents, so to say, the ideal case of observations without any “noise instability” induced by the observing strategy or the instrument. Six different realizations of the SMAS simulation have been performed: the positions and fluxes of the injected sources do not change; the r.m.s. of the Gaussian noise does not change either; only the seed of the random number generator used to produce the Gaussian noise does change and therefore the local noise in each position of the map is different between the 6 SMAS cases. The SMAS has been processed only adopting `blOrderOrig` = 1 because it is not affected by baseline “instabilities”.



For these different data sets, the study of TF consists in measuring the percentage of recovered flux for all sources, and study its dependence on S/N ratio and on iteration number. In this analysis we study also how the noise properties of the NM and FM differ to each other.

Only 1 mm results are shown. A similar reasoning can be applied also to 2 mm data.

### C.2.1 Recovered point-like sources flux

Figure C.1 presents how the fraction of recovered flux varies for each source as a function of iteration number and S/N ratio. The cases of FMAS and NMAS obtained with `blOrderOrig` = 3 are shown. The experiment carried out only with pure Gaussian noise (SMAS) is presented in Section C.2.4. The sources are grouped in bins of S/N ratio. The S/N ratio of a given source changes as the baseline fitting order and the iteration number vary. Therefore, to simplify the comparison between NMAS and FMAS, and to allow to build the full *recovered flux fraction vs. iteration number* curves, it is necessary to fix a reference S/N ratio for each source, to be used in all diagrams. Our choice is to use the S/N ratio measured in the FMAS experiment at the last (12th) iteration, obtained with `blOrderOrig` = 3 for each source.

The Figure demonstrates that for isolated point-like sources in a deep, empty field, 5 iterations are already sufficient to reach convergence on the source's flux. Below the  $5\sigma$  detection limit, the flux loss can be as high as 50%. Even up to S/N=20, if not 30, there might be still a 10% scatter on the measured fluxes, even in the case of these very deep data.

The null map experiment (NMAS) shows a better recovered flux fraction than the results obtained without nulling the original signals (FMAS): smaller scatter and recovered flux fraction closer to unity even in the low S/N tail. This is clearly due to the fact that the null map approach cancels out some of the problems affecting the FMAS.

*This effect suggests that a TF based on the NMAS experiment might be an optimistic description of the properties of the data set.*

We stress again, however, that this is **only an example** aimed to present the methods and their limitations. Here we are operating in the small numbers limit: only few sources have been added to the timelines. Therefore this analysis does not claim to be complete. A publication-grade TF analysis would imply to add thousands of artificial point-like sources, possibly distributed in flux as the observed (or modeled) number counts, and obviously implying several batches of small numbers in order to avoid geometrical confusion.

### C.2.2 Noise properties of Null Map *vs.* Final Map

Proceeding in the comparison of the different experiments performed for point-like sources, Figure C.2 shows the fraction of flux recovered at the last iteration, as a function of S/N ratio, again for `blOrderOrig` = 3.

The distribution of the sources in the NMAS and FMAS is very different, especially at the low S/N end. As mentioned before and as will be shown again in Sect. C.3, the noise properties of NM are different with respect to those of the FM. The noise of the FM is not symmetric around zero and when multiplying every second scan by  $-1$  to produce the NM, these asymmetries have the consequence that the NM noise is not equivalent to the FM noise.

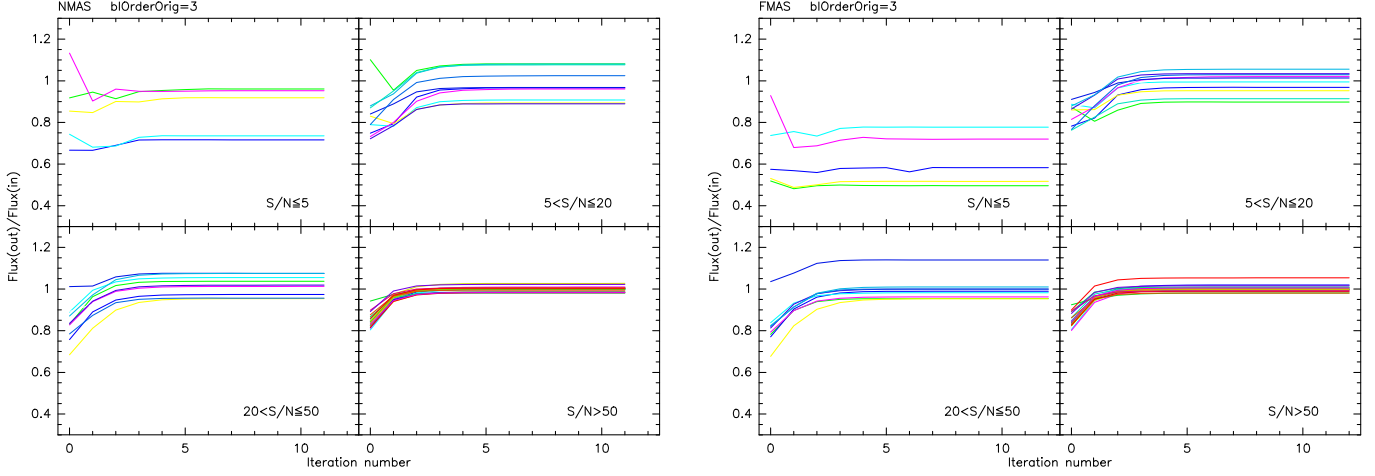


Figure C.1: Fraction of recovered flux in the point-like sources transfer function analysis. For the two experiments under analysis (NMAS and FMAS), this fraction is shown for each source as a function of iteration number, in four bins of S/N ratio. For clarity sake, only the results obtained with `blOrderOrig = 3` are shown. Each colored line belongs to an individual artificial point-like source. For ease of identification, the colors of the lines are the same as the colors of the stars in Fig. C.2.

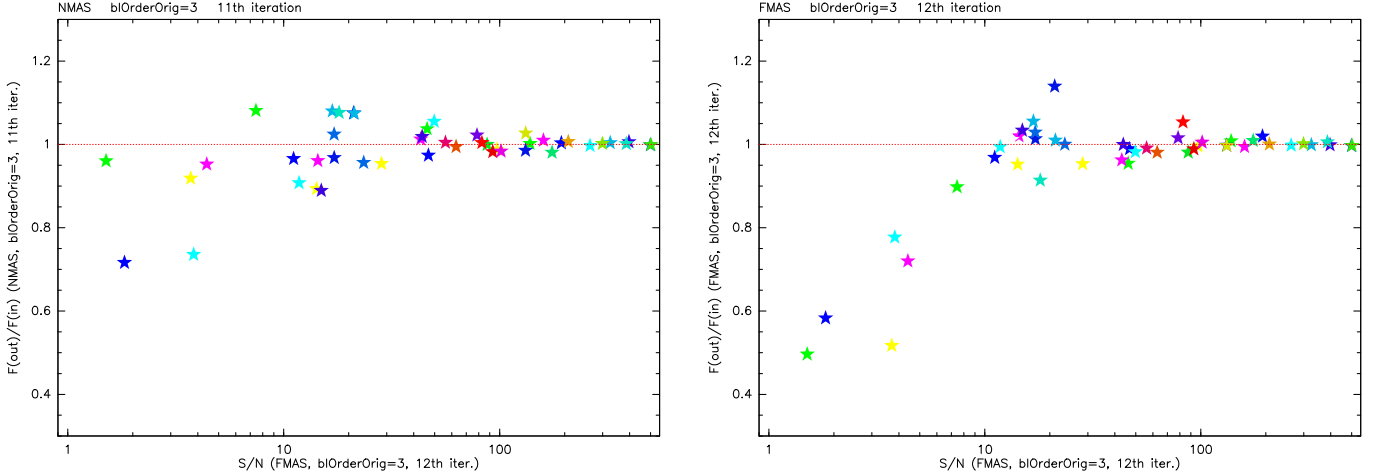


Figure C.2: Fraction of flux recovered at the last iteration, for the two experiments under analysis (NMAS and FMAS), in the case of `blOrderOrig = 3`, as a function of S/N ratio. Each colored star belongs to an individual artificial point-like source. The colors correspond to those of the lines in Fig. C.1.

### C.2.3 The effect of changing baseline fitting order

Each experiment has been performed with five different baseline fitting orders. Figure C.3 presents diagrams similar to Figs. C.1 and C.2 for the NMAS and FMAS, obtained varying the value of `blOrderOrig`.

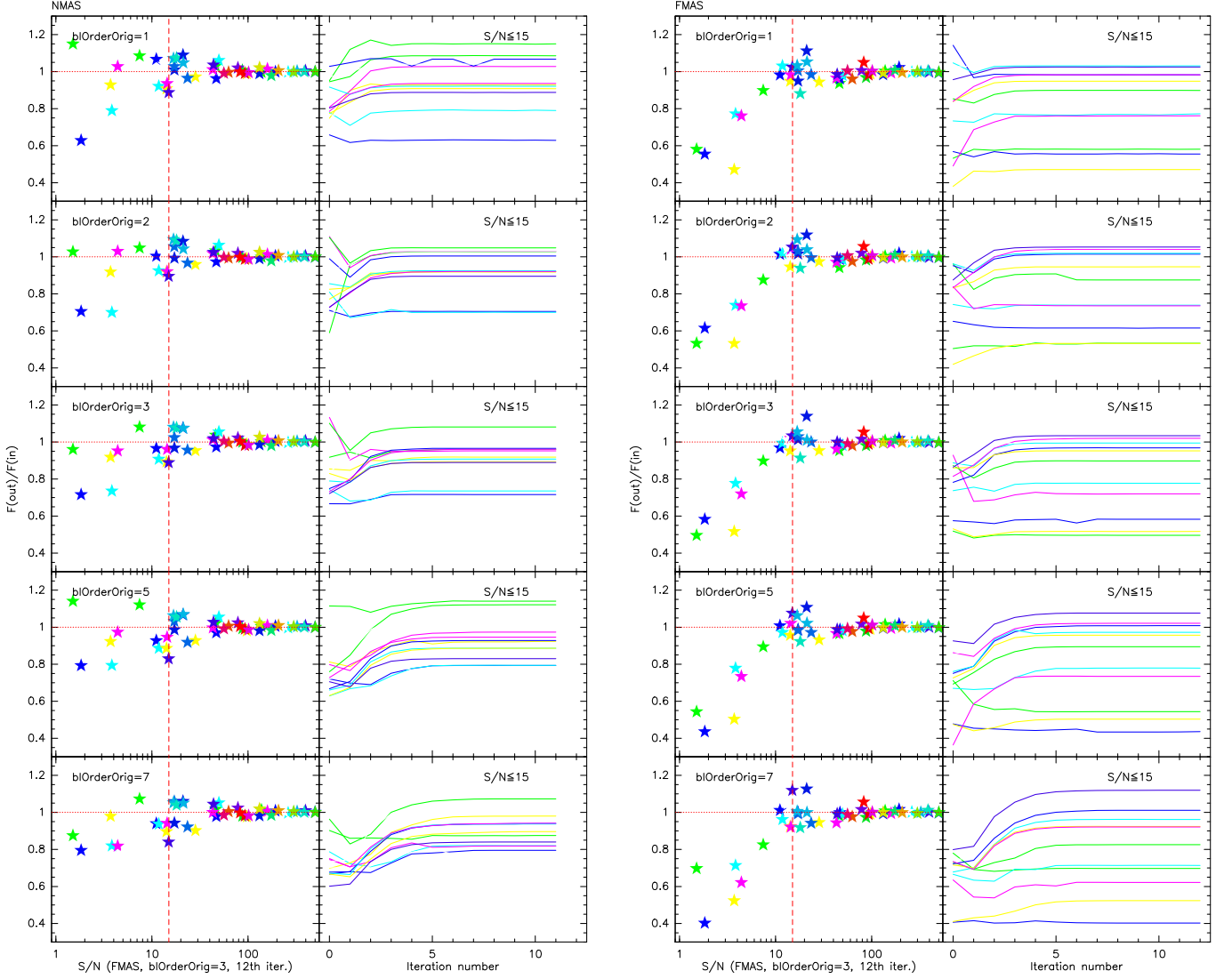


Figure C.3: Effect of changing the baseline fitting order on the point-like sources TF experiments: NMAS (*left*), and FMAS (*right*). For each of these cases, we show: *a*) the fraction of recovered flux at the last iteration, as a function of S/N ratio; *b*) the fraction of recovered flux as a function of iteration number, for sources with  $S/N \leq 15$ . The colors of the stars and of the lines have a 1:1 correspondence. The vertical dashed line marks the  $S/N=15$  level.

As the baseline fitting order changes, the sources move in the diagram. At the low S/N side, this reshuffling is more evident. There is not a systematic rule regulating these movements, which testifies that the residuals of baseline fitting are here playing a role. The sources might lie on a crest or on a depression produced by these residuals (see also Sect. C.3) and the recovered total flux therefore varies. This variation is larger, in relative terms, for fainter objects and/or sources positioned in noisier regions of the map.

The scatter at the low S/N end of the NMAS plot tends to improve for higher values of `blOrderOrig`.

This is not necessarily the case for the FMAS, in which the residuals of the baseline subtraction can be amplified by the non-symmetric properties of the noise.

### C.2.4 The ideal case of simulated pure Gaussian noise

The SMAS simulation has been conducted replacing the timelines with artificial pure Gaussian noise, aimed at representing the NIKA2 instrumental noise and the sky noise. To these timelines, the AS has been added during the processing in the usual way. As mentioned before, six different incarnations of the SMAS have been produced, each of them differing from the other only by the value of the random number generator seed. Only a `blOrderOrig` value of 1 has been used because the data do not have any baseline problems in this case.

Figure C.4 presents the fraction of recovered flux as a function of iteration number, for all the injected sources. As before, the Figure is split into four S/N bins and the S/N is again computed using the FMAS 12th iteration. The same diagram is repeated for all six different SMAS simulations. The panels in Fig. C.4 can be easily compared to those of Figs. C.1 and C.3.

The six different SMAS panels show the limitation of small numbers statistics especially at the low S/N end of the flux distribution of the artificial sources. The same sources, subject to Gaussian noise obtained with the same r.m.s. but with a different random seed, are recovered with very discrepant fluxes if their S/N is lower than 5. This is natura consequence of the fact that we are sampling only very sparsely the distribution of fluxes and noise, using only few sources.

Brighter sources are of course “better behaved”, but even at S/N between 5 and 20 there is still at least a 10% scatter in the recovered total fluxes. This effect is even more evident in Fig. C.5, which depicts the flux recovered at the last SMAS iteration, for all 6 realizations in one single diagram. The classic opening of the flux distribution at low S/N is now clearly seen.

It is worth to note that, even taken together, these six SMAS simulations still are in the small numbers limit and a much larger number of objects should be used to study the flux vs S/N distribution in detail. Moreover, in order to make our point, here we have **not** varied the positions and fluxes of the input sources in each SMAS realization, at odds with what science projects will do.

## C.3 Extended sources transfer function

Also in the case of extended sources, in the analysis of the *transfer function* care must be taken in examining possible spurious effects caused by the limitations of ground-based millimetric observations and by the limitations of the NIKA2 instrument installed on the IRAM 30m telescope.

The example analysis shown here has been carried out with an artificial galaxy including compact giant molecular clouds, added to the timelines of typical NIKA2 extended objects real scans. The null map switch was on, such that the objects originally observed cancel out and only the signal of the artificial object are kept (see Sect. 4.12.1). Tests similar to those presented here can also be performed on other kind of extended sources (e.g. Galactic clouds or SZ negative signals); we invite each scientific project to carry out their specific TF analysis.

Because of the null map technique, the properties of noise on the resulting map are altered with respect to those of the noise of the final map that one would obtain without multiplying each second

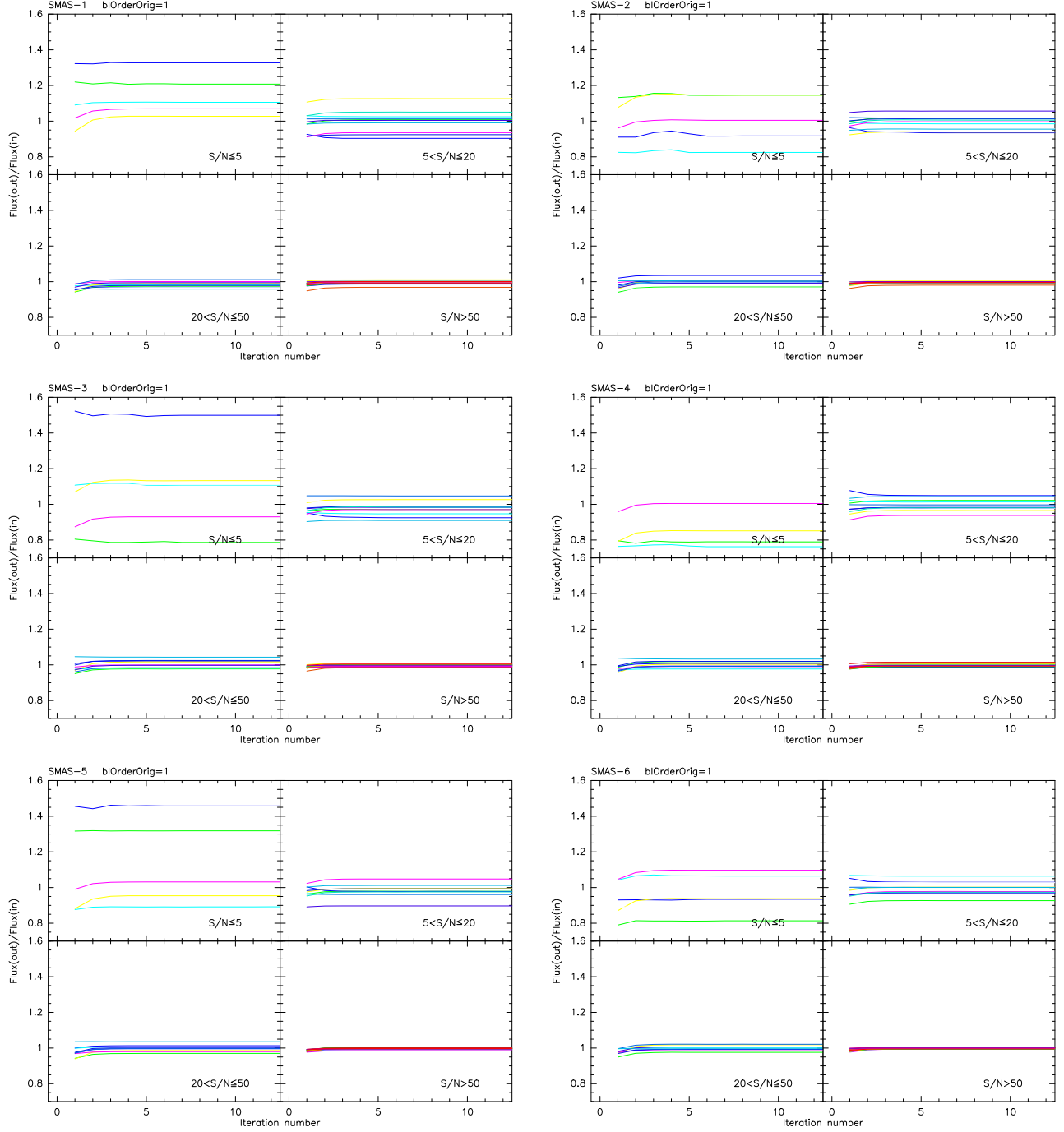


Figure C.4: Result of the six SMAS simulations. The fraction of recovered flux is shown for each artificial source as a function of iteration number, in four bins of S/N ratio. Each colored line belongs to an individual artificial point-like source. For ease of identification, the colors of the lines are the same for the 6 different SMAS and thus belong to the same point-like source. The sources (and the colors) are also the same as in Figs. C.1, C.2, C.5, etc.

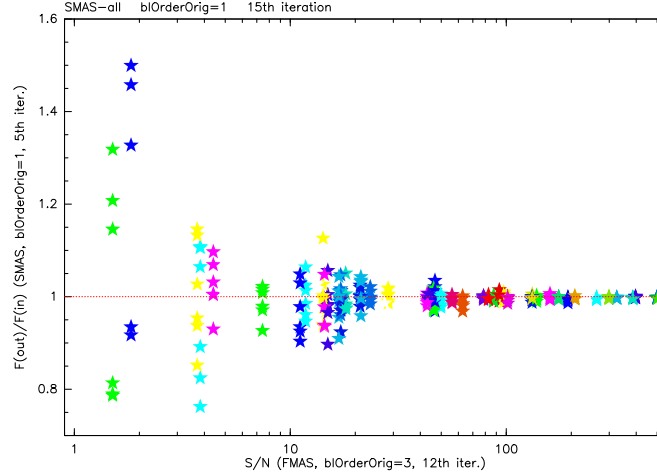


Figure C.5: Total recovered flux in the last iteration of the six SMAS as a function of S/N. See text and the captions of Figs. C.4, C.1 and C.2 for more details.

scan by  $-1$ . As shown before for the case of point-like sources, in fact, the noise on the scans is not perfectly symmetric, because of (sky and instrumental) instabilities, baseline subtraction residuals, etc. Therefore spurious effects can be produced by the null map processing. An analysis of possible caveats related to the NM approach is discussed in what follows. The effects of enhanced noise at the edges of the maps are also studied.

As brief overview, the following cases are analysed and synthetically described in this Section:

1. AS, the artificial map, without any Gaussian noise added, and without PIIC processing.
2. NMAS, i.e. null map plus artificial source, processed with two different RZ values (350 and 550 arcsec), sorting the list of scans only by observation time.
3. NMAS, processed with RZ=550 arcsec, sorting the list of scans by observation time *and* by scan direction.
4. NM, with no artificial source added, processed with two different RZ values (350 and 550 arcsec), sorting the list of scans only by observation time.
5. NM, with no artificial source added, processed with RZ=550 arcsec, sorting the list of scans by observation time *and* by scan direction.
6. NMAS, processed for each scan direction separately, with RZ=550 arcsec and smoothing parameter `smSourcePar`=-3.

Unless otherwise stated, in the NMAS cases the following pieces of analysis are carried out:

- PIIC processing with four different values of the smoothing parameter (`smSourcePar` =  $-1$ ,  $-3$ ,  $-9$ ,  $-15$ ) and three different baseline fitting polynomial orders (`blOrderOrig` = 2, 3, 4).

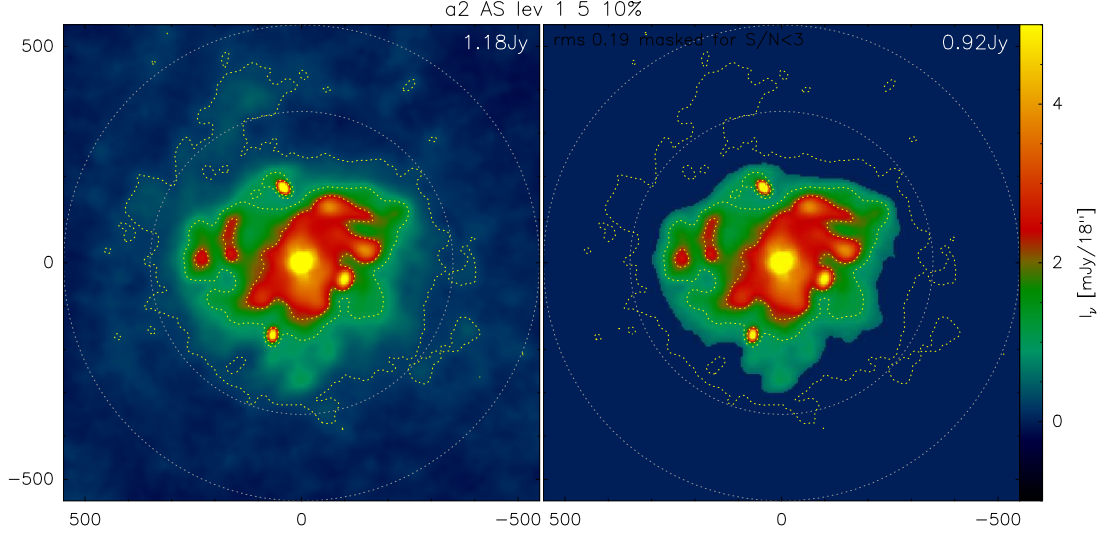


Figure C.6: The artificial source used in the *transfer function* simulation. *Left panel:* the AS as is. The two circles have radii of 350 and 550 arcsec and depict the two different RZ's used in the analysis. *Right panel:* the portion of the AS brighter than the  $3\sigma$  detection limit of the PIIC final map (i.e. cut using the noise r.m.s. of the final processed map). The values reported in the top-right corner of each panel are the total flux of the source (in the right panel it's the flux above the  $3\sigma$  threshold).

- the resulting maps are shown and discussed.
- the total recovered source flux is analysed as a function of the processing parameters and of iteration number.
- the radial (azimuth averaged) power spectrum of the maps is computed and analysed as a function of the processing parameters.

For convenience and ease's sake, only 2 mm examples are discussed. Similar reasonings hold also for the 1 mm data.

### C.3.1 Properties of the input artificial map

As mentioned above, the input AS consists of an artificial galaxy and compact sources meant to represent giant molecular clouds. The outskirts of the galaxy are extended and faint. Consequently, when considering the noise r.m.s. of the map produced by PIIC, the wings are by construction fainter than the  $3\sigma$  detection limit.

Figure C.6 shows the artificial map (left panel). The two circles depict the two different zeroing radii used in the analysis (350 and 550 arcsec). In the right-hand panel, a threshold at the  $3\sigma$  level of the map produced by PIIC is applied, showing that the faint wings of this specific simulated galaxy are lost in the noise of the chosen set of real scans by definition. Above the  $3\sigma$  level, one can expect to detect roughly 78% of the original total flux, in the case of this example. This percentage is therefore by construction the maximum fraction of total flux that one can retrieve after data processing.

### C.3.2 The effect of the zeroing radius

The concept of zeroing radius (RZ) was already described in Sect. 4.5.3: because of enhanced noise in the outer parts of the scan map, it is preferable to set to zero the source map beyond a radius of choice (or outside a user-defined polygon).

We study here the differences in the TF obtained with two different choices of the RZ: a large 550 arcsec radius circle and a smaller 350 arcsec radius one. While building the source map, the latter value allows for “pixel detections” above the chosen S/N threshold only over a smaller region centered in the scan map.

Figure C.7 shows the maps, the percentage of recovered total flux with respect to the known flux of the input artificial map, and the power spectrum of the maps, for all cases under study (i.e. the combination of the following parameters values: RZ=550 or 350 arcsec; `smSourcePar` = -1, -3, -9, -15; `blOrderOrig` = 2, 3, 4). Several effects can be identified.

First of all, when using a larger RZ, the system instabilities (atmosphere + telescope + NIKA2) can create spurious signals due to the enhanced noise in the outer regions (see a proper discussion of causes in Sect. 4.5.3), that are not fully excluded from the source map. In this situation, the fraction of recovered total flux<sup>1</sup> runs away and diverges, because of the spurious positive signal.

The power spectrum of the final maps seems closer to that of the input map when using a larger RZ, especially at the large angular scales (i.e. small  $k$ ), which instead lose more power with smaller RZ. This might be misleading because the power spectrum analysis alone cannot tell that this large scale signal is spurious. On the other hand, note that at the medium scales the ratio of the final maps power spectrum to that of the input map is systematically larger than unity, indicating that the result is not trustworthy.

A smaller RZ guarantees that the outer “problematic” areas are fully excluded from the source map and these spurious positive signals are minimized. As byproduct, Fig. C.7 shows that 20 iterations are not enough to recover the total flux of this kind of extended source with faint wings, but a larger number of iterations is needed to converge to its asymptotic value.

The insurgence of the large scale spurious signal worsens as the smoothing of the source map becomes more important (i.e. large absolute value of `smSourcePar`) and for smaller baseline fitting order (`blOrderOrig` = 2 *vs.* 4).

Finally, the excess of power seen in the ratio of power spectra (inset of bottom plots in Fig. C.7) at  $\sim 2.5$  arcmin ( $k \sim 0.4$  arcmin<sup>-1</sup>) could be due to an enhancement of the source wings due to the thresholding method. When the signal in the wings is close to the adopted S/N threshold, some noise spikes can be detected above the threshold and can enhance the wings’ signal. The scale at which this happens obviously depends on the shape of source’s spatial profile. It is worth to note that, in the experiment presented here, this effect is minimised for RZ=350 arcsec and `blOrderOrig`=4. This indicates that, in combination to the thresholding effect, also the baseline fitting residuals play a non negligible role (see also Sect. C.3.5).

---

<sup>1</sup>the percentage of recovered total flux is computed with respect to the input total flux, without taking into account that by construction only 78% is expected to be above the  $3\sigma$  limit.



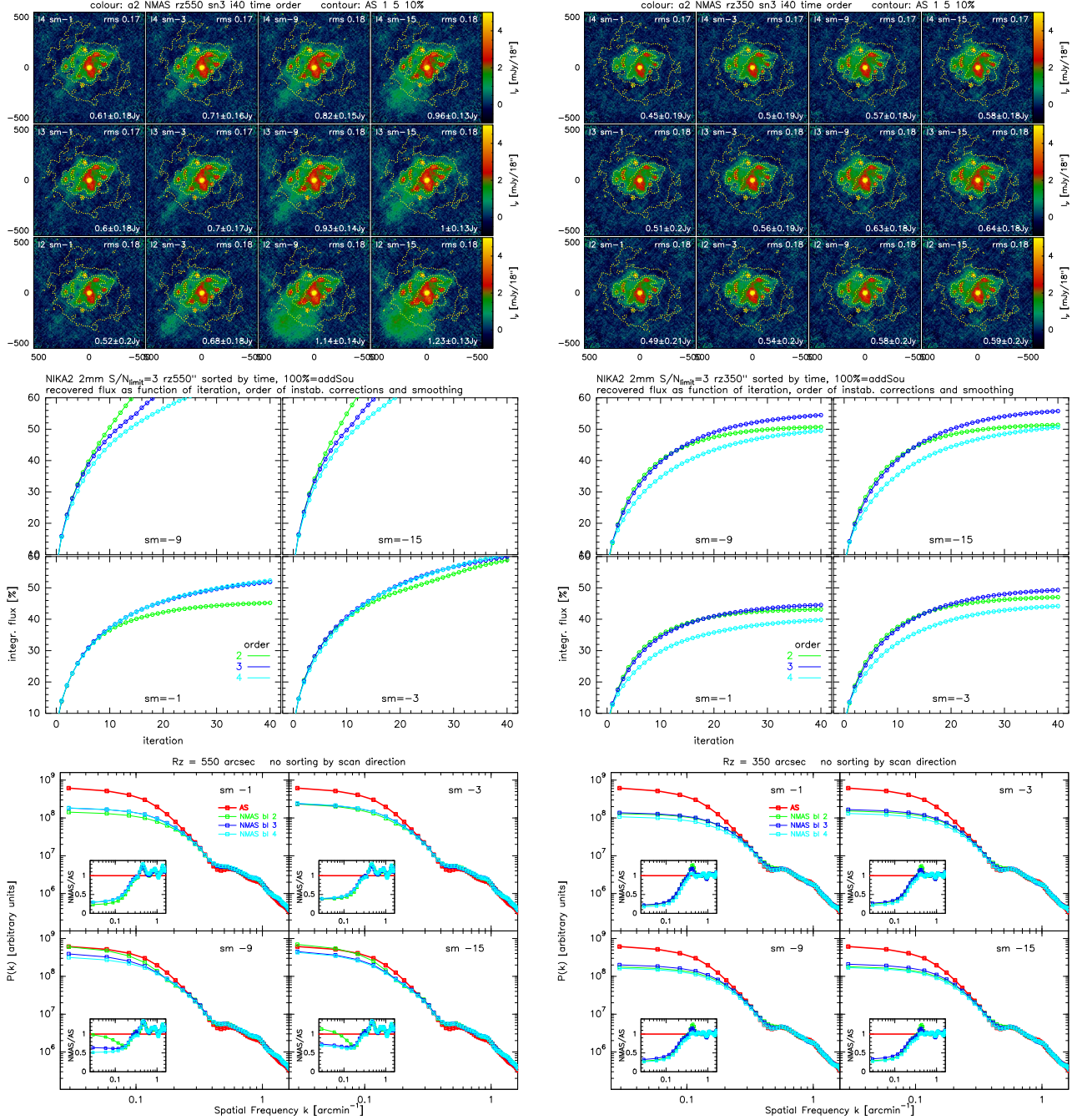


Figure C.7: The effect of different RZ values. *Left* panels show results obtained with RZ=550 arcsec; *right* panels with RZ=350 arcsec. *Top figures*: maps built with three different choices of  $\text{blOrderOrig}$ =4, 3, 2 (rows) and four different values of  $\text{smSourcePar}$  = -1, -3, -9, -15 (columns). *Middle figures*: percentage of recovered total flux for all studied cases. *Bottom figures*: power spectrum of the final map in all studied cases, and ratio to the power spectrum of the input artificial map (inset).

### C.3.3 Re-shuffling the list of scans

The analysis carried out here makes use of null maps. The artificial source is added on the timelines after multiplying each second scan by  $-1$ , so that the original signal for the real object is nullified, otherwise the artificial source would overlap to the real one.

Depending on the adopted observing strategy, it can happen that — in the input list of scans — odd-numbered scans are systematically taken in one scan direction in the sky (e.g.  $+45$  deg in Equatorial coordinates) and the even-numbered scans are systematically in other direction (e.g.  $-45$  deg). As a consequence, when producing the null-map, all scans taken in one direction are multiplied by  $-1$  and all those taken in the other direction keep their original sign. This produces a null map that is indeed “nulled” in the central regions where all scans overlap (and where possibly the target lies) but that it is not in the areas covered by only one of the two scan directions.

This induces an additional difference in the noise properties of the outer regions with respect to the central area, and therefore a potential additional cause of spurious signals caused by baseline fitting residuals, not only in the outer regions but also in the central area itself.

Figure C.8 shows the results of processing obtained after re-shuffling the input scan list. In this experiment, the list is re-organized such that the first  $\frac{N}{2}$  scans were all taken in the first scanning direction (e.g.  $+45$  deg) and the following  $\frac{N}{2}$  scans in the second scan direction (e.g.  $-45$  deg). In this way the  $\pm 1$  multiplicative factor is applied evenly to both scan directions.

Let’s compare these results to those in the *left* column of Fig. C.7. The spurious positive signal, that was produced before, has now mostly disappeared, suggesting that the outer regions have now similar noise properties as the central area of the map. On the other hand, one can notice that the percentage of recovered total flux is lower in this case with respect to the result obtained with  $RZ=350$  arcsec and no re-shuffling of the list of scans. At the medium angular scales the ratio of the power spectrum of the final maps to that of the input artificial map is not systematically larger than unity but is not flat: it has a tendency to be  $< 1$  at  $k \sim 0,6 \text{ arcmin}^{-1}$  and to increase towards smaller angular scales. In other words, simply adopting a smaller  $RZ$  (when possible) seems to be more effective solution than re-sorting the list of scans.

Note, obviously, that more complex configuration can also happen, for example if three, four, or more different scanning directions were adopted.

### C.3.4 Caveats, warnings and null maps

The sorting approach chosen and described above might be sub-optimal and different choices could be made. For example, one could organize the list of scans such that it lists scan directions in couples, i.e. two scans in direction 1, followed by two scans in direction 2, then again two scans in direction 1, and so on, taking care to always keep the scans taken close in time also close in the list.

Note, however, that this alternative approach might be complicated by the fact that scans can be rejected during the processing, because of different reasons (e.g. high noise along the timeline). If this happens then this kind of sorting can easily be altered during the processing. To be effective, one should first verify which scans will be excluded, by running a first “dummy” processing aimed only at identifying them.

The condition that, in order to properly produce the NM, the number of scans multiplied by  $-1$

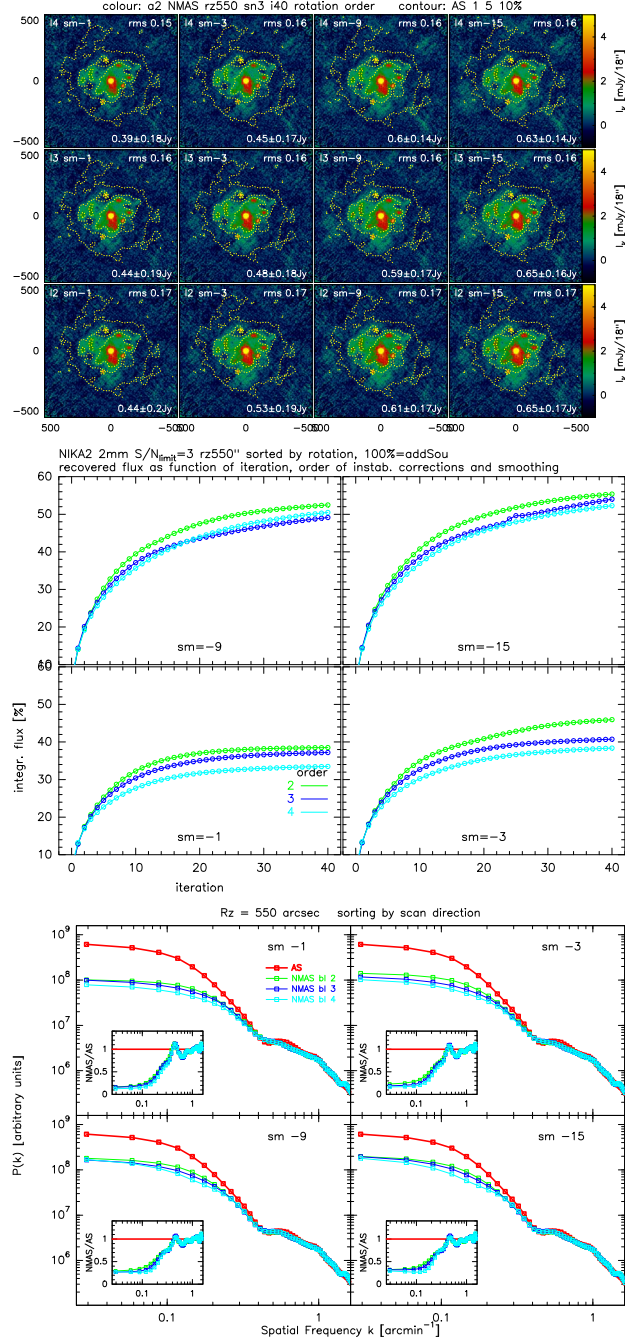


Figure C.8: The effect of sorting the input list of scans by scanning direction, to be compared to the *left* column of Fig. C.7. Here a value of  $RZ=550$  arcsec is adopted. *Top*: maps built with three different choices of  $blOrderOrig=4, 3, 2$  (rows) and four different values of  $smSourcePar = -1, -3, -9, -15$  (columns). *Middle*: percentage of recovered total flux for all studied cases. *Bottom*: power spectrum of the final map in all studied cases, and ratio to the power spectrum of the input artificial map (inset).

needs to be the same number of those “multiplied” by  $+1$ , is a simplification. To be fully correct, the condition is that the number of data records multiplied by  $\pm 1$  must be the same across the whole final map, per main beam angle. A compromise between the two conditions is that the number of maps multiplied by  $\pm 1$  must be the same across the whole final map, per main beam angle. Deviations from these conditions produce NM’s with different degrees of approximation.

In any case, re-sorting the list of scans has some non negligible consequences on the properties of the final maps. Being the calibration of the data never perfect, re-ordering the list of scans necessarily produces different NM (for the reasons written few lines above).

The so-called “system instabilities” can be corrected only to some extent therefore there are residuals. Re-shuffling the list of scans, these residual instabilities are better suppressed when multiplying each second scan by  $-1$  and the null map appears “cleaner”. Figure C.9 shows the NM obtained with usual combinations of `smSourcePar` and `blOrderOrig`.

On the other hand, when dealing with real data to produce the final map (FM), i.e. not using the null map option, these residual instabilities are never suppressed because no scan is multiplied by  $-1$ . The final consequence is that the NM obtained by reshuffling the list of scans is no more representative of the real FM, and therefore the analysis of the TF might not be representative of the effects induced by the data processing on the final measurements (e.g. it could be too optimistic or pessimistic).

For example, if the effect of the residual instabilities is to produce a negative (spurious) signal, then this produces a dip in the FM and the measured flux of the real (positive) source will be lower. Re-shuffling the input scan list, instead, suppresses this effect and the TF calculated from the NM is different from the real TF associated to the FM.

The message here is therefore that re-sorting the input scan list must be done carefully and *only* after an in-depth thinking of the consequences. In the end it’s a matter of purpose: some pieces of analysis might still benefit from re-shuffling the input list of scans, but some others (e.g. the TF described here) might be misled by such choice.

### C.3.5 Instabilities induced by the scanning direction

As known, scanning in the sky crossing different elevations produces large variations of “sky noise”, because the sub-scans cover a wide range of airmasses. Scanning up and down across airmasses produces the “zig-zag” behaviour of the raw signal seen in the top-left panel of Fig 5.1. The baseline polynomial fit removes most of this zig-zag pattern, but after this process there are still KIDs that show the imprint of the total-power zig-zag on much lower level, hidden within the uncorrelated noise. This low-level zig-zag shows up in the final maps and depends on the scan direction in the sky. Maps obtained scanning at smaller angles in Alt-Azimuthal coordinates (i.e. with small variations of Elevation) show the smallest effect.

A thorough study of these instabilities carried out by R. Zylka in Summer 2020 to Winter 2021 has shown that this is just a base line problem and does not affect the flux calibration down to the mJy scale nor the size of sources on the final map. These instabilities visible in the final maps could be in principle minimized via base line fitting, provided that the sub-scans are sufficiently long, i.e. *for each KID* the sub-scans have enough data on both sides of the source. This is not always the



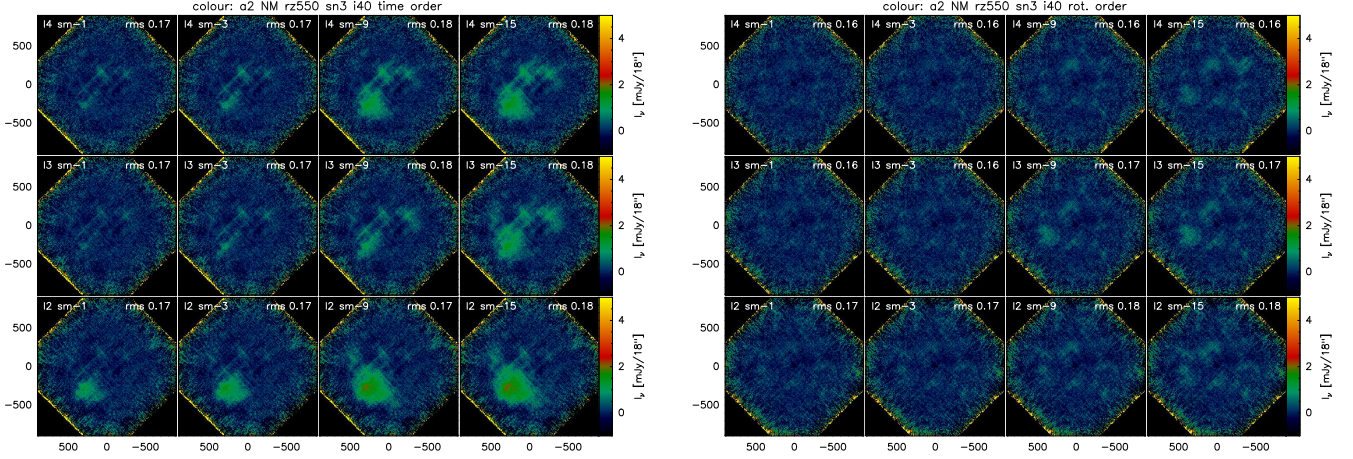


Figure C.9: Null maps obtained without re-sorting the input list of scans (*left*) and re-shuffling it (*right*). A zeroing radius  $RZ=550$  arcsec is adopted. The rows belong to the three different choices of  $blOrderOrig=4, 3, 2$ ; and the columns differ by the four different values of  $smSourcePar = -1, -3, -9, -15$ .

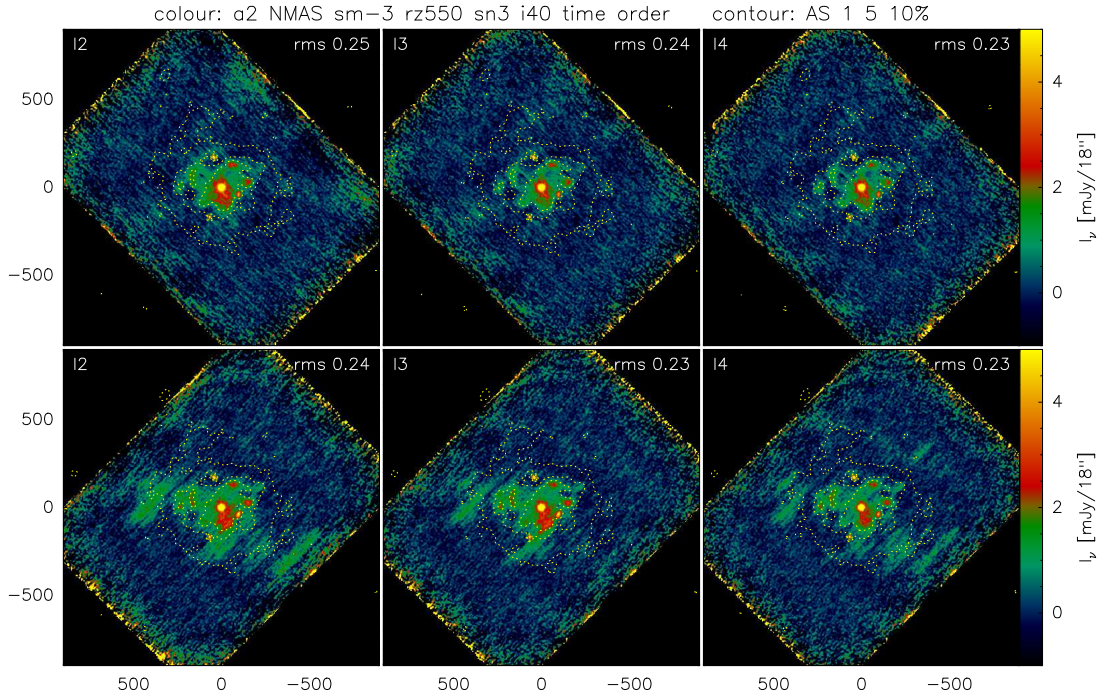


Figure C.10: Spurious signals due to system instabilities can depend on scanning direction in the sky. This example shows the result obtained with  $RZ=550$  arcsec and  $smSourcePar=-3$  for two different scanning directions (*top* and *bottom* rows) and three different values of  $blOrderOrig$  (from *left* to *right* = 2, 3 and 4).

case, therefore in some cases this correction can be performed only approximatively.

The spurious signal induced by instabilities can also depend on scanning direction. The cause is

similar to what described before: if the baseline correction cannot be well characterized, then the residuals can be identified by the S/N thresholding step and can produce “spurious sources”. Since the amplitude of the baseline subtraction residuals depends on scanning direction, also the insurgence of spurious sources depends on it. Figure C.10 shows an example in the specific case of  $RZ=550$  arcsec and `smSourcePar`=-3.

To this scanning effect, also possible intrinsic differences between NIKA2 KIDs and electronic boxes come into play and complicate the way the spurious signals appear. A discussion about these extra effects would be very technical and is beyond the scope of this Appendix.

The residual instabilities depend on the baseline fitting order and typically produce a “wavy” residual structure in the background of the final map, with regions lying on crests and valleys of the waves. The number and position of these crests and valleys depend on the adopted polynomial order (like harmonics). The left, middle and right panels in Fig. C.10 exemplify this effect clearly: the wavy pattern changes depending on baseline fitting order.

# Appendix D

## History of PIIC releases

- **October-November 2019:** first public release of PIIC. It included DAFs valid from June 2018 (NIKA2 run 19) to March 2019 (run 30) and version 1.0 of the tutorial.
- **December 2019:** new DAFs, covering the period from June 2018 (run 19) to November 2019 (run 38).
- **January 2020:** new version of PIIC, including the treatment of records affected by telescope tracking problems and the detection of negative sources, among other changes.
- **March 2020:** new DAFs, covering all NIKA2 science pools so far, from October 2017 (run 12) to March 2020 (run 43).
- **May 2020:** new version of PIIC. The main changes are:
  - new version of the variable `blOrder`, now also depending on scan length (if needed);
  - smoothing of the source map;
  - implementation of `nBest2`;
  - add artificial sources to the timeline;
  - computation of a null-map (a.k.a. “jackknife”);
  - save re-gridded maps of individual scans;
  - pointing correction between scans (incl. intensity corrections);
  - new, updated tutorial (v.2.2).
- **April 2021:** new DAFs, covering all NIKA2 science pools so far, from October 2017 (run 12) to March 2021 (run 51). The DAFs repository now includes also a document that summarizes the quality of calibration for all NIKA2 science runs.
- **May 2021:** new version of PIIC. The main changes are:
  - few parameters moved from the main template script to the further-settings script, including the r.m.s. polygon;

- the new default setup implies that PIIC defines automatically the r.m.s. polygon, with no need of manual intervention by the user.
  - hit maps can now be produced;
  - new scripts available to produce r.m.s. and S/N maps, and to produce source maps;
  - new version of the PIIC tutorial (v.3.1), including a description of DAFs, and the analysis of the effects of gridding on point-like sources.
- **June 2021:** new version of the PIIC tutorial (v.3.5), now including the Appendix about the transfer function.
  - **October 2021:** new version of PIIC. The main changes are:
    - new mode available, saving  $\sim 30\%$  of data reading and pre-processing time (parameter `useDAFsFr`);
    - new “final” cumulative maps available in output, allowing now to run PIIC on sub-sets of data in parallel (`wrCumLast` and `creaAver.piic`);
    - some variables changed name;
    - simplified template script: some variables have been moved to the further settings;
    - new, updated tutorial (v.3.8).